

Design of a Biomimetic Mechanical Stimulator for Engineered Myocardium



*A Major Qualifying Project
Submitted to the Faculty of
WORCESTER POLYTECHNIC INSTITUTE
in partial fulfillment of the requirements for the
Degree of Bachelor of Science*

By:

Daniela Cerkanowicz

MacKenzie Conlen

Shahnaz Ghahremani

Aaron Rosenthal

Date:

25 April 2019

Report Submitted To:

Dr. George Pins, Advisor

This report represents the work of four WPI undergraduate students submitted to the faculty as evidence of completion of a degree requirement. WPI routinely publishes these reports on its website without editorial or peer review. For more information about the projects program at WPI, please see: <http://www.wpi.edu/Academics/Projects>.

Table of Contents

Table of Contents	1
Authorship	6
Acknowledgments	9
Abstract	10
Table of Figures	11
Table of Tables	13
1. Introduction	14
2. Background	17
2.1 Myocardial Infarction & Heart Failure are Irreversible	17
2.2 Current Treatments	19
2.3 Engineering of Functional Myocardium	20
2.3.1 Cardiomyocyte Function	21
2.3.2 Scaffolds and Engineered Cardiac Tissue	22
2.3.3 Cardiac Patches	24
2.4 Mechanical Stimulation	27
2.5 Electrical Stimulation	32
2.5.1 Various Mechanisms for Electrical Field Stimulation	33
2.5.2 Bioreactor Stimulation	34
2.6 Monitoring Physiological Changes due to Stimulation	35
2.7 Review of Commercial Devices	36
2.7.1 Flexcell FX-6000 Tension System	36
2.7.2 Ion Optix C-Stretch 100	37
2.7.3 CellScale Biomaterials Testing Various “Mechanoculture” Products	38
2.8 Need for Engineered Cardiac Patches	39
	1

3. Project Strategy	39
3.1 Initial Client Statement	39
3.2 Defining the Stakeholders	40
3.3 Developing Objectives	40
3.4 Revised Client Statement	45
4. Design Process	46
4.1 Construct Formation	47
4.2 Pairwise Comparison	48
4.3 Needs Analysis	50
4.4 Design Process	52
4.5 Functions and Specifications	53
4.6 Initial Designs	54
4.6.1 Hook Tension Apparatus	55
4.6.2 Stretching Well Plate Apparatus	56
4.6.3 Stretching Well Plate with Walls	57
4.6.4 Inverted PDMS Frame	58
4.6.5 Dynabeads Magnetic System	59
4.6.6 Shear Flow Design	60
4.6.7 Vacuum Chamber Design	61
4.7 Quantitative Analysis of Design Ideas	63
4.7.1 Summary of Pugh Matrix	63
4.7.2 How the Pugh Matrix Works	63
4.7.3 Numerical Analysis of Pugh Matrices	65
4.8 Pugh Matrix Analysis of Design Elements	66
4.8.1 Well Plate Material	66

4.8.1.1 PDMS	66
4.8.1.2 Glass Bottom Well Plate	66
4.8.1.3 Polystyrene	67
4.8.1.4 Results	67
4.8.2 Construct Anchoring	67
4.8.2.1 Built into Well	68
4.8.2.2 PDMS Frame	68
4.8.2.3 Inverted PDMS Frame	68
4.8.2.4 Results	69
4.8.3 Mechanical Stimulation Technique	69
4.8.3.1 Uniaxial	70
4.8.3.2 Multiaxial	70
4.8.3.3 Shear Flow	70
4.8.3.4 Results	71
4.8.4 Force Production	71
4.8.4.1 Stepper Motors	72
4.8.4.2 Vacuum Pressure	72
4.8.4.3 Results	72
4.8.5 Force Analysis	72
4.8.5.1 Load Cell	73
4.8.5.2 Displacement	73
4.8.5.3 Results	74
4.9 Revision of the Pugh Matrix Analysis	74
4.10 Refined Design Ideas	75
4.11 Development of the Final Design	80

4.11.1 PDMS Well Plate System	81
4.11.2 PDMS Lid	85
4.11.3 Stepper Motor	86
4.11.3 Mechanical Stimulation	87
5. Development and Verification of the Final Design	89
5.1 Evaluating Well Plate Designs	89
5.2 Well Plate Deformation Mapping and Image Analysis	91
5.2.1 Finite Element Model of Well Plate in Tension	91
5.2.2 Instron Testing of Polyurethane Well Plate	92
5.3 Preliminary Testing Outcomes	95
5.4 Testing of Molds for PDMS Well Plate and Lid	96
5.5 PDMS Well Plate Lid Testing Through pH Measurements	98
5.6 Final Design	99
6. Validation of the Final Design	101
6.1 Validation of the Mechanical System	101
6.1.1 Instron Testing of PDMS Well Plate	101
6.1.2 Mechanical Stimulation Benchtop Testing	104
6.2 Well Plate and Lid Validation	105
6.3 Fibrin Microthread Diameter Comparison Study	107
6.4 Final Experiment	108
7. Discussion	111
7.1 Mechanical System Analysis	111
7.2 Well Plate and Lid Analysis	113
7.3 Fibrin Microthread Diameter Analysis	113
7.4 Final Design Analysis	113

7.5 Impact Analysis	114
7.5.1 Economic Impact	114
7.5.2 Environmental Impact	115
7.5.3 Societal Impact	115
7.5.4 Political Ramifications	116
7.5.5 Health and Safety Concerns	117
7.5.6 Ethical Concerns	117
7.5.7 Sustainable Usage	118
7.5.8 Manufacturability	118
7.5.9 Applicable Standards	118
8. Conclusions and Recommendations	119
References	120
Appendix A: Pairwise Comparison Chart	125
Appendix B: Pugh Matrices	128
Appendix C: Experimental Protocols	131
Appendix D: Instron Testing of Polyurethane Well Plate	153
Appendix E: CAD Files of PDMS Lid on 6-Well Standard Well Plate	155
Appendix F: Stepper Motor Control Arduino Code	156
Appendix G: Fibrin Microthread Diameter Tables	157
Appendix H: MATLAB Code	158
Appendix I: CAD Drawing of Final Components	161
Appendix J: Final Design Validation Data	167
Appendix K: Bill of Materials with Corresponding Prices	168

Authorship

Section	Author(s)	Editor(s)
1. Introduction	All	All
2. Background	All	All
2.1 Cardiovascular Disease	Daniela, MacKenzie	All
2.2 Current Treatments	MacKenzie	All
2.3 Engineering of Functional Myocardium	Aaron, Shahnaz, Daniela	All
2.4 Mechanical Stimulation	Aaron	All
2.5 Electrical Stimulation	MacKenzie	All
2.6 Monitoring Changes Due to Stimulation	MacKenzie	All
2.7 Review of Commercial Devices	Aaron, MacKenzie	All
2.8 Need for Engineered Cardiac Patches	Daniela	All
3. Project Strategy	All	All
3.1 Initial Client Statement	All	All
3.2 Defining the Stakeholders	MacKenzie	All
3.3 Developing Objectives	MacKenzie, Aaron	All
3.4 Revised Client Statement	All	All
4. Design Chapter	All	All
4.1 Construct Formation	MacKenzie	All
4.2 Pairwise Comparison	MacKenzie, Aaron	All
4.3 Needs Analysis	MacKenzie, Aaron	All
4.4 Design Process	Daniela	All

4.5 Functions and Specifications	MacKenzie, Aaron	All
4.6 Initial Designs	Shahnaz, Daniela	All
4.7 Quantitative Analysis of Design Ideas	Shahnaz, Daniela	All
4.8 Pugh Matrix Analysis of Design Elements	All	All
4.9 Revision of the Pugh Matrix Analysis	Shahnaz, Daniela	All
4.10 Refined Design Ideas	All	All
4.11 Development of the Final Design	Aaron, Daniela	All
5. Testing and Verification of the Final Design	All	All
5.1 Selecting a Stepper Motor	Aaron	All
5.2 Evaluating Well Plate Designs	Aaron, MacKenzie	All
5.3 Well Plate Deformation Mapping and Image Analysis	Aaron, MacKenzie	All
5.4 Preliminary Testing Outcomes	MacKenzie	All
5.5 Verification of Negative Molds for PDMS Well Plate	Daniela	All
5.6 PDMS Well Plate Lid	Shahnaz	All
6. Validation of the Final	All	All
6.1 Validation of the Mechanical System	Aaron, MacKenzie	All
6.2 Well Plate and Lid Validation	Daniela	All

6.3 Fibrin Microthread Diameter Comparison Study	Shahnaz	All
6.4 Validation of Final Design	Shahnaz, Daniela	All
7. Discussion	All	All
7.1 Mechanical System Analysis	MacKenzie	All
7.2 Well Plate and Lid Analysis	Daniela	All
7.3 Fibrin Microthread Diameter Analysis	Shahnaz	All
7.4 Final Design Analysis	Shahnaz	All
7.5 Impact Analysis	All	All
8. Conclusions	Aaron	All

Acknowledgments

The team would like to thank the following people for their assistance, skills, knowledge, and support throughout the project:

Department of Biomedical Engineering

Professor George Pins

Professor Sakthikumar Ambady

Elizabeth English

Meagan Carnes

Lisa Wall

Lynda Hammett

Department of Chemical Engineering

Tom Partington

Department of Mechanical Engineering

Professor Sarah Wodin-Schwartz

Information Technology

Dr. Erica Stults

The student staff of the Foise Innovation Studio Makerspace

Abstract

Heart disease is the leading cause of death worldwide. Myocardial infarction (MI) is a primary symptom of heart disease and results in damaging hypoxia of cardiac tissue and reduction of heart functionality, eventually leading to heart failure. Current treatments for heart disease and MI include pharmacological agents and implanted assistive devices, which may delay complications but do not restore full function to the damaged tissue. Fibrin cardiac patches, which consist of cardiac cells seeded within three-dimensional scaffolds, have recently shown promise as a regenerative solution, but still require improvements to their functional properties and similarity to native tissue. The goal of this project was to develop a low-cost biomimetic mechanical device to stimulate engineered fibrin cardiac patches to improve their functional properties. Cardiac patches seeded with C2C12 cells were used for proof-of-concept and analyzed for myoblast proliferation and alignment. Initial findings indicated that our device is capable of imparting consistent uniaxial strains onto live cardiac patches through diagnostic imaging and analysis.

Table of Figures

Figure 1. Flexcell FX-6000.....	37
Figure 2. Ion Optix C-Stretch	38
Figure 3. Objectives Tree.....	41
Figure 4. Broad concept drawing of design outline	46
Figure 5. PDMS Frame	47
Figure 6. Pairwise Comparison Example.....	48
Figure 7. Hand Drawing of the Hook Tension Apparatus	55
Figure 8. Hand Drawing of the Stretching Well Plate with Posts Apparatus	56
Figure 9. Hand Drawing of the Stretching Well Plate with Walls Apparatus	57
Figure 10. Hand Drawing of the Inverted PDMS Frame Design	58
Figure 11. Hand Drawing of the Dynabeads Magnetic System.....	59
Figure 12. Hand Drawing of the Shear Flow Design.....	60
Figure 13. Hand Drawing of the Vacuum Chamber Design.....	61
Figure 14. Pugh Matrix Example.....	64
Figure 15. Mathematical Model for Weighted Percentages in Pugh Matrices	65
Figure 16. “Jazzy Imaginative Mechanical-Stimulator” concept	76
Figure 17. Four wall inverted PDMS frame	77
Figure 18. Side view of staple stretcher concept	77
Figure 19. Single well isometric top view of staple stretcher concept	78
Figure 20. Single well side view of staple stretcher concept.....	78
Figure 21. Single well isometric bottom view of staple stretcher concept	78
Figure 22. Upside down concept	80
Figure 23. “Butterfly Squares” Well-plate concept.....	81
Figure 24. PDMS frame with walls	82
Figure 25. Finite-element strain profile of the “Butterfly Squares” concept.....	83
Figure 26. ASTM Die C well plate concept	83
Figure 27. Finite-element strain profile of the ASTM Die C well plate.....	84
Figure 28. PDMS lid model with wrapped around ends (grey) on well plate (teal).....	85
Figure 29. PDMS lid model without wrapped around ends (grey) on well plate (teal).....	86

Figure 30. Mechanical stimulator with polyurethane well plate mold	88
Figure 31. Tensile stretch of “Butterfly Squares” well plate	90
Figure 32. ANSYS Results from static uniaxial tension of well plate.....	92
Figure 33. Sample ImageJ displacement measurement (measurement line shown in blue. Also contains top well (A), center well (B), and bottom well (C).)	93
Figure 34. Strain when stretched by 10% of original length (269mm + 26.9mm).....	94
Figure 35. Strain when stretched by 8.6% of total length (269mm + 21.9mm)	94
Figure 36. Strain when stretched by 6.2% of total length (269mm + 16.9mm)	95
Figure 37. ABS well plate mold	96
Figure 38. ABS lid mold (left image: without top piece; right image: whole assembly)	96
Figure 39. Flexible negative polyurethane mold with uncured PDMS	97
Figure 40. 5-piece aluminum mold of well plate (left image: assembled; right image: dis-assembled).....	97
Figure 41. 4-piece aluminum mold of lid (left image: dis-assembled; right image: assembled)..	98
Figure 42. Picture of PDMS lid with 3 T75 flask filter caps on a standard 6 well plate	99
Figure 43. Fully assembled final design	100
Figure 44. Final broken down into all components	100
Figure 45. PDMS well plate Instron test, measured using ImageJ. Yellow line denotes measurement line from the reference point (D). Image also contains a 50mm known length for scale (E), the top well (A), middle well (B), and bottom well (C).	102
Figure 46. Boxplot of axial strain during Instron testing. Wells (x-axis) are labeled in Figure 43	103
Figure 47. Image from mechanical stimulator testing. Yellow line denotes measurement from reference point on stepper motor. Image also contains labeled top well (A), center well (B), and bottom well (C)......	104
Figure 48. Box plot of axial strain in each well during mechanical stimulation. Wells (x-axis) are labeled in Fig. 45.....	105
Figure 49. PDMS well plate with PDMS lid in mechanical system containing 10% FBS DMEM culture media.....	106
Figure 50. Bar graph showing team’s & Pins’ Lab dry and wet microthread diameters.....	108

Figure 51. Fluorescence images of C2C12 cells within fibrin-based scaffolds that show the nuclei (blue) and the actin cytoskeleton (green), as well as the presence of the fibrin microthread. The white arrows indicate the nuclei, the white circles indicate the actin cytoskeleton, and the red, dashed arrows indicate the direction of the applied loading force..... 111

Table of Tables

Table 1. Ideal functional properties of engineered myocardium	21
Table 2. Summary of mechanical stimulation parameters.....	31
Table 3. Summary of electrical stimulation experiments	35
Table 4. Definitions of objectives.....	41
Table 5. Design constraints.....	44
Table 6. Combined pairwise comparison charts	49
Table 7. Design needs.....	51
Table 8. Design wants.....	52
Table 9. Functions and specifications	54
Table 10. Advantages and disadvantages of conceptual designs.....	62
Table 11. Summary of the Pugh matrix scores.....	75
Table 12. Mean axial strain during Instron testing	103
Table 13. Mean axial strain during mechanical stimulator testing.....	105
Table 14. pH values of 10% FBS DMEM culture media without cells.....	107
Table 15. pH values of 10% FBS DMEM culture media with cells.....	107

1. Introduction

Heart disease is the leading cause of death globally, representing 31% (17.9 million) of all fatalities as of 2016. Of those, 85% are caused by heart attack and stroke [1]. Heart disease causes myocardial infarction (MI) in which tissue becomes hypoxic and diseased, leading to reduced heart function and eventually heart failure. Current treatment options include pharmacological agents and surgical devices such as left-ventricular assistive devices and coronary stents, but these solutions do not address the underlying diseased tissue causing the dysfunction [2]. As such, a need exists to regenerate sections of the heart damaged by MI.

Research over the past few decades has sought to find a regenerative solution to the heart disease problem. The emergence of the tissue engineering field has provided a pathway to creating functional replacements for damaged heart tissue. Initial efforts involved injecting cells or synthetic biomaterials into the heart, but cell delivery using this method exposes cells to abnormal signals produced by the diseased extracellular matrix of the native tissue. This altered microenvironment can prevent injected cells from promoting tissue repair or regeneration [3]. Combining cardiomyocytes with a biomaterial scaffold was the next step, with the hope that it would improve integration with the native tissue. Tissue-engineered cardiomyoplasty arose in the early 2000s, and involved transplanting cell sheets or engineered myocardium onto diseased cardiac tissue. Research into 3D biomaterial scaffolds improved upon this, allowing for highly-aligned cardiac tissue constructs that mimic a healthy extracellular microenvironment to be created. A substantial body of research exists investigating scaffold design in terms of material selection, scaffold stiffness, and ability to integrate with native tissue. Natural scaffolds have been created using collagen, fibrin, and alginate; synthetic polymers such as polyglycolic acid, polyglycerosebacate, and polydimethylsiloxane have also been used for scaffolding [4, 5]. Hydrogel constructs have been developed that spontaneously contract, have stiffness properties similar to that of native tissue, and promote axial cell alignment [6-8]. However, the difficulty of integrating these engineered tissues with healthy heart tissue remains.

Cardiac patches are the next step, with researchers seeking to create a platform that will readily integrate with surrounding tissue, promote regeneration, and improve on the contractile and mechanical biomimicry of existing engineered heart tissues. Integration of fibrin threads into

cardiac patches has been found to allow for the fine-tuning of patch stiffness to prevent it from failing under the dynamic loading conditions of the heart [9]. The small scale of cardiac patch platforms also opens opportunities for minimally invasive delivery, with some research proposing endoscopic delivery or injection of shape-memory patches [5, 10].

Despite their promise, the need remains to improve the morphological and contractile similarity of cardiac patches to healthy heart tissue. Though these constructs may be able to contract spontaneously, they exhibit low contractile forces [6-8]. This hinders their feasibility as a suitable replacement for damaged heart tissue. Researchers have sought to address this issue by subjecting engineered cardiomyocyte constructs to mechanical loading that mimics the loading environment experienced by cardiomyocytes *in vivo*. As such, loading modalities investigated include cyclic uniaxial stretch, stepwise uniaxial stretch, various flow conditions including shear flow, and dynamic pressure. Many authors have noted upregulation of genes that positively contribute to myogenesis as well as improved cell alignment, mitochondrial density, myofibrillar density, and increased cell hypertrophy. Despite these promising results, the contractile force generated by mechanically stimulated constructs are three to five times smaller than that of native tissue [8, 9]. Significant work remains to be done to optimize mechanical stimulation regimes to produce more functional engineered tissue.

The Pins Lab at Worcester Polytechnic Institute is currently developing a fibrin-based cardiac patch that incorporates fibrin microthreads to improve the passive stiffness of the patch and cell alignment. While the passive stiffness of the patch has been tuned to match the uniaxial stiffness of native myocardium, further increases to cell alignment and contractile force are necessary to match the functional properties of this cardiac patch to native tissue [9]. Mechanical stimulation is a potential pathway towards improving the function of these cardiac patches and is an important research goal for the Pins Lab. A device that would allow for the repeated uniaxial loading of these cardiac patches while maintaining the necessary environmental controls for cell growth and survival would be a valuable tool for moving this research forward.

This project seeks to address the need to improve the morphological, contractile, and passive mechanical properties of engineered cardiac patches by providing a low-cost platform for mechanically conditioning them. To accomplish this, the system must be capable of cyclically stretching the cardiac patches uniaxially at a frequency mimicking *in vivo* conditions while also

maintaining appropriate cell culture conditions. In designing this device, quantitative analysis was first used to prioritize the most critical aspects of the design that would be necessary to satisfy the needs of the Pins Lab as well as make the device successful. An iterative process was then used in which the team, along with Dr. Pins and members of his lab, brainstormed concepts for components of the design and then numerically ranked them with reference to each of the design objectives. The top-ranked design components were then combined to form a preliminary final design. Preliminary feasibility testing was conducted to determine what specific form each of the components should take, and once the team was satisfied with the performance of each component, a final design was constructed.

To test the final design, validation tests were performed to determine if each of the components met the specifications established by the team. The mechanical system was tested on the benchtop by using image analysis and strain mapping to determine if it would successfully stretch a simulated cardiac patch to a sufficient strain. It was then tested with live cardiac patches seeded with C2C12 murine skeletal myoblasts within a standard cell culture incubator to validate that the mechanical system would run successfully for an extended experiment and that the team's well plate containing the cardiac patches could maintain sterile conditions with appropriate gas exchange. pH measurements were used to confirm that the well plate was facilitating proper gas exchange. A microthread diameter study was conducted to confirm that the microthreads the team used to construct the cardiac patches were similar to those made previously in the Pins Lab. Finally, the overall performance of the entire device was tested using live cardiac patches in a control (polystyrene 6-well plate), the team's well plate, and the team's well plate in the mechanical stimulator. Staining protocols were used to visualize C2C12 proliferation and cytoskeletal changes after 1 day and 6 days of testing.

Following this testing, the team concluded that the specifications for the mechanical stimulator, environmental cell culture conditions, limited monitoring of the experiment, and the cardiac patch were satisfied as laid out in the revised client statement. The only exception was that the team was unable to validate the device for a 2-week experiment due to time constraints. The validation tests showed that this device is capable of providing cyclic mechanical stimulation to Pins Lab cardiac patches while maintaining cell culture conditions and showing improvements to cytoskeletal elongation and alignment. This device can be used moving forward

to investigate the effects of different mechanical stimulation regimes on cardiac patches by adjusting parameters such as frequency, total strain, and duty cycle. This will allow for improvements to the functional properties of the cardiac patches and eventually the matching of their mechanical and electrical properties with that of native myocardium, paving a way for their clinical implementation.

The sections below outline the clinical need to improve the functional properties of engineered cardiac patches in order to provide a regenerative solution to treating myocardial infarction, as well as the bodies of research leading up to the development of the Pins Lab cardiac patch and showing the positive effects mechanical stimulation can have on engineered muscle tissue. The team then discusses the project strategy and details the iterative design process that included brainstorming and quantitative design analysis. Testing of the team's top design options led to the creation of a final design, which then led to the validation tests that confirmed the success of the device. Finally, the impact of the device as well as conclusions and recommendations are presented.

2. Background

2.1 Myocardial Infarction & Heart Failure are Irreversible

Cardiovascular disease is the leading cause of death worldwide [1]. The term cardiovascular disease refers to any disease or condition directly affecting the heart or blood vessels. These conditions can include abnormalities relating to electrical signaling, cardiac muscle function and composition, and the constriction of blood vessels. Further progression of cardiovascular disease eventually leads to loss of heart function and heart failure. While many causes are unknown, poor diet and exercise, congenital defects, drug and alcohol abuse, infection, gender, and age can all contribute to the development of heart disease [11]. Depending on the patient's condition and time of diagnosis, some diseases may be treatable with certain therapies or surgeries. One form of heart disease will most often lead to the formation and progression of another disease.

Though there are many conditions that are categorized as heart disease, some of the most prevalent diseases include arrhythmia, coronary artery disease, and cardiomyopathy. Many of the conditions that are treatable progress to two detrimental conditions, myocardial infarction and heart failure. Several physiological conditions can result in a decrease in blood supply to the heart. Without oxygen, the cardiomyocytes, or heart cells, have little to no time before complete cardiac muscle tissue necrosis occurs [12]. This tissue death is known as myocardial infarction (MI) [11]. There are five different types of myocardial infarction that are categorized according to the presence of biomarkers, the status of dead cells, and the patient's electrocardiogram (ECG) wave [12].

MI is commonly a direct cause of heart failure. Heart failure occurs when the heart is unable to pump enough blood to the rest of the body. Those with a history of myocardial infarction have damage or nonfunctional heart tissue which serves as a significant risk factor for heart failure. The infarcted tissue is unable to contract thus hindering blood flow out of the heart. Depending on the size of the infarct and the degree of tissue death, heart failure can be quite serious. Heart failure leads to other physiological problems such as respiratory problems, fatigue, and edema. Heart failure can occur on either one side of the heart or on both sides of the heart. If the right side of the heart is affected, a patient will experience more respiratory issues due to lack of sufficient blood to the lungs, which can cause edema and further pulmonary conditions. If the left side of the heart is afflicted, there is not enough blood delivered to the tissues therefore causing fatigue and edema in the legs. As heart failure progresses, these symptoms worsen dramatically affecting the patient's quality of life [13].

MI and the resulting heart failure cannot be reversed and the available treatment for these conditions is only palliative. This is due to the biological nature and function of cardiac muscle tissues and cardiomyocytes. Cardiomyocytes are very limited in their ability to regenerate which results in almost instant cell death when cells are damaged, thereby leading to loss of heart function. After injury, cardiomyocytes attempt to self-repair by remodeling their sarcomeric structure, electric signaling, and metabolic processes; however, remodeling dead and injured cells results in the formation of scar tissue, which can cause further dysfunction of the heart [11].

2.2 Current Treatments

Due to a cardiomyocyte's inability to heal itself after an injury, treatments are unable to reverse tissue death and are only palliative solutions. Treatments include medication, surgery, or medical regulating devices. Medications are typically used reduce the occlusion of arteries through reducing plaque buildup, preventing blood clotting, and reducing blood pressure.

While these medications can be preventative of further heart conditions, they frequently cannot prevent blockage in the arteries. The resulting MI is treated with reperfusion immediately after the event. Regaining blood flow in the damaged area of the heart is the primary goal in an effort to prevent further cell death. The reperfusion can be accomplished through thrombolytic therapy in which the blockage is broken up. Fibrinolysis is a technique for this and breaks up the fibrin in the blood clot to encourage blood flow back to the heart. Additionally, the use of stents and balloon angioplasty are useful in opening blocked arteries allowing for reperfusion. The degree of invasiveness of the procedures will depend on the severity of the case and the degree of MI up until that point. Other pharmaceutical treatments, such as anticoagulants and platelet inhibitors, can be used after the event in an effort to prevent another MI event [12, 14].

As previously stated, heart failure cannot be reversed, but the symptoms can be treated, and treatment can slow progression. Initially, heart failure can be treated similarly to MI through medications and lifestyle changes. However, after further progression of the disease, the heart may need more assistance to properly function. In order to overcome the damaged tissue's inability to properly pump, left ventricular assist devices (LVADs) are a treatment method which are surgically implanted and serve as an artificial pump to aid the ventricle in pumping blood. Both LVADs and pacemakers can be used throughout the patient's life span, however, advancements in blood compatibility, more compact devices, and less invasive surgeries can improve overall efficiency of treatment and quality of life [15].

While all these treatments offer a variety of benefits and potential problems, they are all only palliative solutions. There are no current treatments that allow a person to regain 100% of their heart function or enable muscle regeneration following injury to the cardiac cells. Because of this, there is a major need for treatments that can encourage total regeneration or mimic heart function of native host tissue.

2.3 Engineering of Functional Myocardium

The emergence of tissue engineering and biomaterials research fields over the past few decades present an opportunity to address the shortcomings of the current standard-of-care for cardiovascular disease. Myocardial tissue engineering aims to repair or regenerate sections of the heart damaged by MI [4]. Researchers seek tissue-engineered solutions that can mimic the properties of native myocardium such that they will restore the heart to a healthy level of function. Early approaches involved injecting cells, a biomaterial, or both into the heart. Left ventricular restraints, which involve wrapping the ventricle with a biopolymer, have also been explored, but do not regenerate or repair the tissue. Development of engineered heart tissue involves combining a biomaterial with cells to form a matrix and has shown promise as a regenerative solution. Though some research exists in this area, work remains to be done to select the best biomaterial scaffold and cell type as well as improve the contractile and mechanical properties of the engineered tissue. Some authors conceptualize heart disease as a reduction in biomaterial performance, where the biomaterial is the heart tissue. The structure and properties of biomaterials are known to drive their performance [16]. When engineering myocardium, the material properties, contractility, and structure of native heart tissue must be considered if the performance of this biomaterial is to be sufficient for replacing damaged myocardium *in vivo*. Human myocardium experiences a variety of loading conditions during the cardiac cycle, including tension, compression, and shear, and has a nonlinear, anisotropic response. This material behavior is an important parameter when designing the composition of engineered heart tissue, though the challenge remains that it is not yet fully characterized [17]. At the current progression of research, there are a few functional properties that an engineered myocardial construct should have to be clinically viable for the replacement of heart tissue diseased by MI. These properties are key for ensuring that the engineered tissue mechanically and electrically approximates native tissue. Table 1 below lists these properties.

Table 1. Ideal functional properties of engineered myocardium [18]

Functional Property	Specification
Construct Thickness	Roughly 1 cm
Contractile Force Produced	20-50 mN/mm ²
Electrical Conduction Velocity	25 cm/s
Cell Type	Autologous cardiomyocytes

2.3.1 Cardiomyocyte Function

Understanding the growth, differentiation, and morphological structure of cardiomyocytes is critical when engineering cardiac tissue. From the cellular level, cardiomyocytes are muscle cells that in unison form the wall of the heart, the myocardium. These cells are responsible for producing contractile forces, which facilitate the pumping of blood into and out of the heart. If contraction is hindered or not properly functioning, certain areas of the myocardium will not receive adequate blood perfusion spurring cell death. This becomes especially problematic since adult cardiomyocytes have low proliferation capabilities meaning that the damaged cardiomyocytes cannot easily regenerate new, healthy cells.

There are challenges associated with culturing cardiomyocytes for regenerative purposes, notably that low proliferation rates after animal birth and cell isolation requires disruption of the gap junctions that control movement of molecules [19]. Gap junctions allow the transmission of action potentials from myocyte to myocyte, therefore allowing the simultaneous contraction of the cardiac cells. If these junctions are inhibited, the result is disruption or inadequate contraction of the tissue as a whole.

The culturing of neonatal cardiomyocytes has proven to be more successful. The benefit of culturing neonatal cardiomyocytes is that cells can be easily separated from one another during cell isolation, contraction of the cells is possible with stimulation, and the morphological

changes of these cells allows for visualization and detection of intracellular signaling pathways [20].

To produce an engineered cardiac patch, cardiomyocytes must be obtained and grown. The incorporation of human embryonic or pluripotent stem cells are often used in cardiac patches because of their biocompatibility and regenerative capabilities [21]. Human embryonic stem cells derived from 3-5 day old embryos, can grow and differentiate into any type of cell in the body. Similarly, induced pluripotent stem cells (iPSCs) are cells obtained from the skin or blood that are engineered to act as cells that can differentiate into another cell type [21]. The multifunctionality of these stem cells allows them to be ideal platforms for engineered cardiac tissue due to their diverse differentiation capabilities. In comparison to neonatal cardiomyocytes, cardiomyocyte derived-iPSCs produce multinucleated cardiomyocytes and express specific biomarkers indicating proliferation. Engineered cardiac tissue using iPSCs have shown promising therapeutic results in regenerating injured heart tissue, though further work remains to fully understand their suitability for this application [21]

2.3.2 Scaffolds and Engineered Cardiac Tissue

Current treatments for heart disease are limited in that they treat the symptoms rather than the underlying disease. Research has made strides in the development of tissue engineered constructs as a therapeutic platform for treating heart disease. The concept follows from the inception of tissue-engineered cardiomyoplasty in the early 2000s, which transplanted engineered myocardium or cell sheets onto diseased cardiac tissue to assist in restoration of function [5, 22]. Other early approaches involved injecting cells intended to modulate the immune response in diseased regions and recruit endogenous cells [3]. Both methods fall short in that they are limited by the effects of the diseased extracellular matrix (ECM), which has abnormal biochemical components and mechanical properties that compromise the potential regenerative effects of cell-only therapies [3].

Effective biomaterial scaffolds can negate the effects of diseased ECM on regenerative solutions by creating a new microenvironment that replicates the properties of healthy ECM. They can also be designed to send signals that promote tissue repair and regeneration [3]. Natural and synthetic biomaterials have both been used in scaffold design. Naturally derived materials such as animal-derived collagen and fibrin contain cell adhesion ligands and promote cell

infiltration and remodeling. Decellularized ECM scaffolds derived from animals have been used extensively in surgical applications and have the advantage of more closely approximating the native ECM. Preclinical studies using existing products approved by the U.S. Food and Drug Administration as 510(k) medical devices have shown some promise and continue to be an avenue for investigation. Cell-generated decellularized ECM strategies are also being explored, where cells seeded onto a synthetic scaffold secrete a new ECM as the synthetic scaffold degrades, leaving a matrix-only graft after decellularization. Synthetic scaffolds can be modified with peptides to promote cell infiltration and are designed to modulate host response and encourage endogenous repair by controlling scaffold geometry, degradation rate, and pore size [3]. Biomaterial scaffolds can also help engineered cardiac tissue mimic the highly-aligned structure of native myocardium. Suspending myocytes in hydrogels, water-absorbing 3D polymer networks typically derived from fibrin, collagen I, or Matrigel, allows for the application of geometric constraints governing cell alignment and control over the mechanical properties of the construct [6-8].

In vivo cardiac tissue is comprised of cardiomyocytes and other cell types such as fibroblasts, smooth muscle cells, endothelial cells, macrophages, and other leukocytes, leading Zimmerman et al. to conclude that the optimal engineered heart tissue (EHT) construct should be comprised of a biomimetic mixture of non-myocytes and cardiomyocytes. In fact, their research showed that EHTs reconstituted from unpurified heart cell mixtures had a more complex tissue structure and improved force output when compared to EHTs derived from partially purified cardiomyocyte populations. EHTs constituted in this way will contain a well-organized, continuous surface covered with epithelium as well as capillary-like structures penetrating the cardiomyocyte-gel matrix [6]. Bursac and colleagues noted similar ingrowth of blood-perfused vasculature in their tissue-engineered skeletal muscle constructs upon implantation in rats, as well as strong self-regeneration and myogenesis. Similar to Zimmerman's work, these skeletal muscle constructs contained non-myocytes such as fibroblasts and other endothelial cells [23].

Engineered heart tissue has been formed into ring, patch, and pouch-shaped assemblies and grafted onto the hearts of rats. Implantation studies showed their usefulness as assistive grafts, but a number of issues require further investigation, including the understanding of electric coupling with native tissue, identification of a scalable cardiomyocyte source, achieving

muscle tissue dimensions that can support large failing ventricles, and addressing safety concerns [5, 24].

In order to replicate *in vivo* conditions for cardiomyocytes, substrates with varying stiffnesses have been investigated with the goal of producing a scaffold with stiffness similar to that of human heart tissue. The stiffness of native adult human heart tissue ranges from 10 to 500 kPa [9, 18, 25]. Researchers conducted experiments testing the elastic moduli of polyacrylamide gel ranging from 1-25 kPa with mature cardiomyocytes for over one week [26]. It was concluded that contractility of the neonatal rat ventricular myocytes varies with substrate stiffness. Other authors have noted that cardiomyocytes and cardiac fibroblasts generate *in-vivo* contractile force when grown on substrates that match the stiffness of native heart tissue [18]. As the elastic modulus of the substrate increases, cardiomyocyte excitability decreases (when subjected to electrical stimulation). Inversely, with the addition of substrate microposts, calcium channels and sarcomeric organization increased. Sarcomeric organization could be visually observed and analyzed through staining of Rho kinase pathways, integrins, vinculin, and other structural proteins [26].

2.3.3 Cardiac Patches

A cardiac patch is a more focused derivative of the engineered scaffold-cardiomyocyte assembly, with the end goal being integration of the patch with healthy myocardium to replace tissue damaged by MI. In a 2013 review of tissue engineering for heart repair, Radisic and Christman outline the properties of an ideal cardiac patch: a cardiac patch will have a clinically relevant thickness (roughly 1 cm), produce active contractile force on the order of that developed by native tissue (20-50 mN/mm²), propagate electrical impulses (conduction velocity of 25 cm/s), and consist of autologous cardiomyocytes that minimize immune response upon implantation [18]. Current cardiac patch research builds upon existing studies demonstrating the assistive capability of engineered heart tissue [24] and establishing key design parameters including substrate stiffness and cellular composition in order to develop a construct suitable for human implantation [26].

Chrobak *et al.* demonstrated that the stiffness of fibrin hydrogels used in cardiac patch design can be modulated through the incorporation of composite layers of fibrin microthreads

[9]. Fibrin hydrogels alone are mechanically weak and have low stiffness (roughly 0.25 kPa) relative to native heart tissue, but the authors note that incorporation of fibrin microthreads at a 22% volume fraction into a fibrin cardiac patch seeded with neonatal rat cardiomyocytes increased the tensile modulus of the scaffold to a mean of 97.5 kPa, within the mid-range of stiffnesses exhibited by native human myocardium [9]. This addresses two key design parameters of a clinically applicable cardiac patch: (1) it must have similar passive mechanical properties to native myocardium in order to withstand the *in vivo* loading environment, and (2) having a scaffold stiffness similar to that of native myocardium has been shown to result in expression of an *in vivo* phenotype and high active contractile force production (noted in Section 2.3.2). The authors also note increased cell alignment in regions within 100 μm of a fibrin microthread, and hypothesized that static mechanical tension could be used in the future to further improve cell alignment [9]. In terms of active contractile force, however, no significant difference was found between the composite fibrin patch and fibrin gel control. Cell-seeded fibrin hydrogels demonstrate contractile twitch forces of roughly 8 mN/mm^2 [9], so work remains to be done to reach the 20-50 mN/mm^2 contractile force suggested by Radisic and Christman. Similarly, Zhang *et al.* developed a cardiac patch utilizing human embryonic stem cell-derived cardiomyocytes (hESC-CMs) aligned using passive tension and reported average contractile forces of 11.8 mN/mm^2 .

Cellular composition of cardiac patches has been an important area of research. Early development of cardiac tissue constructs utilized purified cardiomyocytes even though adult cardiac muscle is composed of many cell types, including cardiomyocytes, fibroblasts, and endothelial cells. These pure cardiomyocyte constructs failed to adequately recreate a healthy microenvironment for regeneration and growth, driving the introduction of fibroblasts and endothelial cells into 3D constructs. It is now well known that this biomimetic composition of cell types is critical for optimum functioning of engineered heart tissue and improved survival on *in vivo* implantation [18]. However, while fibroblasts can be obtained through autologous biopsy [27], finding a renewable, autologous source of cardiomyocytes is more challenging.

Mesenchymal stem cells have been investigated as a potential cardiomyocyte source and can express cardiac markers, but their ability to develop active force during contraction or exhibit ventricular action potentials is an area of controversy [18]. Pluripotent cell types have

gained traction as of late for their ability to be transformed into a variety of cell types including cardiomyocytes. Pluripotent-cell derived cardiomyocytes generated through spontaneous or directed differentiation are considered immature, despite authors who have noted improved maturity of young cardiomyocytes seeded onto cardiac patches when compared to 2D monolayer culture [18]. Embryonic stem cells (ESCs) specifically have been successfully implemented into a cardiac patch. The fibrin cardiac patch developed by Zhang *et al.* demonstrated high hESC-CM maturity after 2 weeks of 3D patch culture evidenced by conduction velocities of 25.1 cm/s in 90% hESC-CM patches, strong contractile forces as noted previously, longer sarcomeres, and enhanced expression of genes involved in contractile function when compared to 2D monolayers [28]. Cardiac patches based on induced pluripotent stem cell-derived cardiomyocytes (iPSC-CMs) have also been implemented in cardiac patches and implanted in rodent models [18]. iPSC-CMs have an advantage over hESC-CMs in human applications because they are not derived from an embryonic source and thus generate fewer ethical questions.

Additionally, scaffold design remains an important parameter to consider. Recent work found that using fibrin patches as the cardiomyocyte carrier improved the paracrine activity of the engineered tissue. These paracrine improvements drove increases in vascular density at the border zone of infarction sites and regeneration of myocytes from endogenous cardiac progenitor cells, both indications of the therapeutic potential of cardiac patch technology [5].

One of the biggest drawbacks of current cardiac patches is its limited ability to accurately mimic the mechanical and electrical properties of the heart. As such, the contractile function of a cardiac patch must be considered when under development. The contractile function of a patch may also be associated with and affected by the alignment of cells and growth environment to which it is subjected to [29].

Aside from the mechanical and electrical properties, cardiac patches must also meet challenges relating to their overall thickness. The underlying problem that prevents patch thickness development stems from limited oxygen perfusion as a cell is grown [29]. The constraint of thickness to patches limits the vascular supply that may be integrated when implanted. Another drawback of cardiac patch development includes difficulties pertaining to imaging. While there have been many advancements in molecular imaging, the implication of these technologies can be quite difficult when monitoring cell fate and differentiation [29]. Aside

from the growth factors and functionality of cardiac patches, another consideration and drawback is their means of implantation. Integration can be accomplished through suturing the patch, however, this method is highly invasive and can damage the heart tissue further [29]. For the future, researchers aim to create a suture-free patch using thermal energy to strongly adhere the patch to the heart wall [30].

Cardiac patch testing is based on a series of different techniques and methods that are used to qualify the patch as a potential candidate for implantation. One method of analyzing cell count and thickness is through staining of cells. In addition to this, cell imaging is done to visualize the morphological changes of the cells. By staining and imaging the cells, cell infiltration and alignment can also be accessed within the scaffold. Different methods of analysis are currently being developed to properly assess mechanical properties and anisotropy. These methods can also be used to measure its overall elasticity, which is especially important because as age increases, the elasticity of cardiac muscle decreases making it stiffer and thicker. Computational models can also predict implant behavior as well as fatigue properties and conditioning for cell growth. Patch testing before *in vivo* implantation is in the clinical stage of experimentation [5].

2.4 Mechanical Stimulation

Mechanical forces are known to play an important role in *in vivo* myocardial morphogenesis and maturation [31, 32]. Starting with the formation of the cardiac tube during embryonic development, various loading modalities including contraction, cylindrical bending, and fluid shear influence the morphogenesis and remodeling of the heart [32, 33]. These stimuli are critical for the growth and development of mature heart cells; as such, researchers have sought ways to replicate biologically relevant mechanical stressors *in vitro*, which could potentially allow for the creation of myocardium structures in the lab that are sufficiently functional to repair or replace damaged native tissue.

Numerous researchers have investigated the role that mechanical stimulation may play in the functional maturation of cardiomyocytes. These studies examine the effect of different mechanical stimulation parameters including loading modality, frequency of stimulation, and duration. Histological comparison and changes in gene expression are commonly used to evaluate the effectiveness of the loading protocol.

Early investigation of the effect of mechanical loading on immature cardiomyocytes was published by Vandenberg et al., who grew neonatal rat cardiomyocytes on elastic substratum in the wells of mechanical cell stimulators driven by stepper motors. One group of cells was exposed to stretch applied from the bottom of the well, while another experienced uniform horizontal stretch. The authors were concerned with substratum detachment and/or damage in response to stretch. *In vivo* cardiomyocytes must be capable of withstanding repeated mechanical loading for a lifetime as well as spikes in loading intensity caused by changes in beating frequency, blood pressure, and blood volume [34]. They thus hypothesized that their neonatal cells are elastic enough to withstand a total stretch of 180% at a constant strain rate of 15% per minute. Measuring release of soluble creatine kinase, a marker of cell membrane damage, the authors found that even extreme stretches of 180% caused a relatively small amount of creatine kinase to be released. They note that similar mechanical loading patterns caused severe detachment and membrane damage in differentiated skeletal myofibers and adult rat cardiomyocytes, concluding that neonatal cardiomyocytes are uniquely elastic to be capable of handling extreme loads. Additionally, they noted that this loading modality (unidirectional stretch of the substratum without rest) caused the cardiomyocytes to form parallel arrays of rod-shaped cells morphologically similar to the *in vivo* heart [35]. When the neonatal cardiomyocytes were subjected to cyclic stretch of 10-15% for multiple days, the cells aligned perpendicular to the direction of substratum stretch, rather than parallel as was the case in the constant-increase stretch. They conclude that neonatal cardiomyocytes can withstand substantial mechanical stress without accumulating damage and will align depending on the loading pattern.

Nguyen et al. developed a microfluidic cardiac cell culture model (CCCM) that exposed embryonic chick cardiomyocytes to a biomimetic mechanical environment including cyclic fluid flow, heart chamber pressure, and passive tensile stretch. The goal of their experiment was to characterize the cellular response of immature cardiomyocytes to these mechanical stimuli. Their mechanical stimulation regime lasted 4 days and consisted of an 8-15% passive stretch and 10 mmHg pressure applied at 2 Hz, and a fluid volumetric flow rate of 44 μ L/cycle. They examined gene expression and protein synthesis pertaining to calcium regulating proteins, specifically sarcoplasmic reticulum calcium ATPase2a, (SERCA2), phospholamban (PLB), troponin T (TnT), and alpha and beta myosin heavy chain (MHC). They compared both 2D culture and 3D cell constructs exposed to the CCCM stimuli with controls cultured in a static condition, finding

that alpha-MHC, beta-MHC, and PLB increased in 3D constructs exposed to the mechanical loading. They also found that SERCA2a protein synthesis increased in stimulated 2D cultures, though gene expression was similar. The authors note that despite the increased activity of regulatory proteins, biological thyroid hormonal signals may be necessary to fully mature cardiomyocytes in engineered tissues, and true measurement of the ability of immature cardiomyocytes to aid in cardiac repair requires *in vivo* functional analysis study [33].

Although the investigation of biochemical responses to mechanical loading can yield strong indications of cell maturation and growth as noted previously, histological examination of myocyte structural and organizational is essential for understanding the corresponding physical response downstream of gene regulation and protein production. One study showed longitudinal cell alignment mimetic of the neonatal heart, elongation of the cells and nuclei, distinct myofilaments, and improved collagen and sarcomere organization in 3D embryonic stem cell derived structures subjected to 3 Hz cyclic stretch. These physical changes accompanied upregulation in expression of α -cardiac actin, α -skeletal actin, and α -MHC, genes encoding proteins essential to muscle structure and function, and GATA4, a gene essential for embryonic cardiac development. However, these changes were not found in constructs exposed to either 1 Hz or 2 Hz cyclic loading, leading the authors to conclude that the response of cardiomyocytes to mechanical stress is frequency-dependent [36]. Zimmerman et al. showed similar structural improvements after cyclic mechanical stretch in neonatal rat cardiomyocytes. Mechanical stimulation of cardiomyocytes cultured as 3D rings yielded constructs that were similar to native adult heart tissue, having highly organized sarcomeres, adherens junctions, gap junctions, and desmosomes, an extracellular basement membrane, and mature intracellular features including T-tubules and densely packed mitochondria and myofibrils [37].

Following work to establish a renewable cell source for engineered heart tissue, mechanical stimulation of constructs seeded with pluripotent stem cell-derived cardiomyocytes has been conducted. Ruan et al. demonstrated that 4% stretch increments up to 125% total stretch improved the passive tensile stiffness, contractility, and increased the expression of calcium-handling proteins in 3D collagen-based constructs seeded with iPSC-CMs [38]. Similarly, Shimko and Claycomb showed longitudinal cell alignment and sarcomeric banding in ring-shaped collagen constructs seeded with murine ESC-CMs stretched cyclically at 3 Hz to 10% stretch. They note that constructs stretched at 1 and 2 Hz had no effect on the expression of

genes such as GATA4 that drive cardiomyocyte morphogenesis; in fact, the 1 Hz group showed downregulation of GATA4 and consequently alpha-MHC, both of which have been discussed previously as key drivers of maturation and morphogenesis in cardiomyocytes. The authors postulate that this occurred because 1 and 2 Hz is far from the native beating frequency of the murine ESC-CMs, a suggestion with important implications for selecting cyclic frequency in future mechanical stimulation studies [39].

More recently, mechanical loading has been used as a method of improving the functional properties of cardiac patches. Lux et al. used a 1 Hz, 5% uniaxial stretch to stimulate neonatal rat cardiomyocytes seeded in decellularized porcine small intestinal submucosa. These cardiac patches measured roughly 11 cm² and were stimulated for 48 hours. The authors note that mechanical stimulation significantly improved the alignment of cardiomyocytes in the direction of stretch and expression of endothelial genetic markers. They also suggest that their application of 5% stretch when compared to other authors who used 10 or 15% may prevent overstretching of cardiac sarcomeres, which may experience impairment of active force generation when exposed to extra-physiological loads. Like some studies already discussed, the authors found increased expression of alpha-MHC and GATA4. They also found corresponding hypertrophy, noting enlarged cell bodies in stimulated samples [40].

The effect of shear flow on developing myocardium is not as well-researched as that of tensile stretch but may be important as part of a biomimetic growth environment. Hypothesizing that pulsatile flow would result in improved tissue assembly via mechanical conditioning and greater mass transport, Brown et al. created a bioreactor that perfused neonatal rat cardiomyocyte patches with 1.50 mL/min or 0.32 mL/min of culture medium at 1 Hz. They found that the high flow rate condition resulted in a decreased excitation voltage and higher contraction force, while the low flow rate group exhibited hypertrophy with the highest cell length and diameter compared to all experimental and control groups [39]. Other studies have found stimulation via shear flow to upregulate gene expression of some markers involved in cardiac myogenesis [31, 35].

As of 2016, engineered cardiomyocyte constructs are reported to be capable of generating contractile stresses on the order of 5 kPa following different mechanical stimulation regimens. Though promising, these tissues fall short of native human heart tissue, which can develop contractile stresses of between 15 and 30 kPa [32, 37]. Despite having many hallmarks of native

myocardium, various engineered tissue constructs lack some components of mature tissue (i.e. sarcomeric M-bands), have smaller myotube diameter, or may not be capable of contracting [36, 37]. Though it is well understood that cyclic mechanical stretch and dynamic shear flow result in cardiomyocyte hypertrophy, the optimal intensity and duration of these stimuli for producing near-mature cardiomyocyte constructs is unclear. A summary of mechanical stimulation parameters can be seen below in Table 2.

Table 2. Summary of mechanical stimulation parameters

Authors	Parameters being Measured	Cell Type, Scaffold Type	Mechanical Stimulation	Duration of Stimulation	Findings
Vandenburgh et al., 1995	Cell membrane damage, delamination from substratum, cell organization	Neonatal rat CMs grown on silicone rubber	180% total stretch at 15%/min; 10-15% cyclic stretch	Started 1 day post-plating, ends after 180% total stretch	Neonatal cardiomyocytes are highly elastic and withstand extreme stretch; cyclic stretch caused cell alignment in the direction of stretch
Nguyen et al., 2015	Expression of calcium-regulating genes	Embryonic chick CMs seeded on a cross-linked collagen matrix or 2D culture	8-15% passive stretch; 10mmHg cyclic pressure at 2 Hz; cyclic fluid flow at 44 uL/cycle	4 days	Increased activity of regulatory proteins in 3D constructs
Shimko & Claycomb, 2008	Cell construct structure and organization; gene expression	Murine ESC-CMs in ECM scaffold	10% cyclic stretch at 1 Hz, 2 Hz, or 3 Hz	3 days	Longitudinal cell alignment, distinct myofilaments, improved sarcomere organization in the 3 Hz group; gene upregulation in 3 Hz group, downregulation at 1 Hz
Brown et al. 2008	Cell morphology	Neonatal rat CM patches	Perfusion at 1.50mL/min or 0.32mL/min at 1 Hz		High flow rate condition - decreased excitation voltage, higher contraction force; Low flow rate condition cell hypertrophy
Leong, Bursac, Liu, & Liao (2008)	Myotube diameter, genetic markers, elasticity	Skeletal myoblasts on aligned electrospun fibers	5-10% cyclic stretch, 1Hz, Various active/rest periods	1hr on/5hr rest, at least 14 days	Mean myotube diameter increased by 12%, signs of overstretching by day 14

Vandenburgh, Mills, Smiley, & Powell (2002)	Myotube diameter, myofiber area percent	Human bioartificial muscles (HBAMs)	5-15% cyclic stretch	8 days	Improve myotube diameter by 12%, improved myotube area percent by 40%
Lux et al. (2016)	Cell alignment, peak shortening, gene expression	Neonatal rat cardiomyocyte patch	5% cyclic stretch	48 h	Improved cell alignment, gene upregulation, cell hypertrophy
Ruan et al. (2016)	Cell alignment, contractility, hypertrophy, stiffness	Human induced pluripotent stem cell-derived cardiomyocytes	4% stretch increments up to 125% total	30-second intervals, 2 weeks total	Improved passive stiffness, contractility, expression of calcium-handling proteins

Rangarajan, Madden, and Bursac summarize this body of work well, stating that any change in the mechanical stress experienced by striated muscle cells will result in cell elongation and/or cell thickening via sarcomere addition, or apoptosis. Cardiomyocytes specifically are sensitive to the type of overload, pressure, or volume applied. Though not all mechanical stimulation regimes have a positive effect on engineered heart tissue, it has often been found to yield cell growth and/or hypertrophy [41]. A larger muscle generally develops greater forces, so in light of this body of work, mechanical stimulation represents a promising pathway for improving the contractile forces developed by engineered cardiac patches.

2.5 Electrical Stimulation

In order to fully understand the functionality of artificial cardiac constructs and tissues, it is important for the tissues to undergo stimulation that mimics a cardiac environment. The heart experiences significant electrical signaling in order to maintain a sinusoidal rhythm. These signals are activated by the ion exchange that occurs between the cells internal and external spaces. The exchange of ions only occurs in the presence of an electrical voltage. The signals then travel to the rest of the heart across the gap junctions resulting in muscle contraction. Providing tissue construct with this type of stimulation, allows for the tissues to develop in a biomimetic environment, and helps researchers understand how the tissues could couple with living heart tissue. The goal of this stimulation is to condition the cells to allow for coupling and integration into living heart tissue in order to repair damaged heart disease and other conditions [42].

2.5.1 Various Mechanisms for Electrical Field Stimulation

Electrical pacing or stimulation via an electrical field is a common approach to electrical stimulation. Stevens et al. performed an experiment utilizing square electrical waves to stimulate the contraction of human pluripotent stem cell generated patches. These waves were administered onto a six well plate via carbon electrodes. A constant 6V stimulus was administered at a frequency that ranged from 0.5 to 5Hz. It was found that the patches could only contract successfully at frequencies under 2Hz, which can be explained by native human heart conditions that operate at a frequency that ranges from 1-1.7Hz [43, 44]. Frequencies above this threshold did not allow for sufficient cardiomyocyte relaxation, which negatively affected the effectiveness of the contractions [43].

Field stimulation can also be performed with the assistance of the appropriate media. An experiment from Gerbin et al. utilized a Matrigel hydrogel coating to facilitate electric wave delivery. This gel, an extracellular matrix product, provides an *in vivo* mimetic environment for the cells during stimulation [45]. The coated cells were stimulated via a C-Pace Culture Stimulator, which produces electrical pulsation through carbon electrodes on a time controlled delivery [46]. This specific experiment occurred over a period of six weeks and found that the grafts could couple with or match the electrical pulsing of the heart tissue [47]. Similarly, Rupert et al. examined the effect of electromechanical stimulation delivered via platinum electrodes to engineered cells in an isotonic bath of Tyrodes solution [48].

Field stimulation is also possible for long term experiments of more than one week. Ruan et al. also used a C-Pace stimulator, to deliver 5V to cells that were simultaneously undergoing mechanical stimulation for one week [49]. In a study performed by Hirt et al. an electrode stimulation assembly was built using two stainless steel support bars attached to pairs of carbon electrodes. This assembly was placed into the well plates (two electrodes per plate), which contained the tissues and buffer solution. Pacing units were used in conjunction with the electrode assembly, one of which could stimulate four different tissues at the same time. One of the main concerns about electrode and buffer interaction is toxicity; however, that was remediated through short pulses, spaced electrodes, and proper cleaning procedures. 2V was delivered to the electrodes via a Grass S88X stimulator. They found that after 3-4 weeks, a field

strength of 2 V/cm the cells were paced and chronic pacing at lower frequencies induced higher contractile forces [50].

2.5.2 Bioreactor Stimulation

Electrode induced fields, as previously stated, are a popular method of stimulation. In addition to this, researchers have investigated the effects of bioreactor housed stimulation as studied by Barash et al. This study in contrast to those previously mentioned did not group electrical and mechanical stimulation, but instead aimed to integrate electrical stimulation into a perfusion bioreactor. The goal of this bioreactor was to provide all the cells access to the buffer and continuously supply oxygen to the tissue. In doing so, they developed a system that housed a custom electrical stimulation setup consisting of two carbon electrodes that fit into the bioreactor via the tissue fixation points. Carbon electrodes were used due to their high corrosion resistance. The electrical stimulation was altered through a design system which controlled period, time, positive and negative impulse duration, and amplitudes. The cells were first cultured in a petri dish while undergoing 5V of electrical stimulation at 1Hz. The tissue was then moved to the bioreactor to undergo stimulation. A simulation model was generated for this purpose which determined that all cells between the electrodes would experience a 1V uniform field while those on the lateral side of the electrode would not experience stimulation. The team evaluated the effectiveness of the stimulation by measuring changes in cell length and presence of the gap junction protein, Cx-43 via immuno-staining [51].

According to a review done by Massai et al. there are various mechanisms to electrically stimulate cells in a bioreactor. Rectangular or square-wave electrical pulses at a variety of durations, voltages and frequencies are common. According to this study, the voltages can range from 0.1V to 40V. Frequencies varied from 0.2-3Hz to mimic resting heart rate range of 60-100 beats per minute which is equivalent to 1-1.7Hz. The duration of pulses varied from 1 to 10 ms which is also appropriate as the heart stimulation occurs every 1-2ms [44].

In order to better visualize and summarize the state of the art in electrical cell stimulation, Table 3 can be seen below.

Table 3. Summary of electrical stimulation experiments

Authors	Parameters being Measured	Cell Type, Scaffold Type	Electrical Stimulation	Duration of Stimulation	Findings
Stevens et al. 2009	Contraction via contractile amplitude	Human embryonic stem cell patch	Square wave field stimulation 0.5-5Hz	Not reported	Optimal pacing frequency is around 2Hz
Gerbin et al. 2015	Electrical integration and coupling of graft into functional myocardium	Tissue construct of human embryonic stem cells	In vivo- electrode insertion 1-6.5Hz in vitro- matrigel coating paired with field stimulation at 1 and 6 Hz, 5V/cm and 4ms	2- 6 weeks	Grafts coupled with the host tissue in vivo and in vitro most cells could not be stimulated for longer than 4 weeks
Shiba et al. 2012	Electrical coupling with host tissue	Human embryonic stem cell derived cardiomyocytes in vivo	Programmed electrical stimulation (STG-1000) via bipolar electrode insertion into cardiac apex 0-150ms	2-4 weeks (after implantation)	Grafts helps alleviate arrhythmias but were not completely coupled with the host
Hirt et al. 2014	Cell morphology	Rat and human engineered tissue	2V biphasic pulses at 0.5 -2Hz and 4ms carbon electrodes on a stainless steel assembly	3-4 days	Cell organization and contractile force increased in the human generated tissue

2.6 Monitoring Physiological Changes due to Stimulation

In order to understand the effectiveness of electrical and/or mechanical stimulation, it is important to have a monitoring system. Video edge monitoring such as SoftEdge Acquisition from IonOptix is able to detect and image the circumferential edge of a cell. This technique, when used in conjunction with electrical stimulation, allows the user to detect changes in cell morphology [43]. One study used video imaging through an inverted microscope via a high speed camera. Contractions were then visually monitored through usage of a from this using a specific algorithm [52]. Alternatively, cell activity was recorded on a Basler camera mounted on the clear roof of the incubator and light was shown through the bottom of the well plates in order to help image the cells. The contractility of the cells was monitored using a custom software

which examines the length of the tissue and cells over time [52]. Electrocardiogram (ECG), normally used to track the electrical activity of the heart during beating, has been used to analyze how a graft of engineered cells interacted with the surrounding tissue. In this *in vivo* study, the activity of the graft was monitored using GcaMP3 fluorescent tracing the results of which were compared to the ECG of the heart. This data was used to evaluate how well the graft coupled with the surrounding tissue [53]. Mechanical and electrical stimulation are often performed simultaneously to better mimic a physiological environment; therefore, force transducers are utilized to track contractile changes due to mechanical and electrical stimulation in the cells. Therefore, in one study, researchers utilized a force transducer to track the contractile forces of the cells. This transducer was able to provide feedback on for both the electrical and the mechanical stimulation [47].

2.7 Review of Commercial Devices

The growth of the tissue engineering field and need to mechanically stimulate engineered tissues to improve their functional properties has driven the creation of several commercial devices that can apply different types of loads to cell constructs. Devices exist that expose engineered tissues to uniaxial and biaxial tension, compression, shear, and/or perfusion. Some systems are mountable on microscope stages for visualization during experiments.

2.7.1 Flexcell FX-6000 Tension System

The Flexcell FX-6000 tension system is a self-contained and computer-controlled bioreactor that utilizes vacuum and positive air pressure to apply strains to cells or cell constructs. It contains four 6-well plates with flexible bottoms that can deform a substrate up to 33%. Figure 1 below shows the system as well as how it works.

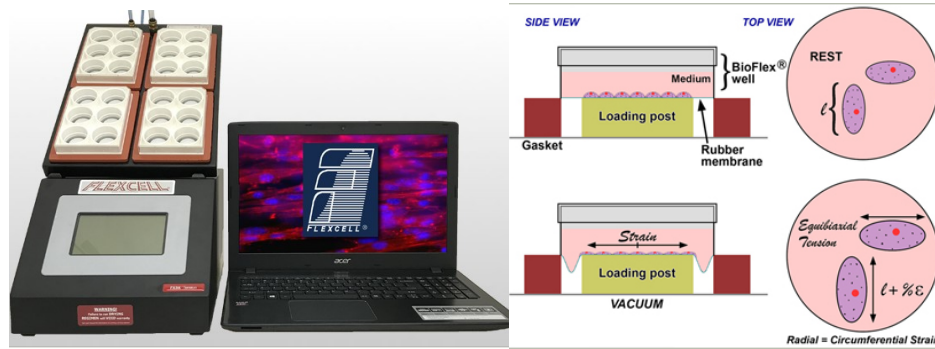


Figure 1. Flexcell FX-6000

Application of vacuum pressure to a circular cross-section produces equally biaxial strain in cell constructs, loading them in both planar directions. Flexcell advertises that this system mimics *in vivo* conditions in cells from muscle, lung, heart, vasculature, skin, tendon, ligament, cartilage, and bone. It is also compatible with other Flexcell culture plates, which allows for the system to apply uniaxial or gradient tension in addition to equibiaxial strain [54].

2.7.2 Ion Optix C-Stretch 100

Ion Optix has developed a machine that can both mechanically and electrically stimulate cells at the same time. The device utilizes a specialized electrode equipped plate to supply electrical stimulation. These electrodes are plated over 6 individually aligned silicone based plates. Each plate is anchored with pins on all four sides. One end of the plate remains stationary while the other is driven by a stepper motor to provide stretch in a uniaxial direction. The device lays within a plastic box to maintain sterility and can be placed in a standard cell culture incubator for the length of an experiment. This system is compatible with the current C-Pace EM device designed by Ion Optix in order to provide electrical stimulation. The device can achieve frequencies up to 10 Hz, strains up to 20% and voltages between $\pm 40V$ [55].



Figure 2. Ion Optix C-Stretch

2.7.3 CellScale Biomaterials Testing Various “Mechanoculture” Products

CellScale currently has four devices on the market that aim to mechanically deform cells or tissue constructs. Each device focuses on a different aspect of *in vitro* mechanical stimulation. The MCB1 focuses on stretching 3D constructs or scaffolds in a biaxial direction. A “snowflake” contains pins arranged in a circle, which the tissue rests on. The snowflake is actuated to pull the tissue outward radially. It can stretch the tissue up to 20% and the experiment can be customized for the user. The MCTR device is used to apply uniform compression onto eight materials and constructs. The device consists of a pressure chamber which exerts a pressure on the well which are filled with liquid and capped with a membrane. The presence of the liquid ensures that the compression is transferred to the material. Results attained through this testing can also be monitored in real time. The MCFX device put out by CellScale is designed to uniaxially stretch cells that have adhered to the bottom of the device’s silicone well plate. The plate contains 16 square wells. Four pin holes are located on the silicone surrounding the wells. The pin holes lie at the four corners of the well, and during stimulation, two pins remain stationary, while two pins move longitudinally. The system can be placed in a standard incubator and is optically clear for easy imaging. Finally, the MCT6 can be used to uniaxially stretch tissue construct, hydrogels, scaffolds and other larger biomaterials. This device is for larger tissues and can hold specimens 10mmX80mm. The MCT6 clamps the tissue at one end and is screw driven to produce longitudinal loading. The compartment holding the tissues can also hold large amounts of media and is sustainable in a standard laboratory incubator [56].

2.8 Need for Engineered Cardiac Patches

Prior research has found mechanical and electrical stimulation to be promising methods of preconditioning engineered heart tissue to more accurately emulate the properties of the heart. In nature, the heart is subjected to constant mechanical strain as well as electrical impulses. While current cardiac patch technology has improved upon prior engineered tissues by being more easily integrated into native tissue, they still fall short of true cardiac tissue in terms of contractile function and tissue thickness. The goal therefore is to design a system to mechanically condition cardiac patches so that their properties may adapt to more closely mimic native heart tissue. By adapting these mechanical properties, higher conduction velocities, organized and longer sarcomeres, and expression of genes pertaining to cardiac contraction can be enhanced, thus created a better and stronger cardiac patch [28]. Current cardiac patches lack proper myocardium structure, elasticity, and sufficient contractility needed to sustain the heart for long term use. By directly mechanically stimulating the cardiac tissue growth in this way, a more functional patch can be developed. Following this goal however, a project strategy must first be attained to properly analyze the best route of action. Further evaluation must also be done on the cardiac patches to consider all possible needs, wants, and constraints.

3. Project Strategy

3.1 Initial Client Statement

The initial client statement guides early needs identification and is a jumping-off point for design discussion for the team and client. Dr. George Pins provided the team with the following initial client statement:

“Design, develop, and characterize an electrical or mechanical stimulator that can be used to reproducibly and cyclically impart stimuli on tissue engineered muscle scaffolds that mimic the native stimuli on tissues.”

3.2 Defining the Stakeholders

As previously mentioned, the client, Dr. George Pins, detailed his expectations of the project to the design team. The thorough explanation of the needs and wants of the project is the client's primary role. The client must detail what they would like to see come out of the design and help guide the design team toward a final product. The user, Dr. Pins's graduate student, Elizabeth English, provides similar feedback on the project, however the user's concerns tend to focus around how the product will function on a day-to-day basis. The feedback of the user is critical to assure that the final product will be useful. The duty of the designer is to integrate the needs, wants, and other feedback of both the client and user in order to produce a product that fits the client's statement. This statement will continue to evolve as the needs of the client and user become more detailed and specific.

3.3 Developing Objectives

Based on background research and a series of discussions with the client as well as the eventual device user, Elizabeth English, a master's student in Dr. Pins's lab, a list of objectives was created to guide the design process. These objectives form the basis for design decisions when they are rank-ordered by importance by the client, user, and design team. The top-level objectives established were *reliability*, *ease of use*, *growth environment*, *visualization*, *sustainability/environmental impact*, and *reproducibility*. Top-level objectives were broken down into sub-objectives when necessary to capture greater specificity. Figure 3 below outlines the objectives and the relationships between lower-level objectives and higher-level objectives. Table 4 elaborates on how the team defined each objective and sub-objective in the context of this project.

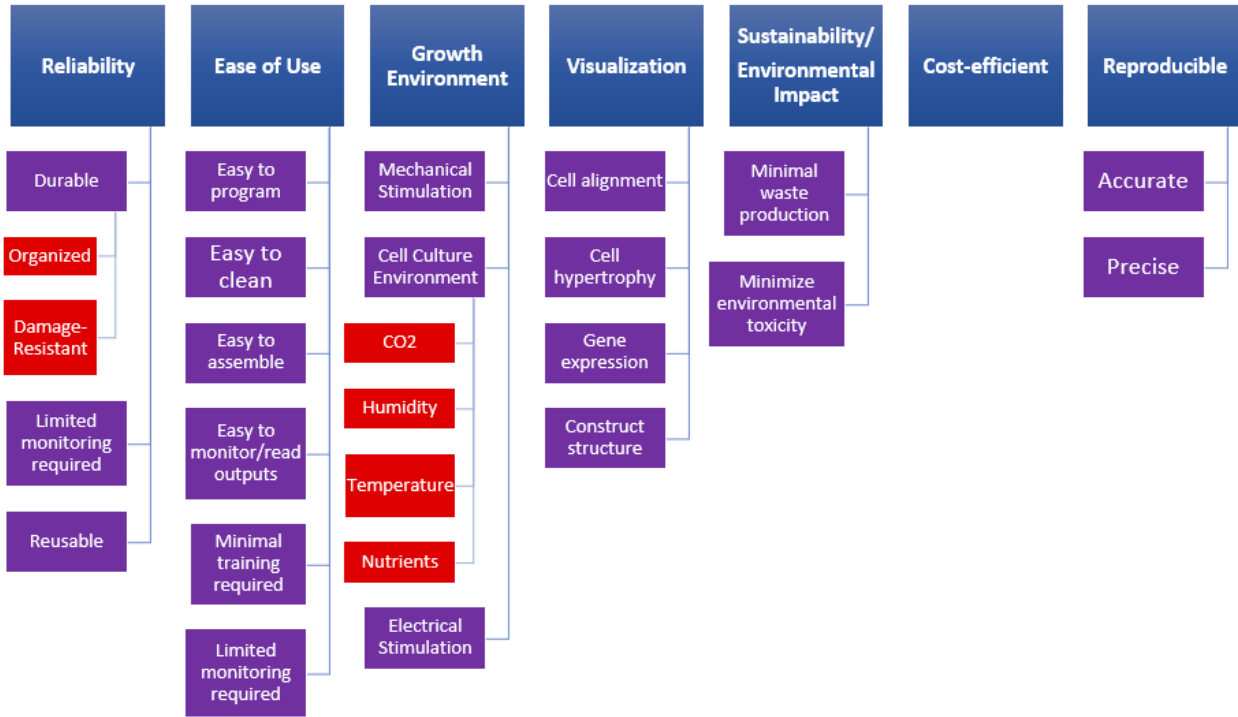


Figure 3. Objectives Tree

Table 4. Definitions of objectives

Objective	Definition
Reliable	The device should function properly and not require any repair throughout the duration of an experiment. If the device is re-used, its components should not require frequent replacement.
Durable	The device should be able to withstand any wear and tear that occurs during normal operation and throughout an experiment without falling apart, breaking, or corroding. Additionally, the device components will be neat and organized to facilitate portability and ease of use.

Limited Monitoring Required	The device should not require constant monitoring during experiments, allowing for experiments to run unsupervised. Any device outputs will be autoregulated, meaning that once the user sets up the device and begins the experiment, no further user input will be necessary to maintain proper function of the device.
Reusable	The device can be used for more than one experiment.
Reproducible	The actions performed by the device as well as any measurements taken must be both accurate and precise. This allows for the results of any experiment to be achieved more than once given the same conditions.
Accurate	Accuracy refers to how close a measurement is to the correct value in the case of a measurement tool, and in the case of the device, how close a device output (i.e. temperature) is to what the control was set to. An accurate device will perform exactly as designed, with little to no difference between intended outputs and actual outputs.
Precise	Measurable outputs of the device during use should lie in a specified range each iteration.
Ease of Use	The device will be simple and user-friendly.
Easy to Program	The user will be able to easily input or change experiment parameters.
Easy to Clean	All components of the device will be disinfected easily and effectively.
Easy to Assemble	The device will be simple to set up and not contain too many wires or complex external accessories.
Easy to Monitor	The device will output data in a straightforward way so that the user can easily and quickly understand the status and controls of the experiment.

Minimal Training Required	The procedure for setting up and operating the device will be simple and not require extensive training for the user.
Limited Monitoring Required	The device should not require constant monitoring during experiments, allowing for experiments to run unsupervised. Any device outputs will be autoregulated, meaning that once the user sets up the device and begins the experiment, no further user input will be necessary to maintain proper function of the device.
Cost efficient	The materials used to synthesize the device as well as the manufacturing costs are affordable.
Visualization	The device should have visualizing components that enables the experimental results to be analyzed or viewed either with an imaging technique or with the naked eye.
Cell Alignment	Cells may align and organize to emulate the band structure of cardiac muscle in response to the stimulus applied by the device.
Cell Hypertrophy	Cells may grow in response to the stimulus applied by the device.
Gene Expression	Cells may express specific genes that can indicate further growth and functionality.
Construct Structure	Each component of the patch may be layered, aligned, and integrated to form a proper functioning composite. The presence of a micro-anatomy such as endothelium or a vascular network may develop in response to the stimulus applied by the device.
Sustainability Environmental Impact	The device should aim to minimize environmental waste and toxicity.
Minimize Waste Production	Must considerably minimize the amount of materials used and the user must be conscious of the amount of medium and other growth supplements the cells need in order to grow.

Minimize Environmental Toxicity	The disposed materials should be nontoxic to the environment.
Growth Environment	The cells must be provided with the environment they need for proper growth <i>in vitro</i> .
Mechanical Stimulation	The device must be able to apply a mechanical stimulus to the cells that mimics the physiological environment in the heart.
Cell Culture Environment	Proper conditions that cardiomyocytes need in order to proliferate and grow such as CO ₂ , humidity, specific temperature, and nutrients.
Electrical Stimulation	The device must be able to apply a electrical stimulus to the cells that mimics the physiological environment in the heart.
Sterility	The cells must be provided with a clean environment without the disturbance of bacterial growth.

Design constraints represent the “deal-breakers” inherent in the project; the system absolutely must meet these constraints to be successful. Through discussions, the design team, user, and client reached the following design constraints, outlined in Table 5 below:

Table 5. Design constraints

Constraint	Description
Must maintain live cardiomyocyte culture	<ul style="list-style-type: none"> - Cell culture environment must be sterile - Cell culture environment must not be cytotoxic
Must provide mechanism for biomimetic stimulation to cardiomyocytes	<ul style="list-style-type: none"> - Primary client goal
Must detect changes in cell morphology	<ul style="list-style-type: none"> - Necessary for validating the efficacy of the above stimulation
Must cost less than \$1000	<ul style="list-style-type: none"> - Maximum WPI budget for a team of four students

Must be achievable by April 2019	- Must be completed before project deadline and graduation
----------------------------------	--

3.4 Revised Client Statement

This is the team's current conceptualization of the initial client statement and it will be continuously improved upon after further information is gathered from the client. The following is the revised client statement that the team crafted:

*Engineered cardiac muscle tissue need to withstand mechanical or electrical loading during tissue development, regeneration, and healing. The system will provide **a cyclic mechanical stimulus of 5-15% uniaxial stretch at 0-2 Hz** to fibrin-based cardiac patches for a two week period to **improve their functional properties**. The cardiac patches will be removable from the mechanical stimulation system for imaging and analysis of morphological changes and gene expression. The system will be sterile and contained within a standard cell culture incubator in order to **maintain the environmental conditions of 37°C temperature, 95% relative humidity, and 5% environmental CO₂**. The mechanical stimulation settings should be variable and computer-controlled to allow for investigation of different regimes and automated to limit necessary user input.*

4. Design Process

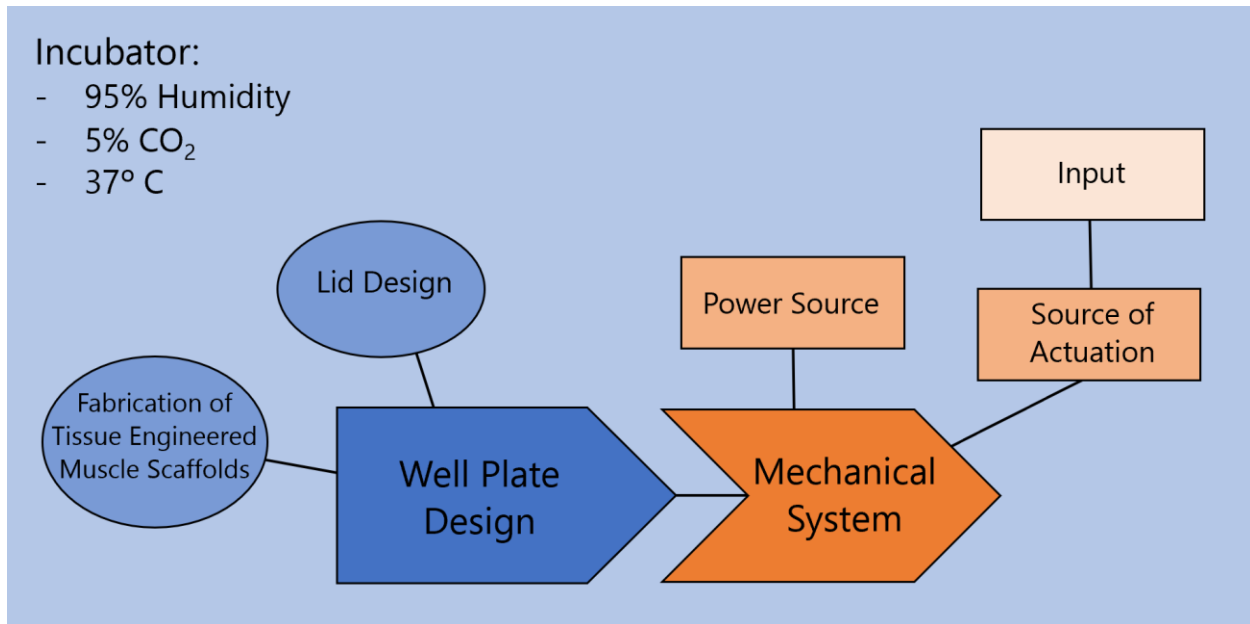


Figure 4. Broad concept drawing of design outline

The cardiac patch created in Dr. Pins's lab by Chrobak and colleagues builds on existing engineered heart tissues and cardiac patches by using fibrin microthreads to match the stiffness of native myocardium, and by extension, increasing active contractile force development. However, to further improve the functional properties of the Pins Lab cardiac patch, the team was tasked with creating a mechanical stimulator system that would apply biomimetic loads to the cardiac patches, with the expectation that the observations of the positive effects of mechanical stimulation on cellular growth, morphogenesis, and contractility as discussed in Section 2.4 would hold true.

Following this task, the team created a concept drawing outline to further organize and breakdown the different components, as shown in Figure 4. This concept map outlines the different components the team will need to evaluate and design for. The outline is centered around two main components; the well plate and mechanical system. In order to grow the cardiac patch, some kind of well plate will need to be properly designed so cell culture can successfully be achieved. Coming off of this design, a lid will also need to be custom made to properly fit the designed well plate and tissue engineered muscle scaffolds will need to be fabricated as a proof of concept place holder to ensure proper function. All this together will be appropriately fitted

into some kind of mechanical device. In order to have a functioning mechanical device, the system must have some sort of power source and way of actuation to mechanically operate. Coming off of the source of actuation, an input code must be implemented in order to give the mechanical system proper instructions on what to do. The overall device in series will then be placed in a standard lab incubator with set parameters of 95% humidity, 5% CO₂, and 37°C.

4.1 Construct Formation

The cardiac patch used in the Pins Lab utilizes fibrin threads in conjunction with a fibrin hydrogel in order to create a layered construct to mimic properties of the heart. Fibrin threads are made of a mix of thrombin and fibrinogen and are extruded into buffer and are then stretched and secured to dry. The fibrin threads are then attached to a PDMS frame via silicone adhesive. The multilayer gel is then even cast over the fibrin threads mounted on the frame. The PDMS frame is a rectangular, clear, gel-like apparatus. It has four posts, one on each corner, that extend vertically out of the well. There are ridges on all ends of the frame that surround the construct. The construct is attached to the short ends of the rectangle and extends longitudinally down it. The four posts are fixed with O-rings which keep the frame from floating when placed in media. The designers were challenged with ensuring that the mechanical stimulation apparatus would be able to stimulate this specific construct in order to further the development of these patches for in vitro testing. The frame can be seen in Figure 5 below [9].



Figure 5. PDMS Frame

4.2 Pairwise Comparison

The pairwise comparison chart is a quantitative tool used to evaluate the relative importance of the project objectives. Every objective within the objectives tree (see Section 3.2) is placed along the horizontal and vertical axis of the matrix. The individual filling out the chart moves down the vertical axis, comparing each objective on that axis to each objective on the horizontal axis (see example in Figure 6). If the vertical axis objective is considered more important than that on the horizontal, a “1” is placed in the cell common to both. If both objectives are considered equally important, a “0.5” is placed in that cell. If the objective on the horizontal is more important, a “0” is placed in that cell.

Top-Level Objective	Reliability	Ease of Use	Growth Environment
Reliability		1	0
Ease of Use	0		0
Growth Environment	1	1	

Figure 6. Pairwise Comparison Example

The figure above demonstrates how the objective along the vertical axis (“Ease of Use”) is compared to the objective on the x-axis (“Reliability”). In this case, ease of use was not considered to be more important than reliability, so a “0” was placed in the cell common to the two objectives. Since the pairwise comparison chart is a symmetric matrix, only half of the chart needs to be filled out to make a direct comparison between every objective, upon which the values are mirrored to the remaining half of the matrix. Once all objectives have been compared, the numbers in each row are summed to obtain a final score for each of the objectives.

The design team, user (Elizabeth English), and client (Professor Pins) individually filled out a pairwise comparison chart before coming together to discuss the results. The total score results of each pairwise comparison chart are shown along with their weighted average scores in Table 6 below:

Table 6. Combined pairwise comparison charts

	Total Score	Total Score	Total Score	
Top-Level Objective	Designer	Client	User	Weighted Avg.
Reliability	4.5	4	3	3.7
Ease of Use	1.5	2	3.5	2.5
Growth Environment	5	5	5	5
Visualization	4	4.5	1	3
Sustainability/Environmental Impact	0.5	0	0	0.1
Cost-efficient	1	1	4	2.2
Reproducible	4.5	4.5	4.5	4.5
Reliability				
Organized	2	0	2	1.2
Corrosion Resistant	4	3	2	2.8
Damage Resistant	0.5	3	2	2.1
Limited Monitoring Required	2	1	4	2.4
Reusable	1.5	3	0	1.5
Ease Of Use				
Easy to Program	4.5	2	2	2.5
Easy to Clean	0.5	3.5	3	2.7
Easy to Assemble	1.5	3.5	2.5	2.7
Easy to Monitor/Read Outputs	4	5	2.5	3.8
Minimal Training Required	1	1	0	0.6
Limited Monitoring Required	3.5	0	5	2.7
Growth Environment				
Mechanical Stimulation	2.5	1.5	3	2.3
CO2	2.5	3	3	2.9
Humidity	2.5	0	3	1.7
Temperature	2.5	5	3	3.7
Nutrients	2.5	5	3	3.7
Electrical Stimulation	2.5	1.5	3	2.3
Sterility	6	5	3	4.4
Visualization				
Cell Alignment	2	2.5	1	1.8
Cell Hypertrophy	2	1.5	0	1
Gene Expression	0	0	2.5	1
Construct Structure	2	2	2.5	2.2
Sustainability/Environmental Impact				
Minimal Waste Production	0	1	0.5	0.6
Minimize Environmental Toxicity	1	0	0.5	0.4
Reproducible				
Accurate	0	0	0.5	0.2
Precise	1	1	0.5	0.8

To produce the weighted averages, the client's and user's scores were assigned a value of 40% respectively and the designer scores were assigned a value of 20% to reflect the importance of the voice of the customer in engineering design.

The notable results from this exercise appear in the first section of Table 6 under the portion labeled "Top Level Objectives", where reliability, reproducibility, and maintenance of a proper cell growth environment were ranked as the three most important objectives. The user, client, and designers agreed that the pairwise comparison charts accurately reflect their opinion about the objectives. Following this agreement however, a few clarifications were made, namely that "growth environment" and "corrosion resistance" are constraints that the design must satisfy rather than objectives which may or may not be more important than the others. The fact that both objectives were ranked highest in their categories does reflect that all stakeholders considered them to be indispensable to the project. At the end of the discussion, the client and user recommended that the design team brainstorm primarily for growth environment, reliability, visualization, and ease of use, with reproducibility being more of a concern as the device is tested. The overall results of the pairwise comparison charts were used going forward in making design decisions. The raw data from each pairwise comparison chart appears in Appendix A.

4.3 Needs Analysis

The design team determined design needs and wants based on the outputs of the pairwise comparison charts and discussions with the user and client. The combined pairwise comparison chart (see Table 6) contains score that was averaged from the objective scores given by the user, client, and designer. Based on those rankings, each objective was designated either a constraint, a need, or a want. Constraints are "deal breakers" that form the design space within which the team must operate. Needs are conditions that must be satisfied for the design to satisfy the client statement. Wants are "nice-to-haves" that are not critical to the functioning of the device but would add additional functionality and usability to the design. Constraints were previously defined in Table 5. Needs and wants were determined by taking the top-ranked sub-objective from the three most critical top objectives: reliable, ease of use, and visualization. Since the objective reproducible, which was ranked highest, only has two sub-objectives, it was considered a need instead of breaking it up.

Table 7. Design needs

Design Needs:
1. Limited Monitoring Required
2. Easy to Assemble
3. Easy to Clean
4. Easy to Monitor/Read Outputs
5. Visualize Construct Structure
6. Reproducible

As mentioned, the output of the pairwise comparison charts as well as feedback from the client and user were used to determine the design needs which can be seen in Table 7. The device must be corrosion resistant in order to comply with the cytoculture constraint (see Table 5), therefore the next highest ranked objective under reliability was chosen as a need. Limited monitoring required was ranked first in the reliability category, because it is critical that the device be able to run without requiring inputs overnight. Ease of assembly, easy to clean, and easy to monitor/read outputs were all taken from the ease of use category, because all were considered important by the client, user, and design team. Ease of assembly and ease of cleaning both facilitate regular usage of the device in the lab. If the device is assembled incorrectly or is not cleaned properly, it might malfunction in subsequent experiments and produce inconsistent results. Easy to monitor allows the device user to ensure the device is performing as intended while the experiment is running. In the visualization category, visualizing the construct structure was the top objective in both the pairwise comparison charts and in discussions. Changes to the construct structure including the size, orientation, and shape of the cells as well as development of micro-structures such as vascularization have been used by researchers as indicators of the effects of cell stimulation as noted in Section 2.4. Reproducibility is critical if the results of experiments are to be trusted. Poor accuracy and precision of the components of the device will yield experimental results with high variation, which will be statistically unacceptable.

Table 8. Design wants

Design Wants:
1. Damage Resistant
2. Easy to Program
3. Gene Expression

The wants were established through discussion with the team, client, and user and can be seen in Table 8. Damage resistance is important to consider for the user who would prefer that the device can withstand minor bumps and small drops. However, shatter resistance or drop proof are not significant design considerations. It was decided that easy to program would be convenient and helpful for the user in order to ensure that the device can be operated efficiently and effectively. However, this was not considered to be absolutely necessary to the functionality of the device. Gene expression was not the next highest-ranking objective in the visualization category, however after discussions with the project team, gene expression was decided on the best secondary way to measure the progress and changes of the project. Testing the construct for gene expression after stimulation is often used to measure development according to the user and is a common method found in literature [33, 39, 57], but this is not a primary concern for the development of the project.

4.4 Design Process

After evaluating the design priorities from the Pairwise Comparison Charts, each team member individually conceptualized design ideas, then met with the client and the user to brainstorm initial design concepts. The design concepts were developed around the consideration of two additional growth environment constraints: fitting within a standard cell culture incubator and withstanding its environment without experiencing material decay or cell damage. After analyzing the advantages and disadvantages of each design concept, the team utilized Pugh matrices to numerically score the functionality of each design. A Pugh matrix is a mathematical tool used to compare and contrast different ideas against each other in a quantitative manner. In order to organize and evaluate each individual component of the designs, the team categorized

five specific design elements: the well plate material, the construct anchoring, the mechanical stimulation technique, the force production, and the force analysis. The Pugh matrices were used to evaluate each design element and scored them according to the constraints and top objectives from the function means analysis. Based on the top scores from the Pugh matrices, the design team completed a secondary brainstorm session which focused on combining the initial design concepts into three final design ideas.

4.5 Functions and Specifications

A key function of the device comes from the constraint that it must maintain a proper cell growth environment, so the cardiac patches survive the experiments. In order to carry out this function, the device must remain sterile. Otherwise, contaminants could harm the cells, which could alter or entirely invalidate the experiment. Additionally, it must allow for sufficient heat and gas exchange with the cells in order for them to reach thermal equilibrium with the provided environment. This environment consists of standard cell culture conditions of 37 degree Celsius ambient temperature, a relative humidity of 95%, and a CO₂ concentration of 5%.

According to the client statement and needs the device must allow for biomimetic mechanical stimulation of the cardiac patch. The patch must be stretched uniaxially and a benchmark of 5-15% elongation was obtained from the literature. The device will operate at a frequency of 0-2 Hz based on values found in literature, this value also mimics that of a healthy heart. The team must also be able measure the elongation throughout the experiment accurately in order to understand the effects on the patch.

The device must also be compatible with the cardiac patches currently used in Professor Pins's lab. The dimensions of the PDMS frame that holds the patch is 2.5cm by 1.9cm, so this was set as the minimum specification for well area. The wells must also be deep enough to allow for full submergence of the cardiac patch in culture media, which was found to be 3mL in volume.

Finally, the experiment must be able to sustain an experiment for up to 14 days as specified by the user and client. Additionally, the design must be able to operate successfully without supervision for an overnight 12-hour period as requested by the user.

Table 9. Functions and specifications

Function	Specification
Cell Growth Environment	<ul style="list-style-type: none"> ● Remain sterile for 2-week continuous experiment ● Allow enough gas exchange to maintain culture media pH of 7.4. ● Provide an environment of at least 95% humidity ● Maintain a temperature of 37°C ● Maintain 5% CO2 concentration
Mechanical Stimulation	<ul style="list-style-type: none"> ● 5-15% uniaxial elongation of cardiac patch ● Allow user control over stimulation frequency and duty cycle ● Frequency range of 0-2 Hz
Hold Cardiac Patches	<ul style="list-style-type: none"> ● Anchor cardiac patch in well without cells coming into contact with plate ● Well size to accommodate 2.5cm x 1.9cm cardiac patch ● Hold 3 mL of culture media
Require limited user input	<ul style="list-style-type: none"> ● Sustain an experiment duration of 2 weeks ● Run at least 12 hours without user input

4.6 Initial Designs

As a team, initial designs were hand drawn and evaluated based on the pairwise comparison charts. The following sections outline the initial brainstormed designs in detail; Table 10 highlights their advantages and disadvantages.

4.6.1 Hook Tension Apparatus

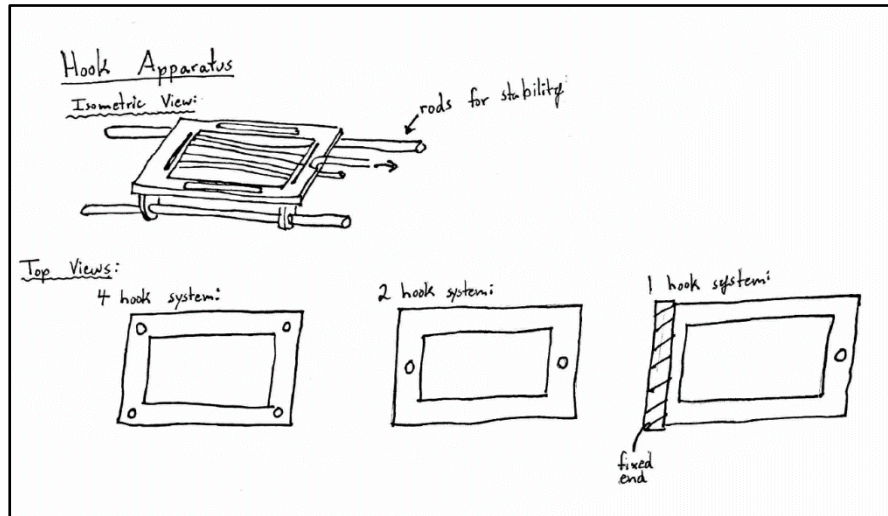


Figure 7. Hand Drawing of the Hook Tension Apparatus

The first design concept utilizes a hook tension apparatus which pulls on each end of the PDMS frame, in turn, stretching the cardiac patch (see Figure 7). The design uses linear actuators to drive the hooks into tension using a standard or custom made well plate. To control the force applied, a load cell would be implemented along with a microcontroller to easily program, control, and display the force. The design would incorporate one or up to four hooks: one hook pulling from only one side in the middle of the frame, two hooks with each pulling on one side in the middle of the frame, or four hooks with one pulling on each corner of the frame. The use of rods within the construct frame could also be incorporated as another component in the design to create more stability for the PDMS frame and cardiac patch when mechanical stresses are applied. The rods would be used as a guided track for the ends of the PDMS frame to slide up and down when the hook(s) are pulled. One major challenge for this design is the fitting or manipulation of the standard or custom well plate which includes the attachment of the hooks to each well and increased well size to allow for greater displacement of the cardiac patch during stimulation.

4.6.2 Stretching Well Plate Apparatus

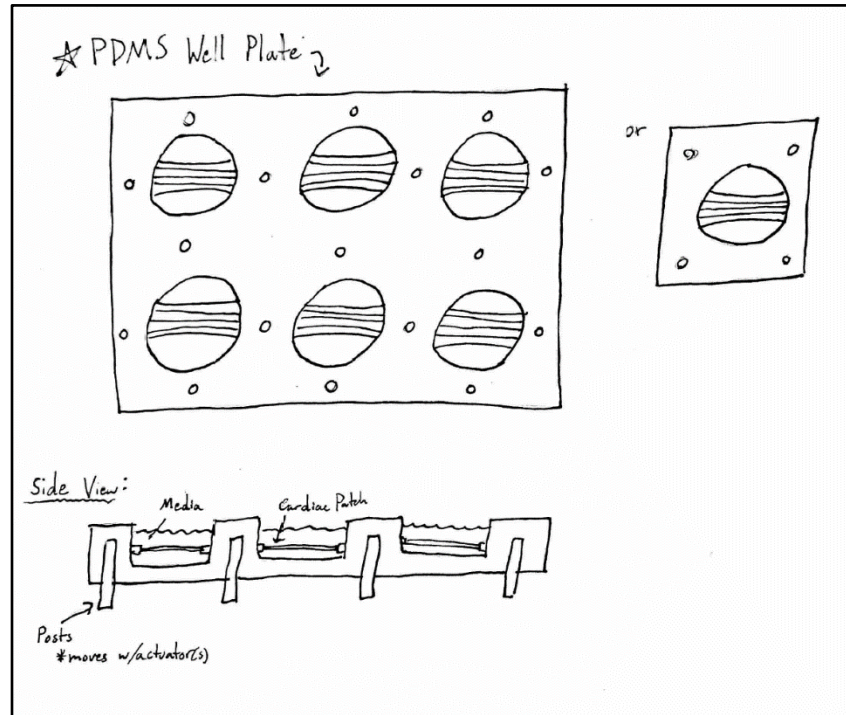


Figure 8. Hand Drawing of the Stretching Well Plate with Posts Apparatus

The second design concept brainstormed, incorporates a custom PDMS six well plate with posts within the plate from underneath to provide mechanical stimulation. The design would feature the PDMS frame molded and built into the PDMS well plate thus, allowing for the entire well plate to be stretched, providing mechanical stresses along each well and cardiac patch. The system uses an actuator to move the posts within the well plate which will provide tension by stretching of the plate. Posts would be positioned on four sides of each well or the four corners of each well as shown in Figure 8 above. This design will allow for a direct force application to the patch as well as easy assembly, manufacturing, and control of the plate. The challenges surrounding this design concept include the inability for the patch to be taken in and out of the well.

4.6.3 Stretching Well Plate with Walls

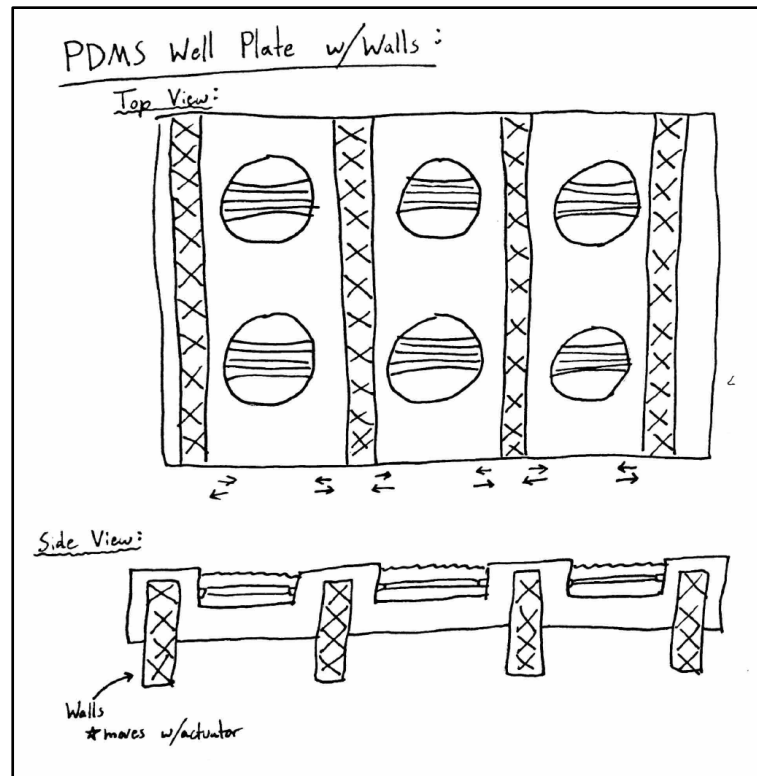


Figure 9. Hand Drawing of the Stretching Well Plate with Walls Apparatus

Progressing from the previous design concept of a PDMS well plate with a built in PDMS frame, the accordion inspired design alternatively uses walls instead of posts to create a more uniform strain distribution. The design utilizes the same tension system; however, it utilizes walls instead of individual posts. For a six well plate, there would be one or up to four walls between two sets of wells (seen in Figure 9 above). This design presents the same advantages and disadvantages as the previous stretching well plate design with the exception of a more uniform strain distribution.

4.6.4 Inverted PDMS Frame

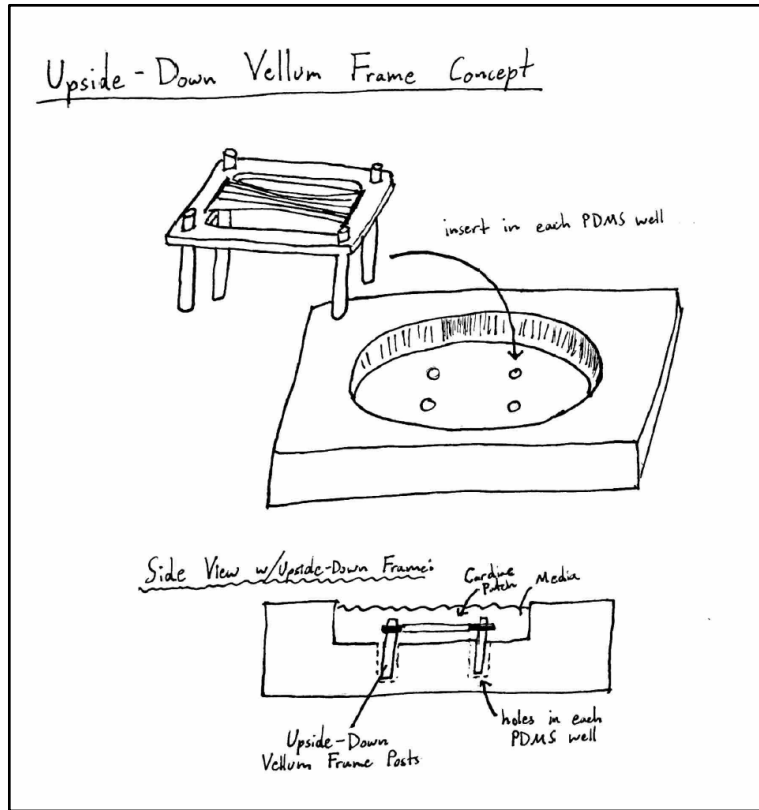


Figure 10. Hand Drawing of the Inverted PDMS Frame Design

The inverted PDMS frame, inspired by the concept of a Lego, is an alternative design feature added to the built in PDMS well plate apparatus. Instead of the frame being attached to the well plate, four holes are molded into each well of the PDMS plate to hold the inverted PDMS frame (see Figure 10). The posts of the PDMS frame would fit into the molded holes when the frame is inverted allowing for easy removal of the patch without strenuous damage to the PDMS well plate. A load cell would be implemented to control the force applied to the constructs. The key advantage and purpose of this design feature is to easily remove the cardiac patch throughout experimentation for visualization of morphological cell changes. A challenge of this design is finding the proper material properties of the PDMS posts to make sure they do not warp or bend improperly during stimulation. Another major disadvantage is the analysis of the forces being translated between the well plate, PDMS frame, and cardiac patch which may be hard to calculate and measure.

4.6.5 Dynabeads Magnetic System

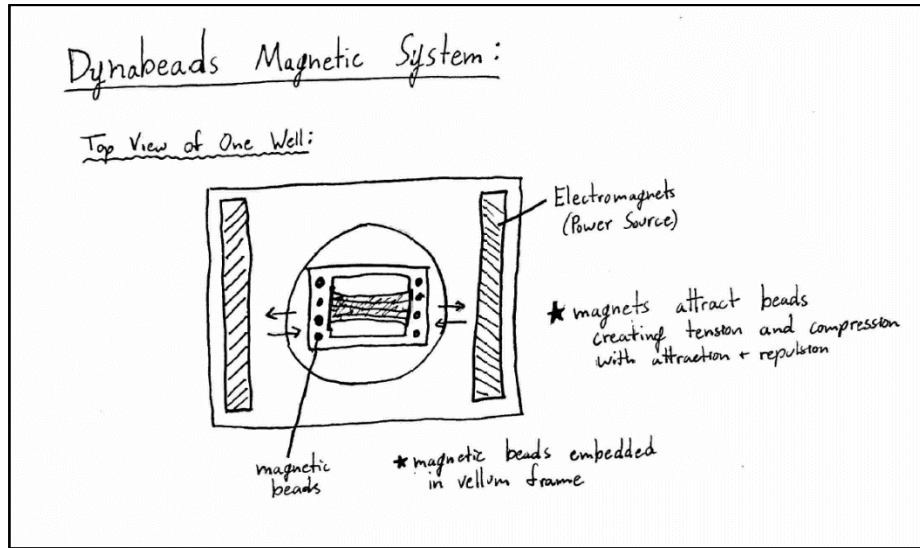


Figure 11. Hand Drawing of the Dynabeads Magnetic System

The Dynabeads Magnetic System incorporates Thermo Fisher Scientific's Invitrogen Dynabeads within both the left and right sides of the PDMS frame as seen in Figure 11. The goal of the magnetic Dynabeads is to uniaxially stretch the patch within a standard cell culture well plate. The power source is supplied by electromagnets that create magnetic poles which pull the cardiac patch in opposing directions producing tension along the patch. The electromagnets would be controlled via wires and a microcontroller. The force needed to pull the construct and patch could easily be altered based on the amount of electric current running through the electromagnets. Possible challenges that could arise however, would be interferences of the electric field and calibrating the magnetic force production system.

4.6.6 Shear Flow Design

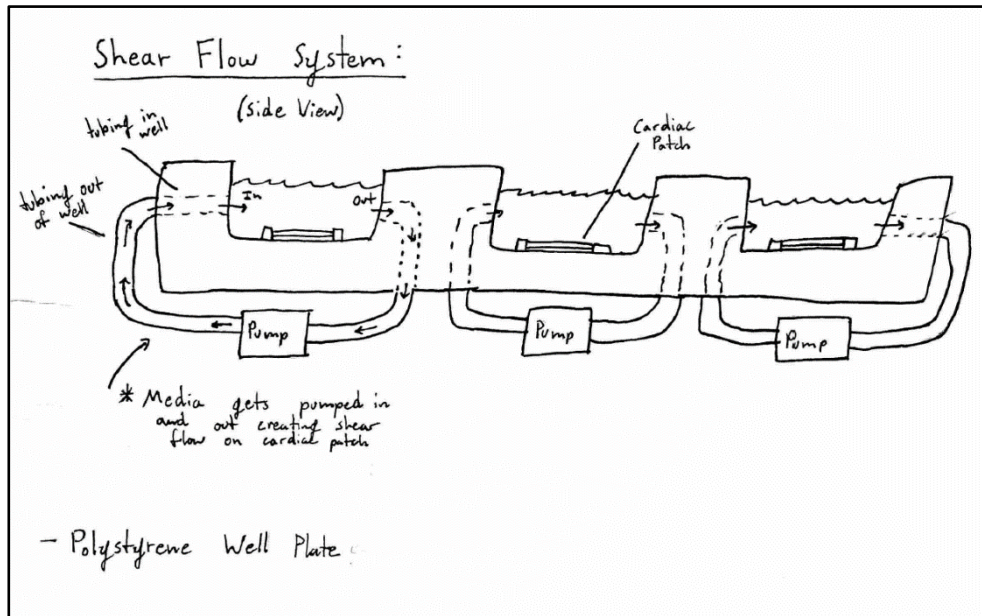


Figure 12. Hand Drawing of the Shear Flow Design

The Shear Flow Design seen in Figure 12 uses machined holes that act as flow channels within each well to cyclically perfuse media through the well. This design creates a biomimetic shear force, mimicking blood perfusion through the heart muscle tissue. The cardiac patch would be anchored to the well allowing for a calculable shear flow distribution throughout the patch. A pump will drive the cyclic media flow through the wells in a standard well plate with the channel modifications. A major disadvantage of this design is the usage of multiple pumps within the whole system, thus posing size challenges. Since the system requires more than one pump, the cost of the system as a whole would be otherwise expensive.

4.6.7 Vacuum Chamber Design

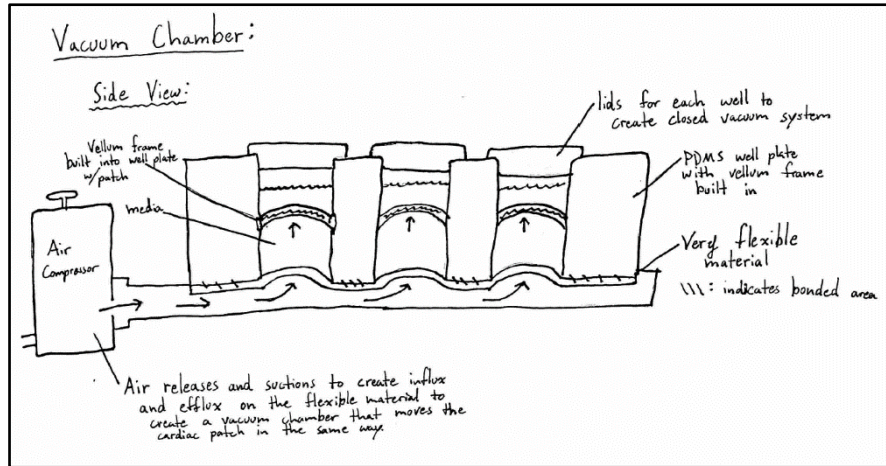


Figure 13. Hand Drawing of the Vacuum Chamber Design

The Vacuum Chamber seen in Figure 13 design utilizes a custom PDMS well plate which will be bonded to a flexible material at the bottom. The design incorporates an air compressor that would actuate the flexible well plate bottom through a channel, thus creating a vacuum chamber to flex the material up and down in order to induce multi-axial tension and compression in the cardiac patch. The force exerted onto the patch would be controlled via air pressure of the vacuum system and the shear flow of the media within the system. One major challenge with this design is finding the right flexible material that will not yield after cyclic air flow and possess strong bonding properties. Another challenge to this design is ensuring that movement from the media will not induce shear forces onto the cardiac patch.

Table 10. Advantages and disadvantages of conceptual designs

	Advantages	Disadvantages
Hook Tension	<ul style="list-style-type: none"> • Direct and easy to control forces with load cell • Uses standard well plate 	<ul style="list-style-type: none"> • Difficult to assemble <ul style="list-style-type: none"> ◦ Requires modification to standard well plate
PDMS well plate with posts	<ul style="list-style-type: none"> • Ease of manufacturing • Properties of PDMS can easily be tailored • PDMS frame is directly attached to plate allowing for direct and easy to control forces onto the patch 	<ul style="list-style-type: none"> • Non-linear strain distribution; hard to apply same force to all patches • Cannot be imaged through • Patches have to be cut out once completely done with experiment • May need multiple actuators
PDMS well plate with walls	<ul style="list-style-type: none"> • Uniform strain distribution • Ease of manufacturing • Properties of PDMS can easily be tailored • PDMS frame is directly attached to plate allowing for direct and easy to control forces onto the patch 	<ul style="list-style-type: none"> • Cannot be imaged through • Patches have to be cut out once completely done with experiment • May need multiple actuators
Inverted PDMS frame	<ul style="list-style-type: none"> • Patch is removable to allow for imaging throughout the experiment • Properties of frame can be tailored 	<ul style="list-style-type: none"> • May creating bending forces or yielding of well plate • More indirect and complicated force production onto cardiac patches
Dynabeads Magnetic System	<ul style="list-style-type: none"> • Uses standard well plate • No load cell • Easy to assemble 	<ul style="list-style-type: none"> • Possible interference with electrical stimulation • May be difficult to calibrate • May be hard to sterilize • May interfere with incubator interface
Shear Flow Design	<ul style="list-style-type: none"> • Uses standard well plate 	<ul style="list-style-type: none"> • Difficult to manufacture • Each well requires its own pump system • Effects of shear flow is hard to document and evaluate
The Vacuum Chamber	<ul style="list-style-type: none"> • Multi-axial stretch • May be imageable 	<ul style="list-style-type: none"> • Requires custom or modified well plate

4.7 Quantitative Analysis of Design Ideas

4.7.1 Summary of Pugh Matrix

The team utilized Pugh matrices to quantitatively evaluate several design ideas for the five specific elements. The team based the design elements off of the preliminary conceptual designs. The design elements were scored based on a rubric that represents whether or not the design element met the constraints (C) and how well the design element achieves each objective (O) it is scored against. In terms of the constraints, the design elements were scored on a yes (Y), maybe (M), and no (N) scoring system with yes being that the element followed the given constraint, maybe being that the element possibly followed the constraint, and no being that the element did not follow the constraint. The elements were rated on a 1-5 scale, with 1 being that the design element did not meet the objective well and 5 being that it fully met the design objective. The team determined the 1-5 score for each element following a thorough investigation of the possible design ideas for each element. Following a unanimous vote from the team, the top idea for each element was chosen based off of the team's decisive score and a mathematical model the team followed. The top ranked or the top two ranked element ideas were used to create three narrowed down design ideas which led the team to their final design idea.

4.7.2 How the Pugh Matrix Works

The Pugh Matrix below (see Figure 14) represents an example of the team's quantitative analysis of one of the five design elements. Each element was evaluated in a separate Pugh Matrix so the scores stayed consistent with the applicable objectives they are being scored against. Applicable design objectives were chosen from the objectives and sub objectives in the pairwise comparison charts if the design element met all the constraints and the team deemed it applicable (see Table 6). The team chose to focus on five applicable objectives, which are highlighted in blue in Figure 14: reproducible, reliability, visualization, ease of use, and cost efficient. Although the growth environment objective is the highest ranked objective within the team's PCC, the team chose to label the growth environment as a constraint. This being that the device must be limited to a standard cell culture laboratory incubator and maintain sterility and

cell growth. Depending on the design element, specific objectives or sub-objectives were blacked out (see Table 4) if the team felt they did not apply to the given element. Although different objectives are blacked out in varying Pugh Matrices, the weighted percentages remained the same throughout all matrices in order to provide consistency of numerical weighted percentages.

In the event that the design element did not meet all the constraints, the design objective and sub-objectives were not considered and the total score of the element was not measured nor applicable to the analysis.

Well Plate Material		PDMS	Glass Bottom	Polystyrene (standard)
Constraints				
C1	Sterile	Y	Y	Y
C2	Functions within Lab Incubator	Y	Y	Y
C3	Completed before April	Y	Y	Y
C4	Cost Below \$1000 Budget	Y	Y	Y
C5	Cell Viability	Y	Y	Y
Objectives:		Scores		
O1	Weight % Reliability			
17.60%	Durable	4	2	4
	Limited monitoring required			
	Reusable	2	1	1
	Total Score:	6	3	5
	Weighted Sum:	1.056	0.528	0.88
O2	Weight % Ease of Use			
11.90%	Easy to Program			
	Easy to Clean	5	5	5
	Easy to Assemble	4	5	5
	Minimal Training Required	4	5	5
	Total Score:	13	15	15
	Weighted Sum:	1.547	1.785	1.785
O3	Weight % Reproducible			
21.40%	Accurate			
	Precise			
	Total Score:			
	Weighted Sum:			
O4	Weight % Visualization			
14.30%	Imagable	4	5	5
	Total Score:	4	5	5
	Weighted Sum:	0.572	0.715	0.715
O5	Weight % Cost Efficient			
10.50%		4	4	5
	Total Score:	4	4	5
	Weighted Sum:	0.42	0.42	0.525
	Total Score:	3.595	3.448	3.905

Figure 14. Pugh Matrix Example

4.7.3 Numerical Analysis of Pugh Matrices

In order to accurately analyze each objective within the Pugh Matrix, weighted percentages were calculated (seen to the left of Figure 14 under each objective), for all objectives including the ones not shown in the matrix. The weighted percentages were determined based off of the pairwise comparison charts as mentioned previously in Section 4.2. The weighted averages from the pairwise comparison chart were added together to obtain a sum of 21. The weighted average for each specific objective was then divided by the total sum of 21 and multiplied by 100 to derive a weighted percentage for each. The mathematical model for the weighted percentages can be seen below in Figure 15.

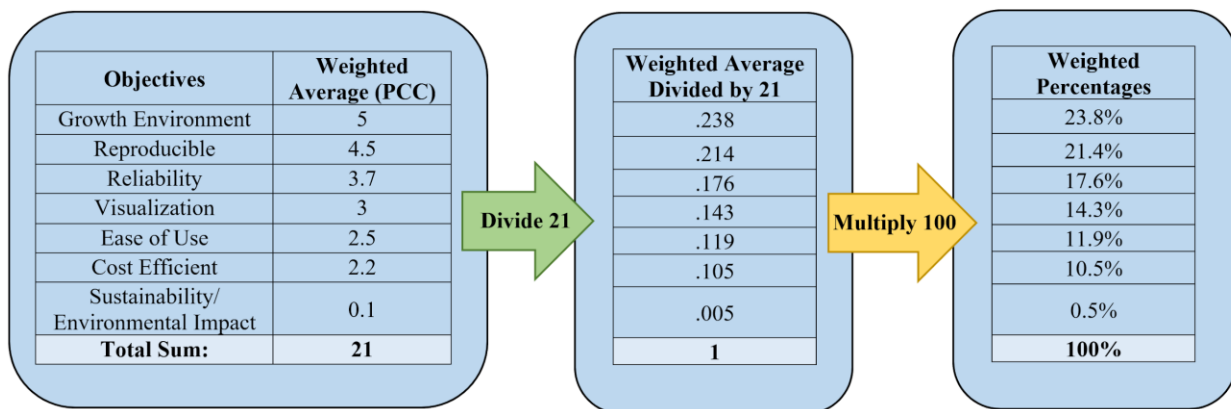


Figure 15. Mathematical Model for Weighted Percentages in Pugh Matrices

The team determined scores of 1-5 for all the applicable sub-objectives based on the functions and specifications of the design element. Once the sub-objectives scores were given, the sub-objective scores were then added up and multiplied by the weighted percent of the specific objective to give the total weighted sum for the specific objective. For example, in Figure 15 under PDMS, the sub-objective durable has a score of 4 and the sub-objective reusable has a score of 2. The sum of these two sub-objectives give a total of 6. The total sub-objective score of 6 is multiplied by the weighted fraction of 0.176. This yields the weighted sum of the reliability objective- 1.056. Once the weighted sums of each objective is calculated, all the weighted sums for the given design element are summed up to give a total design element score. For example, in Figure 15 under PDMS, 1.056, 1.547, 0.572, and 0.42 are added together to give a total design element score of 3.595.

4.8 Pugh Matrix Analysis of Design Elements

The advantages and disadvantages of the different design elements were explored in order to quantitatively narrow the design field. The scores for sub-objectives were obtained based on the compiling of research and analysis of the design element.

4.8.1 Well Plate Material

The first design element the team explored was the use of three different well plate materials which included polydimethylsiloxane (PDMS), a glass-bottom well plate, and polystyrene (the standard well plate). After thorough research, the team confirmed that all materials did not violate any constraints within the Pugh matrices. The team also decided to neglect monitoring, ease of programming, and reproducibility for this section of the Pugh matrices, as it is not applicable to well plate materials.

4.8.1.1 PDMS

The first well plate material the team analyzed was polydimethylsiloxane (PDMS), which is an elastic silicone that has relatively low fabrication costs. Even though it is easy to fabricate, it can be more cumbersome to produce since it involves mixing reactants, degassing gel, and curing within an oven. Though PDMS is transparent, imaging capabilities through PDMS can be improved by minimizing the surface roughness through polishing. Despite this method of modification however, it is still difficult to produce high-quality images through PDMS with a microscope. The material and mechanical properties of PDMS may also be easily altered through the mixing ratio of polymer or by adjustment of the temperature at which it is cured. This material is easily sterilized by ethanol, dri-clean detergent, high temperature autoclaving, and UV light treatment, which means PDMS can be reused as long as no stimulation is present [58].

4.8.1.2 Glass Bottom Well Plate

The second well plate material the team chose to focus on was glass-bottomed well plates because of their improved visualization capabilities. The glass coverslip that is tightly bonded and sealed to the bottom of the well plate allows for high quality microscopic images. Glass-

bottom well plates are cheap to purchase, sterile, and can be re-sterilized. Their inability to be reused however, also makes them easy to clean since it is just disposed of. Unlike PDMS, the brittle glass well plates shatter easily making them not as durable compared to other materials.

4.8.1.3 Polystyrene

The final well plate material explored was polystyrene, which the material a standard cell culture well plate is made of. Much like the glass bottom well plate, the polystyrene well plates are not reusable; they are a single use material. Since polystyrene is less brittle than glass but more brittle than PDMS, its durability is better than a glass plate, less durable than PDMS in terms of large drop forces (ex. Being knocked down from the benchtop). Though PDMS is less brittle than polystyrene, its durability is also affected by fatigue due to mechanical stimulation. Polystyrene well plates are the most accessible well plate material because of their frequent use and availability within the lab. It is also a transparent material, making it easy to image with a microscope.

4.8.1.4 Results

Following the objective scoring, the polystyrene well plate scored the best in relation to the objectives with a weighted average of 3.905 (see Appendix B). The PDMS material scored the next highest with a score of 3.595 followed by the glass-bottom well plate with a score of 3.448. The polystyrene scored the highest in the ease of use objective due to its ease of disposal. The glass-bottom well plate and the polystyrene well plate scored similarly for their ease of use and visualization, however, due to the brittle property of glass, the glass-bottom well plate fell short in the durable sub-objective.

4.8.2 Construct Anchoring

To ensure that a cardiac patch can be stretched inside a well plate, the construct must be secured before mechanical stimulation can be applied. For this design element, the team decided to investigate three different mechanisms for anchoring the construct: building a frame into the well plate, using the PDMS frame, and using the inverted PDMS frame. After thorough research,

the team determined that the all techniques would not violate any constraints. The team also decided that reproducibility, limited monitoring, and reusability were not applicable for this design element. The remaining applicable objectives were used to score the three different anchoring techniques.

4.8.2.1 Built into Well

A frame built into the well would be created using a PDMS well plate. The mold for the PDMS would feature a construct frame near the bottom of the well which the fibrin threads and construct could be attached to. This would alleviate the need to anchor the PDMS frame to the bottom of the well plate, which would likely require an adhesive. Therefore, this design would have a decreased chance of being damaged or coming apart during operation. With this design however, the entire well plate would need to be re-fabricated for every experiment meaning that if any of the cardiac patches became broken or misshapen, the entire plate would have to be discarded, not just the construct itself. The only training required would involve the knowledge of how to properly assemble the well plate by mixing the PDMS. Finally, the construct would have to be carefully cut out of the well only at the end of the experiment making resection of the construct more difficult for imaging.

4.8.2.2 PDMS Frame

As previously mentioned, the current application of the cardiac patch is anchored to a PDMS frame with fibrin threads extending through the patch and glued on both ends of the frame. Leveraging an existing component would allow for the same ease of assembly and limited training necessary which is already beneficial in the current design. Concerns however lay with securing the frame to the well plate which will impede on its level of durability since it is not actually permanently anchored. Imaging for this design will still remain simple, quick, and easy especially compared to the built-in frame as previously discussed.

4.8.2.3 Inverted PDMS Frame

As previously mentioned, the inverted PDMS frame would involve a frame with posts that extrude downwards into slots in the plate. For this design, a well plate with a stretchable

bottom would need to be utilized. Similar to the regular PDMS frame, the inverted PDMS frame would allow for easy removal and imaging throughout the course of the experiment. While durability may increase due to a lock-and-key fit with the posts and slots, there is a major challenge with deformation of the well plate following fatigue of the posts. The nearly identical design of the inverted PDMS frame to the regular PDMS means that cleaning and assembly would remain easy and quick to accomplish.

4.8.2.4 Results

Following the objective scoring, the inverted PDMS frame scored best in relation to the objectives with a weighted average of 3.21 (see Appendix B). The PDMS frame scored the next highest with a 3.139 and following that, the built-in frame with a 2.957. While the built-in frame scored high in durability it fell short to the PDMS designs in all other categories. A large contributing factor which negatively affected the score for the built-in design was its lack of imageability due to the requirement of cutting and moving the frame out of the well at the end of the experiment. The PDMS frame scores were comparable to the inverted version but fell just short in almost every category except cost efficiency.

4.8.3 Mechanical Stimulation Technique

The next design element the team researched was different mechanical stimulation techniques for stretching of the cell constructs. The team decided to narrow their focus to three different stimuli techniques: uniaxial, multiaxial, and shear flow. When evaluating this design element using the Pugh matrix, the team concluded that all design techniques complied with the constraints. Further analysis also determined that durability, level of training, ease of cleaning, ease of assembly and easy of programmability could not be evaluated for this specific design element due to inapplicability. Visualization and cost were also not taken into account when determining the best course of action for the stimulation.

4.8.3.1 Uniaxial

Uniaxial strain refers to the application of force being exerted in only one direction. Because of this, high and variable stresses tend towards the anchoring points of the structure and a more uniform stress distribution in the direct center. The effect of this technique may also depend on the material's Poisson's ratio where a perpendicular force acts on the material construct [59, 60]. Due to this ratio and uneven distribution of stresses, the effects of this technique can be hard to quantify and present itself with less accurate and precise data. Shear stresses can also result from unintended friction or imperfect loading but can be alleviated with careful design [60]. The effects of these faults mean some monitoring is necessary for this technique however, since the technique is performed in only one direction, assembly and programming is easier.

4.8.3.2 Multiaxial

The second stimulation technique the team analyzed was multiaxial stimulation which distributes strain in multiple directions. The use of this technique can eliminate shear stresses experienced in uniaxial stimulation and allow quantifiable force distribution that is more accurate and precise. Because multiaxial stimulation requires more direction, assembly and programming becomes slightly more difficult. Similar to uniaxial stimulation, multiaxial may also require a certain amount of monitoring, but should remain reusable [59, 60]

4.8.3.3 Shear Flow

The final technique evaluated was shear flow which is defined as shear stress that is induced by fluid flow. One advantage to this technique is its ability to provide an environment that mimics blood flow through the heart. Despite this major advantage, there are many drawbacks to this design including difficulty in measuring and calculating the amount of stress on each cell. To overcome this, computational fluid dynamics modeling would need to be utilized which would require training [59]. Furthermore, the media used for a shear flow system would need to be replaced over time for growth and sterile purposes. Additionally, each well will

need its own individual shear flow system to avoid contamination which makes assembly, programmability, and reusability of this technique more difficult [61].

4.8.3.4 Results

After fully researching and analyzing each technique, multiaxial stimulation scored the highest with a 4.350 due to its high precision and accuracy (see Appendix B), followed by uniaxial with a 4.046. Both multiaxial and uniaxial stimulation ranked the same for reliability however, multiaxial simulation proved to provide better force distribution, thus giving it a higher score in the reproducible category. Though uniaxial had a higher score than multiaxial for ease of use, the reproducible category was deemed more important and therefore had a greater weighted average making multiaxial the top ranked technique. The least ranked technique was shear flow which resulted in a score of 2.922. Most of this score was affected by its lack of reproducibility and reusability.

4.8.4 Force Production

In order to provide mechanical stimulation, different force production techniques were analyzed. The team agreed to assess three different techniques: stepper motors, vacuum pressure, and magnetic beads. First and foremost, these techniques were evaluated to confirm that they did not violate any of the constraints. After further research, it was determined that stepper motors and vacuum pressure systems would not infringe on any constraints. The magnetic beads, posed possible interference with the lab incubator due to the metal trays it holds as well as its difficulty to be easily sterilized. Because of these tentative results, the team decided to eliminate the magnetic beads and further invest their time into the possible use of stepper motors and vacuum pressure. These two force production techniques were assessed based on the top four objectives since the visualization objective is not applicable for this design element.

4.8.4.1 Stepper Motors

Stepper motors are a commonly used rotating actuator which converts digital signals by steps into mechanical movement [62]. The small size of the device and use of an open-loop controller allows for little maintenance and easy assembly with programmable abilities. These motors work in a wide range of speeds while still remaining fairly inexpensive. They are designed with precise positioning and repeatability, however tend to have a low accuracy of 3-5% of a step [63]. Due to their lack of contact bushes in the motor, they are reliable and dependable compared to other resources. They are also easy to clean and require very minimal training.

4.8.4.2 Vacuum Pressure

One of the biggest advantages of using a vacuum pressure system is its ability to create multiaxial strain. Durability and reusability also make them a great design element for applications that are especially concerned with limited monitoring. Despite their multiaxial strain production, the system is only somewhat accurate and precise due to errors that may easily occur during installation, operation, or calibration. Although it is easy to operate and clean, it does require minimal training.

4.8.4.3 Results

Based on this background research, stepper motors were calculated to be the best method for force production over vacuum pressure. Stepper motors resulted in a summed score of 5.602 (see Appendix B), while vacuum pressure followed not too far behind with a 5.364. Although both methods were rated to have equal reliability, reproducibility, and cost efficiency, the difference was in their ease of use, which made stepper motors the winner. Unlike vacuum pressure systems, stepper motors are much easier to assemble with little to no training necessary.

4.8.5 Force Analysis

In order to understand the degree of force being applied to the construct, a force analysis tool is needed. The team decided to investigate two options: a load cell and displacement system. For the load cell component, two different types of load cells were analyzed; the strain gage and

hydraulic load. Research proved that all components did not violate any constraints. The design objectives visualization, ease of assembly, and ease of cleaning were disregarded due to their inapplicability.

4.8.5.1 Load Cell

A load cell is a type of force transducer that converts force into an electrical voltage. The team looked at two major types of load cells, strain gage and hydraulic, which are useful for the goal of this project. Strain gage load cells are the most commonly used, and operate based on the change in resistance of a strain gage as it physically deforms. Strain gage load cells come in a variety of accuracies and configurations and can range from incredibly cheap hobby-store units to highly accurate calibrated industry units. They are suitable for measuring many loading modalities, including tension, compression, and bending. Hydraulic load cells measure weight (force) in terms of a change in the pressure of the fluid within the cell. Properly calibrated hydraulic load cells can be accurate to 0.25% of the full scale or better. They have no electrical components making it useful in hazardous areas but monitoring of the output may be challenging. Load cells as a whole are considered to be accurate and precise as well as easy to program.

4.8.5.2 Displacement

Another option is direct measurement of displacement for the system. Displacement is a simple way to measure a force and represents the degree to which the object deforms in one or more directions under load. It can be measured with something as simple as a ruler, or via an imaging algorithm such as pixel mapping. For this application, the team would be interested in how much the cardiac patches deform in the direction of the load. Durability for this case would not be of concern, however more monitoring would be needed since measurements of the displacement would have to be taken over time in order to obtain consistent and accurate data. Proper measurements for displacement would also require some training for the user. There are challenges in maintaining accuracy and precision for this system since it is very susceptible to user error.

4.8.5.3 Results

Based on the team's research, load cells were found to be the best fit for this design element with a score of 5.977, while displacement measurements scored a 4.469 (see Appendix B). Load cells were considered superior to displacement measurement in all categories except durability because of their high precision, ease of programming, and affordability. In the case of durability, the team was concerned that the humidity within the incubator would affect load cell performance.

4.9 Revision of the Pugh Matrix Analysis

Due to new information about design parameters that were given to the team by the client and user, the team re-organized their Pugh matrices to encompass the updated needs and wants from the client and user. It became apparent that the team did not need to consider the multi-axial design element in the mechanical stimulation technique Pugh matrix (see Appendix B) since the client and user merely wanted to stretch the cardiac patches in a uniaxial direction. Therefore, the multi-axial design element was blacked out in the updated mechanical stimulation technique Pugh matrix (see Appendix B). Table 11 below shows the top ranked design ideas that the team chose to focus their refined design ideas upon. However, since the team had not become aware of this mechanical stimulation technique change until after the refined design ideas had been solidified, multiaxial stimulation is still considered in Section 4.8 above.

Table 11. Summary of the Pugh matrix scores

Design Element	Ideas	Scores
Well plate material	PDMS	3.595
	Glass Bottom	3.448
	Polystyrene	3.905
Construct anchoring	Built into well	2.957
	Vellum frame	3.139
	Upside down Vellum	3.210
Mechanical stimulation technique	Uniaxial	4.046
	Shear flow	2.922
Force production	Stepper motor	5.602
	Vacuum pressure	5.36
Force analysis	Load cell	5.977
	Displacement	4.469

4.10 Refined Design Ideas

Following the initial design components that were thoroughly and quantitatively analyzed within the Pugh matrices, the team came up with more detailed and refined designs. All three designs were created with the constraint that the device must operate and fit within a standard cell culture incubator in order to maintain a proper cell growth environment.

The first design concept developed centers around an off-the-shelf polystyrene well plate and was nicknamed the “Jazzy Imaginative Mechanical-Stimulator”, or “JIM”, for short. In this design, the PDMS frame, which holds the cardiac patch, is placed within the well and attached to a linkage system that connects to a stepper motor to uniaxially actuate the walls of the PDMS frame. The linkage would be based on a rack and pinion mechanism with two parallel rails connecting to a stepper motor via gears. The rails would then extrude down through machined holes in the polystyrene well plate lid to attach to the walls of the PDMS frame. The tensile force would be applied to one wall while the other wall is fixed to the well plate, so only one wall of each frame needs to be clamped. The mechanical linkage and PDMS frame walls would be composed of metal and rigid plastic respectively which will not deform significantly under the load required to stretch the cardiac patches. This makes the transfer of forces from the stepper motor to the cardiac patches more direct, allowing the cardiac patches to be stretched more

uniformly. One major advantage to this design is its use of a standard well plate which is less expensive than manufacturing a custom plate. Despite this however, a new lid would need to be manufactured which may compromise the sterility and sealing of the well plate. Difficulty in sealing may also come from the junction between the well plate lid and the rail extrusions. This is a major concern for the well plate environment and provides more difficulty for assembly for the user. This design is also mechanically complex, and could present difficulties for ease of assembly, which was a key concern of the client and user.

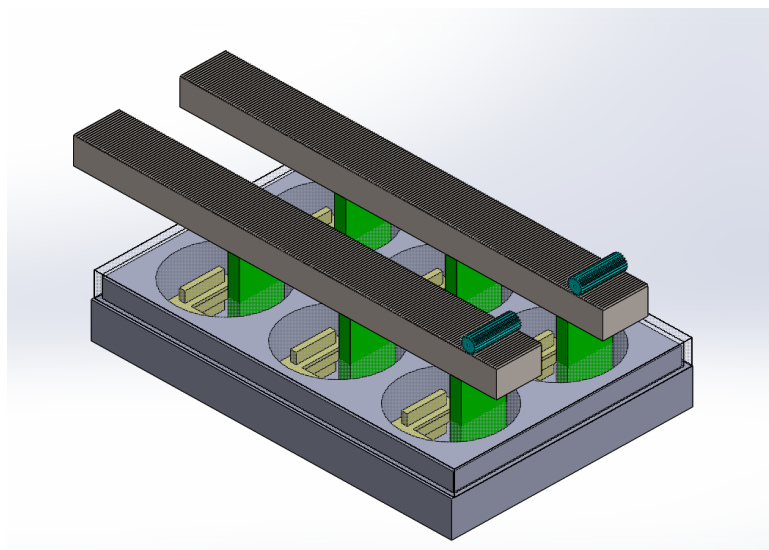


Figure 16. “Jazzy Imaginative Mechanical-Stimulator” concept

The second design concept was alternatively developed around the use of a PDMS well plate and was given the name Staple Stretcher. To create the custom PDMS well plate, a reusable negative mold would be designed and 3D printed allowing for fabrication of the well plate. The design utilizes a revised version of the inverted PDMS frame concept as mentioned previously in Section 4.5.4. For this design however, the frame will incorporate four extended walls instead of four posts and which fit into small cavities within each well (see Figure 16). This will function as an anchoring system while also allowing for easy removal. Exposed cutouts underneath the PDMS well plate will be positioned around the rigid walls fitted within each well where a gripping system will clamp the walls through the PDMS as shown in Figure 18. Clamps that lie within these spaces would connect to stepper motors to produce the mechanical stimulus in both the x and y directions. Though this design offers a more direct linear force distribution across the

construct, certain concerns lie in the complexity of the design and cost of the custom PDMS well plate. Detailed drawings of this design can be seen in Figure 17 and Figures 19-21.

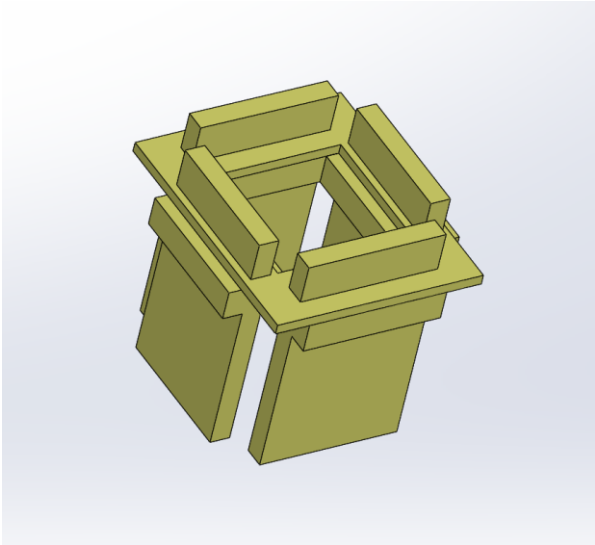


Figure 17. Four wall inverted PDMS frame

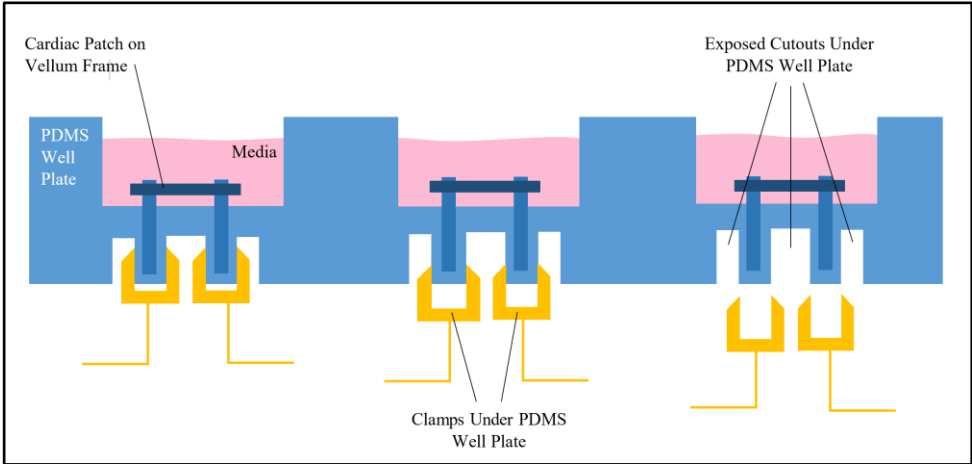


Figure 18. Side view of staple stretcher concept

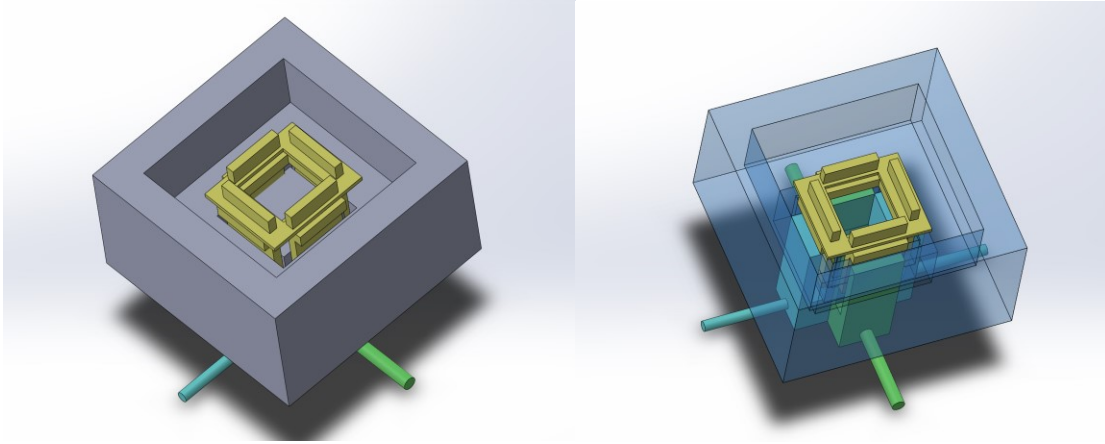


Figure 19. Single well isometric top view of staple stretcher concept

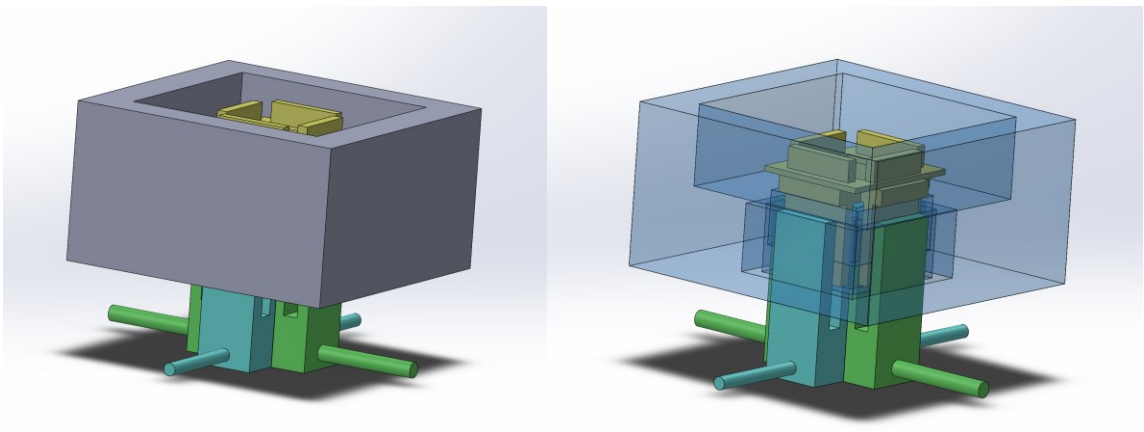


Figure 20. Single well side view of staple stretcher concept

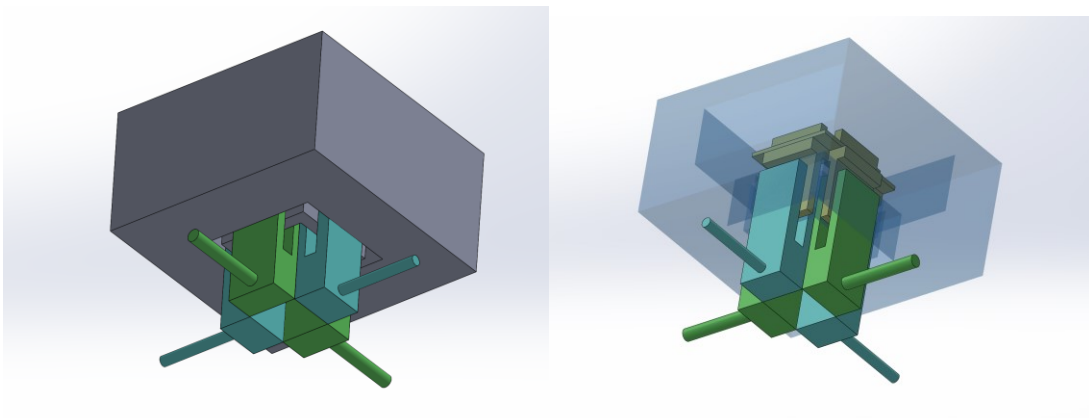


Figure 21. Single well isometric bottom view of staple stretcher concept

The third design concept has elements similar to the staple stretcher design described above, such as the use of a PDMS well plate and improved inverted PDMS frame. However, in this design, the well plate would have six wells all aligned in a row. The mechanical system for this design will encompass two horizontally extended walls for lateral stimulation and two end posts for axial stimulation (see Figure 22). These walls and posts will be located underneath the PDMS well plates within duvets that will push and pull the construct in both directions. The horizontal walls may promote a more uniform and direct force distribution than posts since it will sit directly in front of all six wells. The directions of the mechanical stimulation will work independently from one another to prevent resistance and distortion of forces. In other words, the posts will provide an axial stimulation to the construct, return to its original position, stop, and then proceed to initiate lateral stimulation from the horizontal walls. The goal of this design concept aimed to provide multiaxial stretch to the cardiac patch, thus yielding an adequate biomimetic stimulation. This design was advantageous because of its simplicity in comparison to the Staple Stretcher and J.I.M. Additionally, the inverted PDMS frame makes for easy removal for imaging throughout the experiment. The team however, was concerned about the force distribution due to the shape of the design and non-linear nature of PDMS.

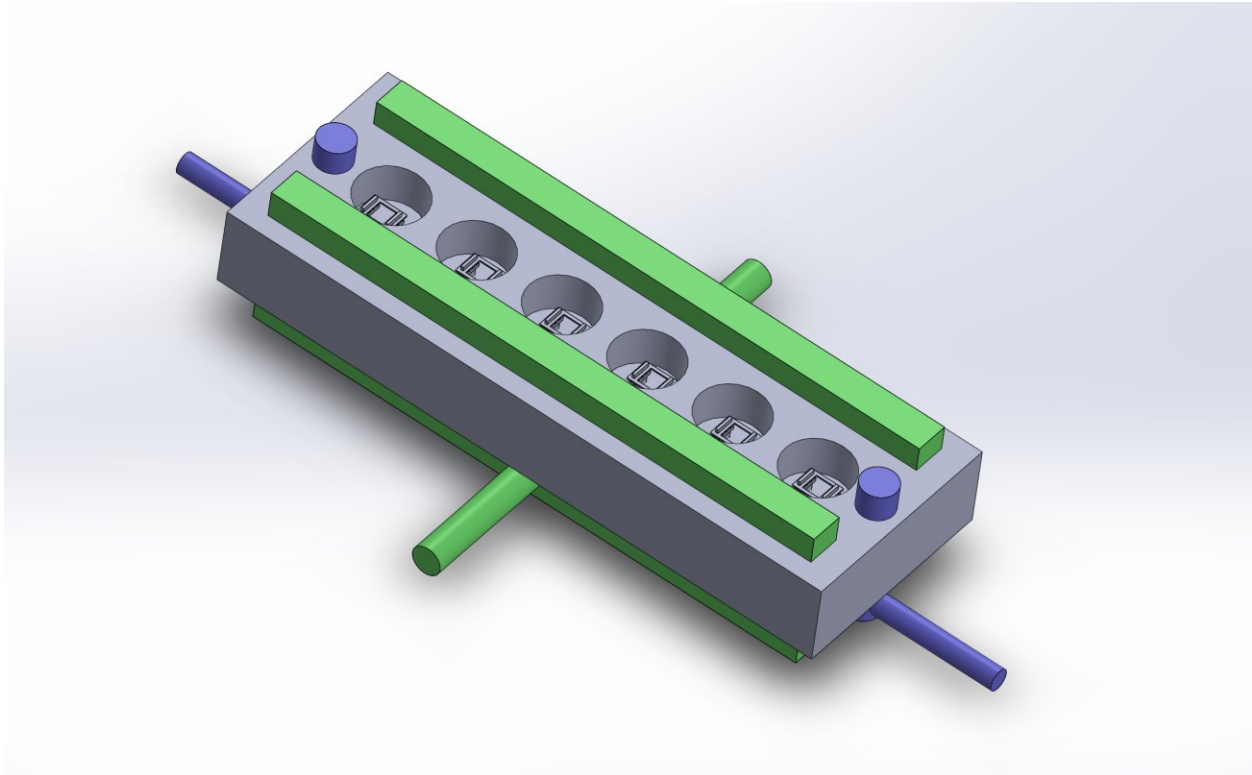


Figure 22. Upside down concept

4.11 Development of the Final Design

Following the analysis of the Pugh matrices and narrowed down concepts, the team voted and agreed that the final design will be based off of the inverted PDMS frame with the PDMS upside down well plate model. After this decision was made, the team further analyzed the design in detail to review all components and assess feasibility. Once the team agreed on the design, CAD drawings were created using Solidworks 2018 (Dassault Systems), followed by finite element analysis (FEA) (Solidworks 2018, Dassault Systems) to visualize and mechanically map out the applied stresses in the design. The drawings and FEA map was then shown to the client and user for approval and further evaluation of the design. The team then agreed on a conceptual mechanical system which involved the use of a stepper motor. The idea was to use one stepper motor coupled to a lead screw to move one end of the well plate, which will be secured with clamps. The opposing end was to be fixed in a stationary position, to minimize the need for additional components and ensure uniform strain. The overall design was

broken down into four different components: the well plate, the lid, the PDMS frame, and the mechanical stimulation. These four components are further outlined in the following sections:

4.11.1 PDMS Well Plate System

The first component of the final design consists of a molded PDMS well plate. A negative cast of this well plate was 3D printed and used as a reusable mold for easy assembly. The mechanical properties of the PDMS can be altered by changing the mixing ratio of curing agent to base [64]. The well plate was also designed to have a ‘dog bone’ shape in order to ensure the cardiac patches in the wells experienced uniform strain. The wells were aligned in a 2x3 formation identical to that of a standard well plate in order to minimize the size of the design for placement in the incubator. The well plate was molded with designated holes on each end for easy placement of the metal posts for mechanical stimulation as described in section 4.9.3 below, along with rectangular cavities within each well for placement of the PDMS frame.

Multiple concepts for the PDMS well plate were created using Solidworks. Initially, the team was concerned primarily with creating a shape for the well plate that would yield a distributed linear strain profile in the wells. This is important for ensuring that the cardiac patches are stretched uniformly. Tentative dimensions reflecting the overall size of the well plate were not considered in the following two designs, as shape was the main focus.

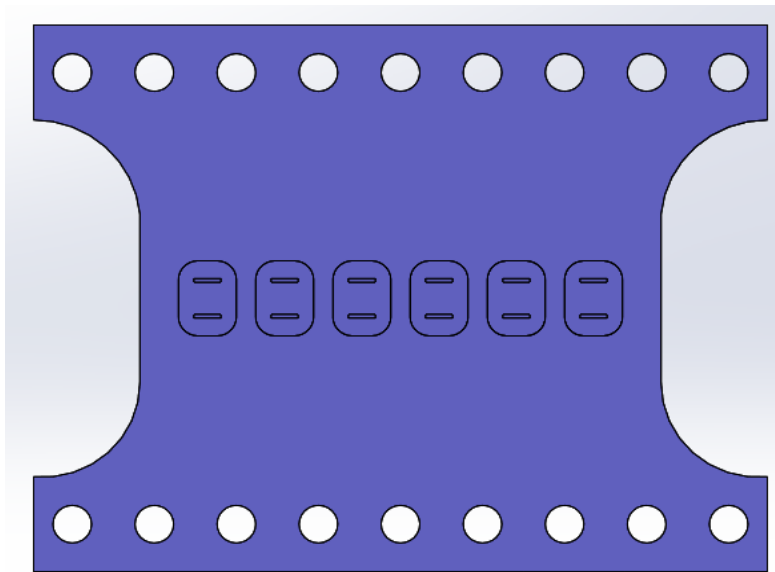


Figure 23. “Butterfly Squares” Well-plate concept

Figure 23 above shows the top view of the Solidworks model of the first well plate concept, named “Butterfly Squares” by the team for its shape. It features six rounded-square wells (for easier media transfer) in a row with extruded cuts to accept the re-designed PDMS frame with extruded walls, shown below in Figure 24.

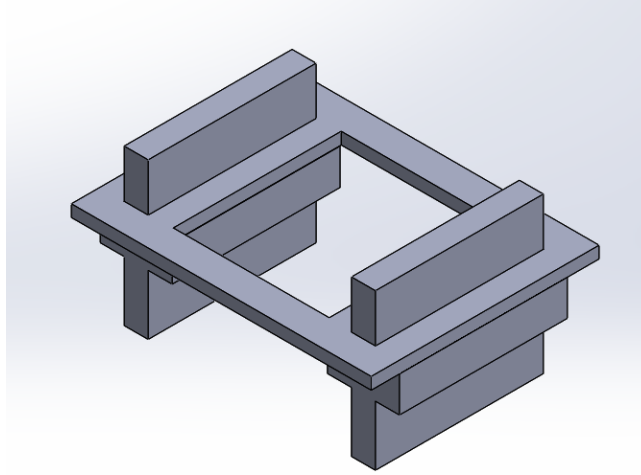


Figure 24. PDMS frame with walls

To evaluate the potential of the “Butterfly Squares” design, a simple Solidworks finite-element model was created. Tentative material properties of Sylgard 184 PDMS cured at 25 degrees Celsius were used to determine the force required to achieve 10% strain in a center cross-section of the well plate [65]. Based on literature documenting the tensile properties of bulk Sylgard 184, we assumed that the PDMS exhibits linear elastic stress-strain behavior up to 10% strain [65]. Thus, the stress (σ) needed to produce 10% strain can be calculated using Hooke’s law and the Young’s modulus of the PDMS, 1.32 MPa:

$$\sigma = E\varepsilon = (1.32 \text{ MPa}) * (0.1 \text{ mm/mm}) = 0.132 \text{ MPa}$$

From there, the force required can be calculated using the stress and the cross-sectional area (A) of the well plate in the center:

$$F = \sigma A = (0.132 \text{ MPa}) * (60 \text{ mm}) * (270 \text{ mm}) = 2138.4 \text{ N}$$

A static simulation in Solidworks was created where the tensile force was applied to one end of the well plate, with the other end being fixed in place. The model was then meshed and solved. Figure 25 below shows the strain profile calculated by Solidworks.

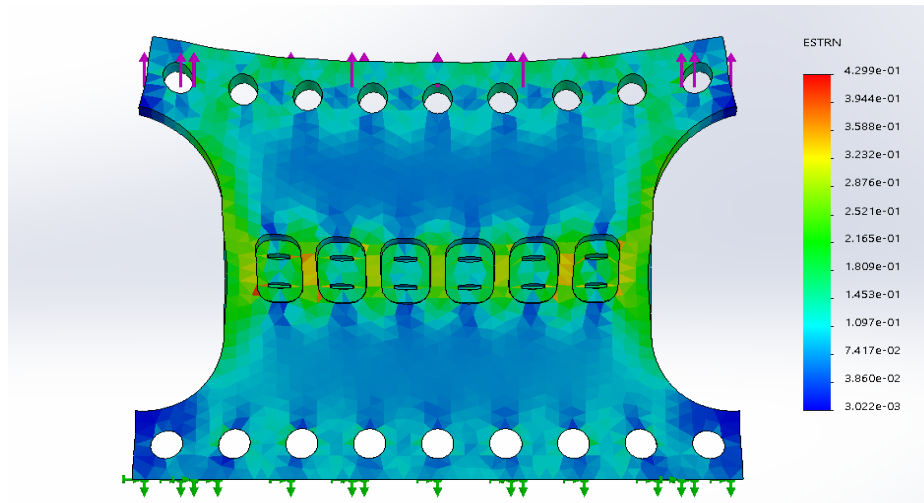


Figure 25. Finite-element strain profile of the “Butterfly Squares” concept

The finite element model, being a static study where the force is applied in a single step rather than in multiple small iterations, is not the most suitable model when strains exceed 6% (Solidworks, 2018). This limits the conclusions that could be drawn from the simulation; however, the strain within the wells ranged anywhere from roughly 10.1% to 25% on average, and even as high as 43% in some small regions of the mesh. Though at this stage it was undecided what an acceptable strain tolerance was, a tolerance band of .1 mm/mm + .25 was unacceptable.

In an effort to improve the strain profile in the region of the wells, a new concept was created in Solidworks that was essentially a scaled-up version of the “Die C” dog-bone test specimen geometry from ASTM D412-16, a standard test method for tensile testing of vulcanized rubbers and thermoplastic elastomers [66].

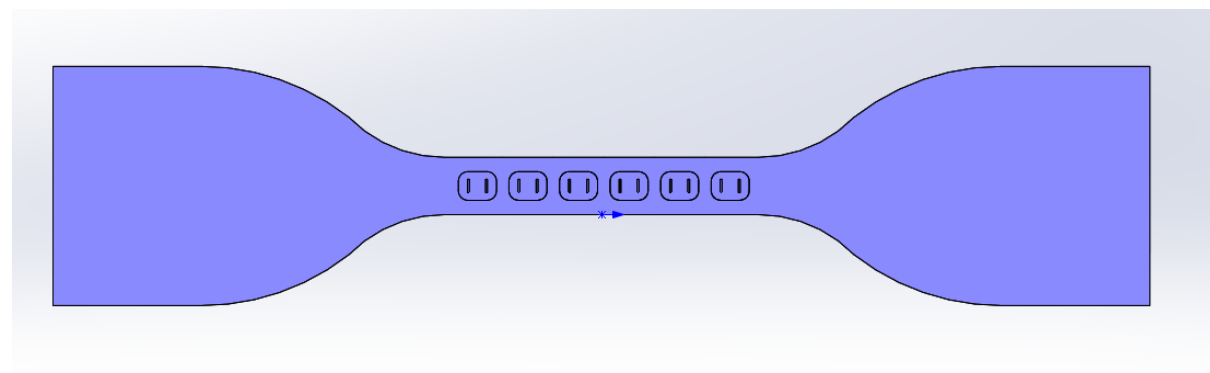


Figure 26. ASTM Die C well plate concept

This dog-bone shape reduces the effect of the high forces experienced at the ends of the specimen when pulled in tension, so it was thought that the same property would hold if it was scaled up (seen in Figure 26). A finite element model was created similarly to the “Butterfly Squares” design. The force was calculated as

$$F = \sigma A = 0.132 \text{ MPa} * 60 \text{ mm} * 60 \text{ mm} = 475.2 \text{ N}$$

The equivalent strain calculated by the Solidworks simulation is shown below (see Figure 27)

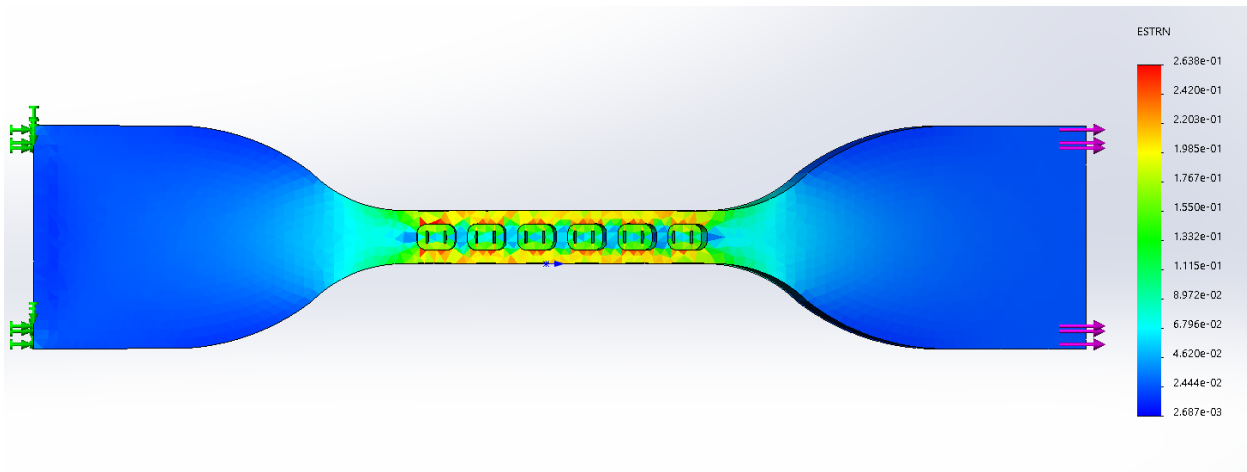


Figure 27. Finite-element strain profile of the ASTM Die C well plate

The strain in the well regions ranged between about 4.6% to 17.7%, which would correspond to a strain tolerance band of 0.1 mm/mm \pm .177/ - .054. While this improves on the previous design, it is still a substantial deviation from the target strain of 10%.

To further develop the final design of the well plate, the team looked at the dimensions of the previous two designs, particularly the overall size. In both cases, the cross-sectional areas of the well regions are quite large, requiring nearly 500 lb and over 100 lb of tensile force respectively. The hardware required to produce this force will undoubtedly be cost-prohibitive on a budget of \$1000. Additionally, the overall lengths of both designs exceed 1 foot, with the ASTM D412 Die C design being nearly 4 feet in length. With the limited incubator space available to the team, both designs would be impractical as they would not fit in an incubator, especially considering the extra hardware required for the force production system.

With the constraint of fitting the entire system on a shelf in an incubator, the team worked to minimize the size of the well plate designs. Both the “Butterfly” and “ASTM Die C” well plate concepts were remodeled with a smaller length, width, and depth. The dimensions of each well were also adjusted to allow them to contain sufficient media to sustain the cardiomyocyte patches. Additionally, the two grooves in each well were removed following tensile testing that will be detailed in Chapter 5.

4.11.2 PDMS Lid

In addition to the PDMS well plate, a custom PDMS lid with a mixing ratio of 20:1 would be created in correspondence to the shape of the well plate and allow for proper gas diffusion to promote cell culture conditions, while also minimally affecting the mechanical stress applied to the wells of the well plate. To achieve this goal, a three piece negative mold was printed so the lid may perceive identical shape relations to the top surface of the well plate. To compensate for the clamps that will hold the ends of the well plate, the lid was designed to wrap around the border of the well plate as shown in Figure 28.

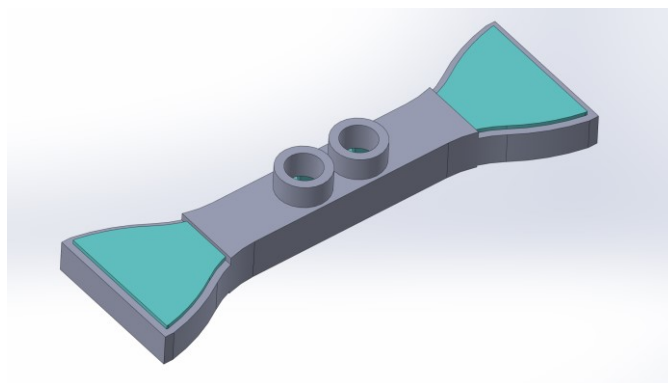


Figure 28. PDMS lid model with wrapped around ends (grey) on well plate (teal)

With this method, a proper seal would be achieved with minimal effects on the translated strain throughout the well plate. This design however, may create shear forces and require higher force production from the stepper motor due to the additional rubber band effect of the lid. In an effort to overcome this problem, the team also theorized the idea of cutting off the ends of the lid that wrap around the well plate and instead have it only be laid over the wells (see Figure 29).

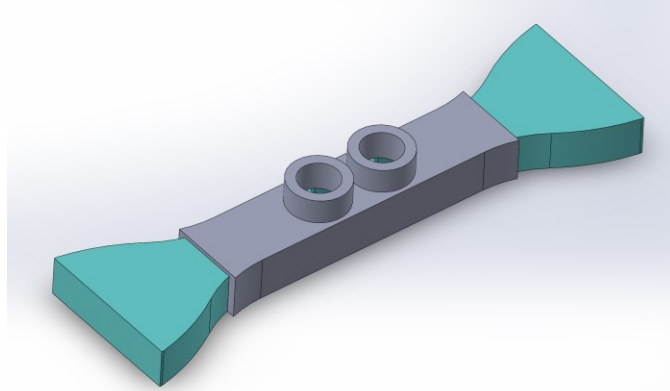


Figure 29. PDMS lid model without wrapped around ends (grey) on well plate (teal)

The implementation of this method will allow for less forces to interfere with the overall stretching of the well plate and force required by the stepper motor. The design may or may not however be properly secured around the well plate. Mechanical stimulation and cell culture tests would be done to validate and determine which method would be most compatible with the well plate. Aside from the shape, a key element of the lid design was the usage of filter caps from tissue culture flasks (otherwise known as T-flasks). T-flask filter caps are designed to allow for proper gas diffusion needed to maintain cell culture. In order to utilize this pre-designed tool, the lid was molded with two cylindrical protrusions, with each protrusion sitting between two wells. The protrusions are to be hollowed out by puncturing a circle with a round steel hollow hole punch tool with a diameter of 15 mm. Therefore, the T-75 flask filter caps may be placed onto the hollowed protrusions, thus allowing for properly filtered air diffusion for the cells.

4.11.3 Stepper Motor

In order to select a stepper motor that would be capable of cyclically producing 10% strain in the wells, the team first considered the force required to produce that strain. The stress needed to produce 10% strain in the narrow gage-length section of the well plate is calculated as follows, assuming the PDMS material has a Young's modulus of 1.32 MPa [65]:

$$\sigma = E\varepsilon = (1.32 \text{ MPa}) * (0.1 \text{ mm/mm}) = 0.132 \text{ MPa}$$

From there, the force required can be calculated using the stress and the cross-sectional area (A) of the well plate in the center, subtracting the cross-sectional area of the well cutouts:

$$F = \sigma A = (0.132 \text{ MPa}) * (20 \text{ mm} * 26 \text{ mm} - 21.4 \text{ mm} * 17.8 \text{ mm}) = 18.4 \text{ N} = 4.14 \text{ lbf}$$

The torque (T) required to produce that force at constant velocity can be calculated using the screw lead (L) and the rated efficiency of the screw (e). ACME lead screws that we were likely to use in the design range in efficiency from 30% to 50%, so a worst-case value of 25% was used for this calculation [67]. The following calculation is for a 12.7 threads per inch lead screw, with a lead of 0.0787 in * 4 starts = 0.3148 in:

$$T = F * \frac{L}{2\pi e} = 4.14 \text{ lbf} * \frac{0.3148 \text{ in}}{2\pi(.25)} = 0.8297 \text{ lbf} * \text{in} = 13.28 \text{ oz} * \text{in}$$

With this torque requirement in mind, the team sought out a stepper motor that would be easily integrated with an Arduino microcontroller. Adafruit's NEMA-17 stepper motor suited our needs, as there is substantial documentation for its use with an Arduino via a stepper motor controller shield and an Arduino code library allowing for easy programming of the system. Since this stepper motor is rated to a maximum holding torque of 28 oz*in, using this motor will yield a safety factor of 2.108, leaving room for frictional demands and acceleration torque.

4.11.3 Mechanical Stimulation

In order to improve ease of assembly while maximizing the mechanical output of the design, one end of the well plate would be clamped to a stationary platform while the other end would be clamped to a moving platform driven by a lead screw. On the stationary end of the platform, a stepper motor would be fixed onto a bottom base surface and attached to the lead screw via a shaft coupler. A tapped pillow block would also be implemented near the stepper motor as well as the other end of the lead screw to provide additional stability for the lead screw. An aluminum cube with a lead screw nut fixed in the center to thread the lead screw through, will be attached underneath the moveable platform. In order to provide stability and alleviate additional forces such as weight and friction, two rods would also be added in parallel to the lead screw. The rods would be secured to the base surface with tapped clamping mounts on each end and linear ball bearings would be implemented to minimize friction. Polystyrene would be used to construct the mechanical system's platforms and base surface, because of its ability to be easily cut and shaped, as well as its compatibility with cell culture incubators. The remaining

nuts, screws, and additional parts would all be made of stainless steel, galvanized steel, or aluminum due to the materials corrosion resistance.

When the mechanical system is under operation, the moving platform will move uniaxial in the direction of the rods and lead screw. The ball bearing attached to the moving platform will allow for easy guiding, stability, and movement on the two parallel rods. The lead screw directly center and below the platform will actuate the movement of the platform via a lead screw nut that is held with an aluminum block and attach to the platform. The lead screw is driven by the stepper motor described previously and controlled using an Arduino microcontroller. The Arduino is programmable, allowing for the stretch rate, total stretch, and duty cycle to be controlled by user input. The PDMS well plate will rest on top of both the moving and non-moving platform a polyurethane plate can be seen in Figure 30 below which was used for preliminary testing that is described in Section 5.2. The well plate will be secured to each platform with make shift removable clamps. The clamps will be placed on the ends of the well plate and secured down by tightening the nuts in which screws will go through as seen in Figure 30.

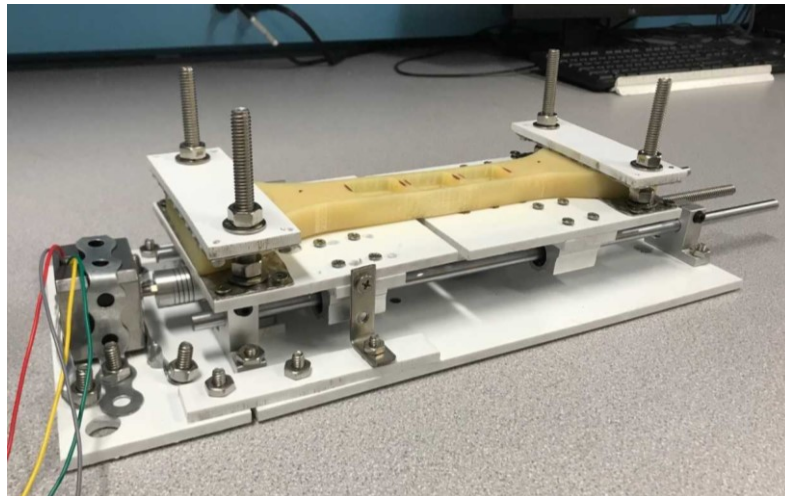


Figure 30. Mechanical stimulator with polyurethane well plate mold

5. Development and Verification of the Final Design

5.1 Evaluating Well Plate Designs

In order to begin testing the well plate designs, the molds for the well plates needed to be fabricated. For prototyping purposes, the team acquired a container of Smooth-On Reoflex 50 (Smooth-On, Macungie, PA), a two-part polyurethane rubber. Negative molds of the well plate designs described in Section 4.11.1 were modeled using Solidworks and printed using additive manufacturing. The molds were each made out of polylactide (PLA) plastic for its low cost and availability in the rapid prototyping labs. Following this, the polyurethane was properly measured and mixed, then poured into the PLA molds. Since PLA has a low glass transition temperature, the rubber was left to cure at room temperature overnight. Initial stretching of the finished polyurethane well plates by hand led the team to the realization that the PDMS frames which were inserted into the cutouts of the wells, were not stretching with the plate. To solve this problem, the team opted to anchor the PDMS frames into the wells using stainless steel pins at each corner of the frame and remove the cutouts from the bottom of the wells. New molds and polyurethane plates were then created using this design.

To evaluate the deformation of each well plate design when stretched to 10% of its original length, tensile testing was performed using an Instron 5544. Each well plate was stretched for 5 cycles at 800 mm/min while force and extension data were collected by the Instron. Representative force-displacement curves can be found in Appendix D.

During these tensile tests, the deformation of the wells were observed. Since the “Butterfly Squares” well plate was gripped by the Instron at only one point in the center with a substantial overhang, the center well appeared to stretch significantly more than the wells on either side, as opposed to a uniform grip. This effect can be seen below:



Figure 31. Tensile stretch of “Butterfly Squares” well plate

The tensile test shown above does not adequately capture the mechanical properties of the “Butterfly Squares” well plate, as gripping it in the center creates distortion under load. To better mimic how we planned to create our final mechanical stimulation system with this design, the team would need to test this well plate with a fixture that gripped it across its width rather than at a small section in the center. The team was unable to find parts in the lab or fabricate parts that would allow for a uniform grip across the well plate by the Instron, without using up a substantial amount of time and funds. Given the time and material costs of trying to accommodate for this however, the team decided against this well plate. The “Butterfly Squares” well plate also has a considerably larger cross-sectional area in the narrow section than the dog bone well plate, making it much stiffer in comparison. A stiffer design would require more torque than the existing stepper motor could produce. This would compromise the system factor of safety, reduce the life of the stepper motor, and potentially prevent the stepper motor from being able to cyclically stretch the well plate at 1 Hz. For these reasons, the team decided to move forward with the dog bone well plate design.

5.2 Well Plate Deformation Mapping and Image Analysis

After deciding to use the dog bone shaped well plate, the team needed to gather experimental data to verify that the PDMS well plate experiences strains within our design specifications when cyclically stretched. Table 9 lists the established nominal strain at $10\% \pm 5\%$. To achieve this, a test protocol (found in Appendix C) was developed for an Instron 5544 universal tensile tester in order to perform a preliminary test on a well plate fabricated from polyurethane. The test was done to ensure that the well plate was able to be cyclically stretched to achieve a 10% stretch within each well of the plate. An acceptable strain range of $10\% \text{ strain} \pm 5\% \text{ strain}$ was established from the literature; 10% strain was used as a target goal. Before analyzing the data, the team established an acceptable range for well strain based on the literature as seen in Table 2. From this literature the team decided upon a target of $10\% \text{ strain} \pm 5\% \text{ strain}$ at 1 Hz. This was also used to verify if uniform strain could be achieved within each of the three wells during tensile testing. Analysis of video recordings taken of each test yielded strains experienced by a PDMS frame anchored in each well during the uniaxial stretch.

5.2.1 Finite Element Model of Well Plate in Tension

A finite-element model was created for the tentative dog bone well plate shape using ANSYS 19.1 (ANSYS, Canonsburg, PA) in order to determine whether the shape would facilitate even strain in each of the wells when the well plate was placed under tension. A static structural study format was used, and the well plate was fixtured at one end and given a tensile force at the other end. The calculations for the force required to stretch the well plate can be found in Section 4.11.3. In running this simulation, it was assumed based on the literature that PDMS exhibits Hookean linear elastic isotropic material behavior at 10% strain, so these properties were assigned to the well plate in ANSYS with an elastic modulus of 1.32 MPa and Poisson's ratio of 0.49 [65]. A top view of the well plate showing the strain in the direction of the load along with callouts illustrating the strain at various points in the wells can be seen below.

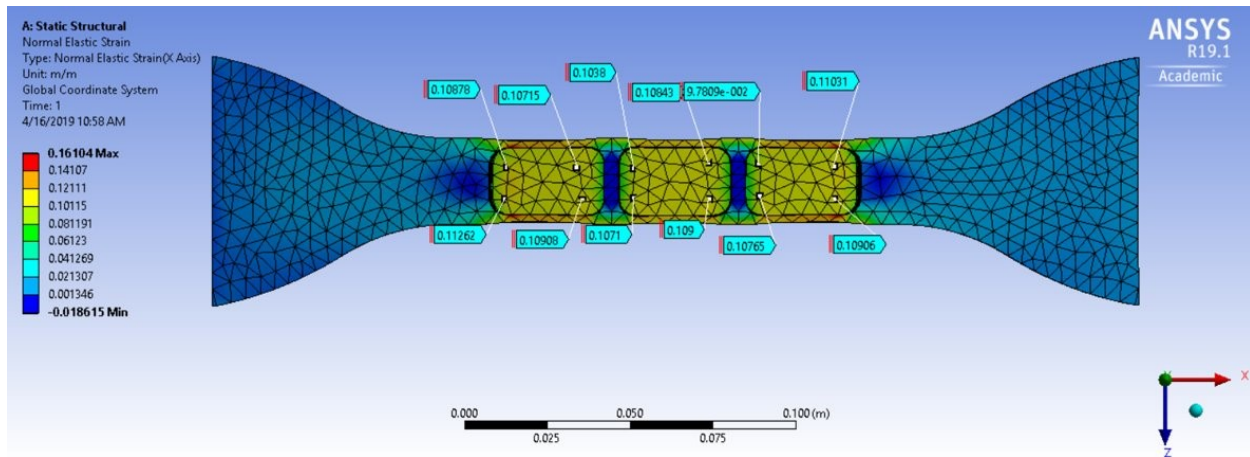


Figure 32. ANSYS Results from static uniaxial tension of well plate

The bottom of the wells where the cardiac patches would be placed, appeared uniformly yellow when loaded, which corresponded to roughly $10\% \pm 1\%$ strain according to the callouts. The team felt that this data predicted that the strain would be even in each well and proceeded to physical testing of the well plate.

5.2.2 Instron Testing of Polyurethane Well Plate

Following the predictive modeling of the well plate design, the team then looked to see if the plate could produce the uniform strains of $10\% \pm 5\%$ within each of the three wells. This was tested on a preliminary basis through an Instron 5544 tensile test of a polyurethane well plate. The cyclic stretch test, featuring five cycles, was recorded using a mounted camera with the length of the well plate present in the field of view. An object of a known length was included in the field of view to provide a scale for the image analysis as described in the protocol found in Appendix C.

Three different testing conditions were explored to evaluate which elongation technique yielded the most accurate strain results while also minimizing force applied to the stepper motor. The plate was first stretched to 10% of the original length of the entire well plate, then 8.6% and 6.7% for the two subsequent trials. In other words, the plate was 269 mm long, so in the first test it was stretched to a total a final length of 295.9 mm (269 mm + 26.9mm), stretching the well plate to its original length plus 10% of its length. This was performed for both the 8.6% and 6.7% trials, which represented 5mm and 10mm decreases in the amount stretched relative to the

first trial. For the 8.6% trial an extra 21.9mm was added to the original length of the plate, and an extra 16.9mm was added to the original plate length for the 6.7% trial. The full Instron test was recorded for each of the three trials and 10 freeze frame images of the well plate were taken following each test. For one test, two images, stretched and unstretched, were analyzed from each of the five cycles, thus accumulating to a total of 10 images per test. The displacement of the PDMS frame in each well was then measured from the images using ImageJ software. The setup and a sample measurement can be seen in blue in Figure 33 below.

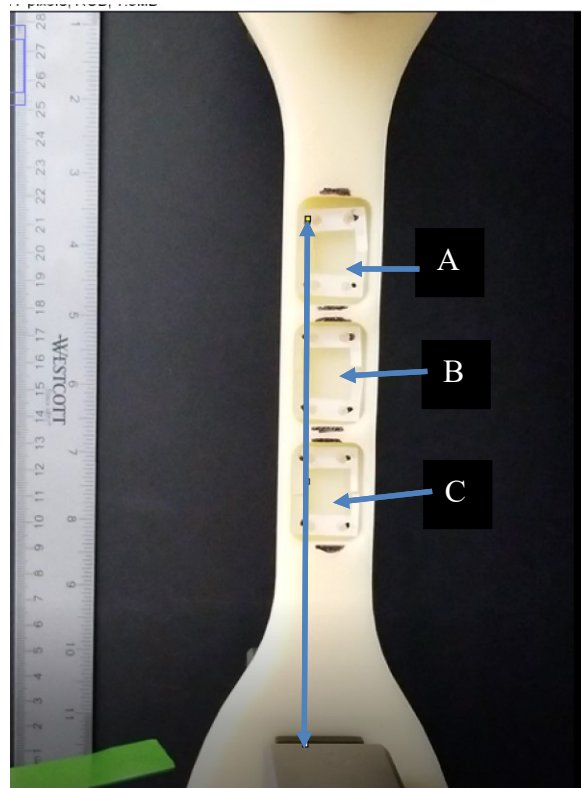


Figure 33. Sample ImageJ displacement measurement (measurement line shown in blue. Also contains top well (A), center well (B), and bottom well (C).)

All measurements were taken relative to a stationary anchor point, the bottom Instron grip. The distance between the well was determined by subtracting the distance of the top dots to the grips from the distance of the bottom dots to the grips. Raw data from the test can be found in Appendix D. After the values were taken, plots were created to show how well the strain data fit into the range of $10\% \pm 5\%$. These graphs can be seen in Figures 34-36 below. Asterisks on the graph mark the place where the mean occurs.

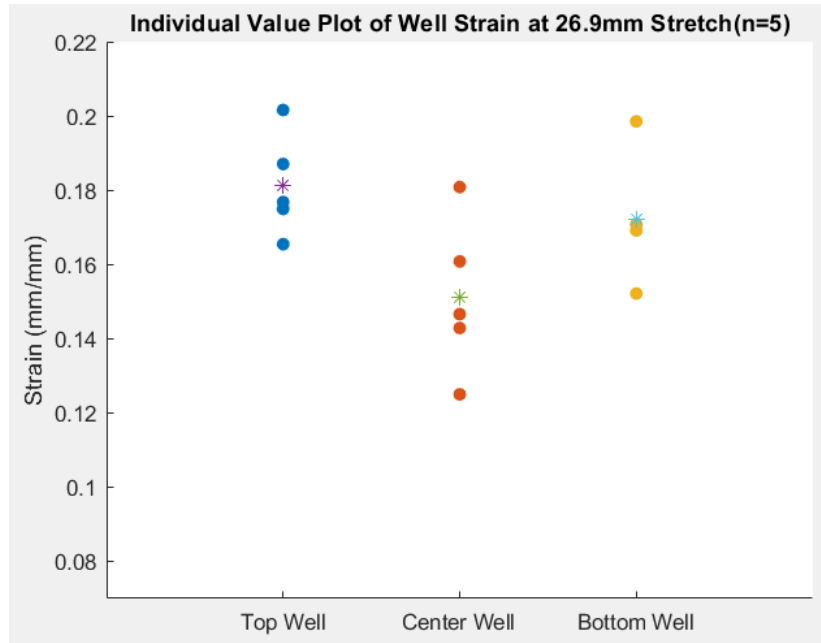


Figure 34. Strain when stretched by 10% of original length (269mm + 26.9mm)

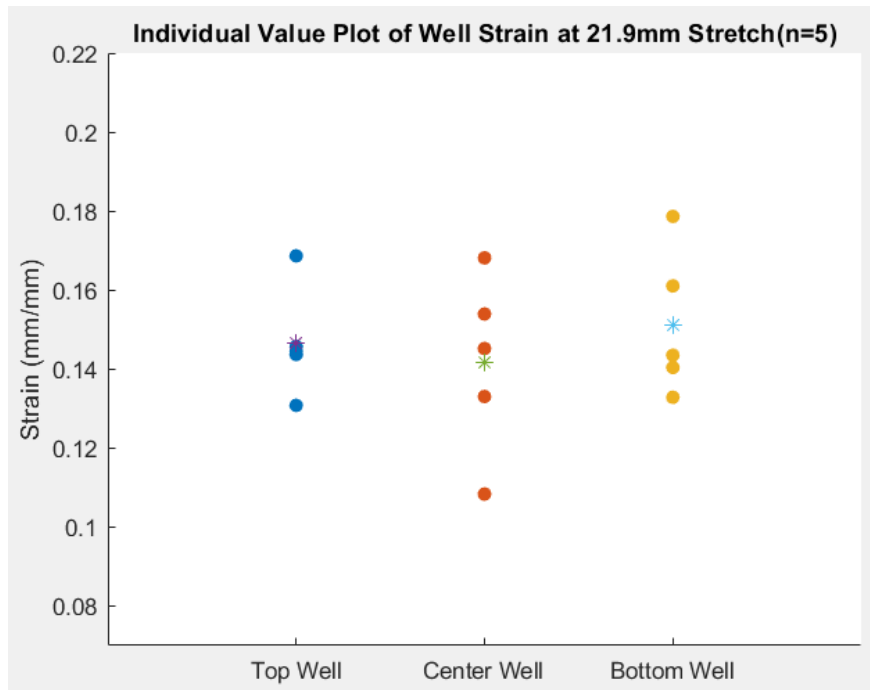


Figure 35. Strain when stretched by 8.6% of total length (269mm + 21.9mm)

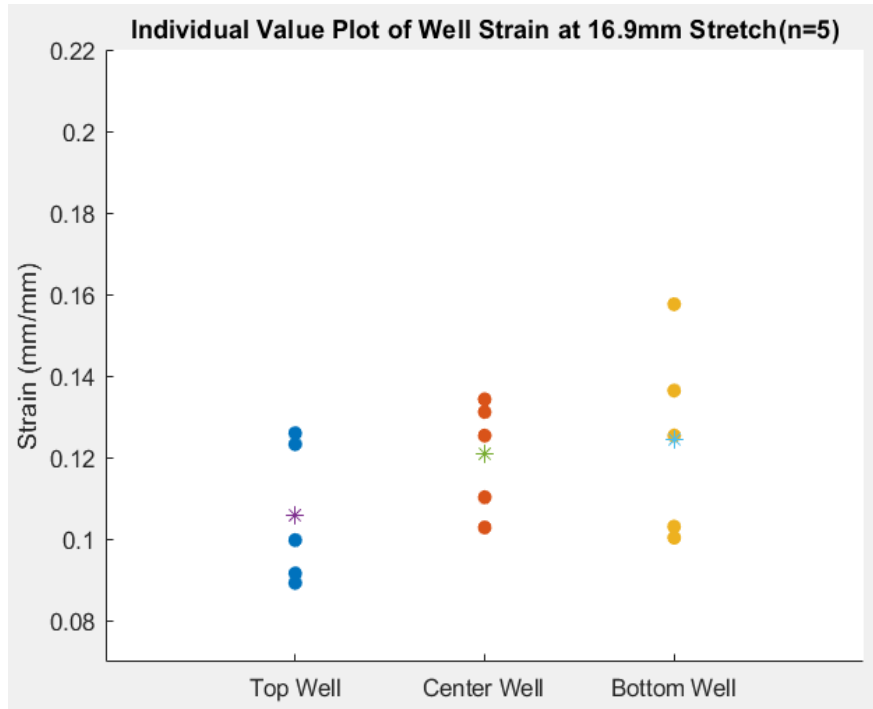


Figure 36. Strain when stretched by 6.2% of total length (269mm + 16.9mm)

It can be seen from Figures 34-36 above that the 8.2% stretch most closely was associated with the target range of 5-15% strain developed by the team.

5.3 Preliminary Testing Outcomes

From this preliminary polyurethane testing, the team was able to gather further information about the best way to test the upcoming PDMS mold. For instance, a consistent gauge length should be set for the plate each time it is tested. This means that every time the plate is put into the Instron the length between the two frayed ends of the dog bone must be the same for every trial to ensure consistency. This gauge length will also be used to determine how much the well plate is stretched. Instead of stretching the plate to 10% of the original length, the plate would be stretched to 10% of the gauge length which is approximately 12.8mm. Additionally, the grip must be tightened to the plate at the exact same location for every test to ensure consistency and that the plate is not pulling farther to the left or right. This consideration became important as the preliminary data showed that there were strain discrepancies between the left and right sides of the same wells. All of these testing changes would be implemented when the final PDMS well plate was mechanically tested.

5.4 Testing of Molds for PDMS Well Plate and Lid

After retrieving our team's 3D printed negative molds of acrylonitrile butadiene styrene (ABS) for the well plate and lid designs, PDMS was measured out with a 20:1 ratio, degassed, and poured into the well plate mold. The mold and PDMS were then placed in an oven at 85°C and cured for 100 minutes [68].



Figure 37. ABS well plate mold

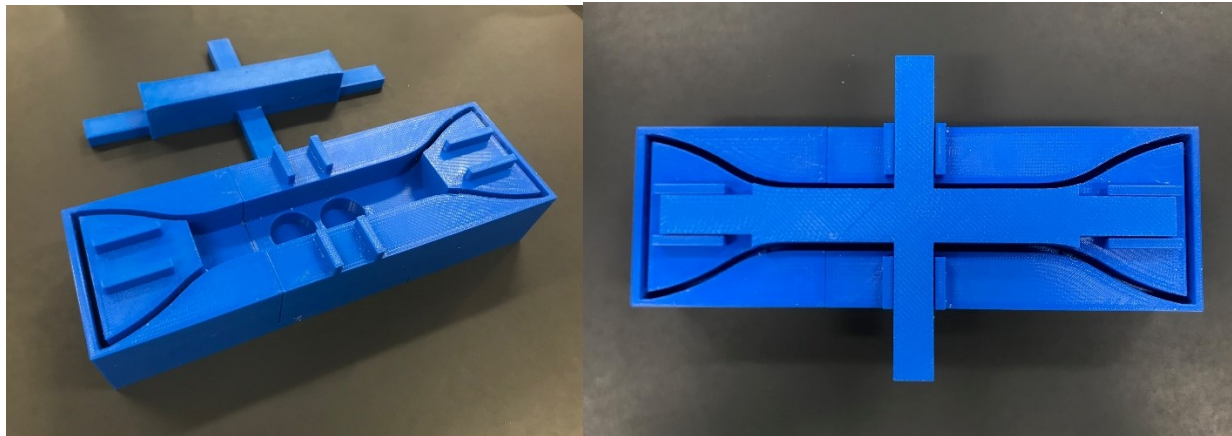


Figure 38. ABS lid mold (left image: without top piece; right image: whole assembly)

Upon trying to remove the PDMS from the mold, it was found that the PDMS bonded to the interfaces of the ABS mold. The narrow channels on the sides of and between each well, were especially hard to remove. Removing this portion of the well plate could not be achieved without ripping the PDMS. To overcome this, the team tried placing the mold in the fridge after fully curing and before demolding. The theorized idea was based off of thermal conductivity in that cold temperatures may shrink the PDMS, thus causing it to separate from the ABS mold

allowing for easy removal. Upon doing so however, the team was unsuccessful and discussed trying a flexible mold. To make a flexible mold, the team used the ABS negative mold to create a polyurethane flexible mold by creating a series of positive and negative molds (see Figures 37 and 38). PDMS was then poured into the new flexible mold and cured once again for 100 minutes at 85 degrees Celsius. Although the flexible mold allowed for the PDMS to be removed very easily, the surfaces of the PDMS remained uncured and sticky. The result believed to be due to the surface interaction between the polyurethane and PDMS. This experiment proved that a flexible mold works as an excellent tool however, for PDMS a more compatible flexible material must be selected to ensure proper curing of the PDMS to avoid leaching.

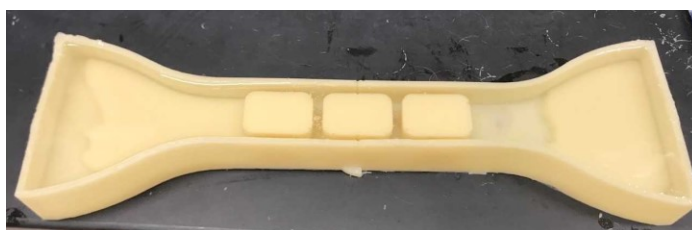


Figure 39. Flexible negative polyurethane mold with uncured PDMS

This led the team to believe that machining an aluminum mold may be the best approach. In doing so, a five-piece aluminum mold was machined for the well plate and a four-piece aluminum mold was machined for the lid (seen in Figure 40 and 41).

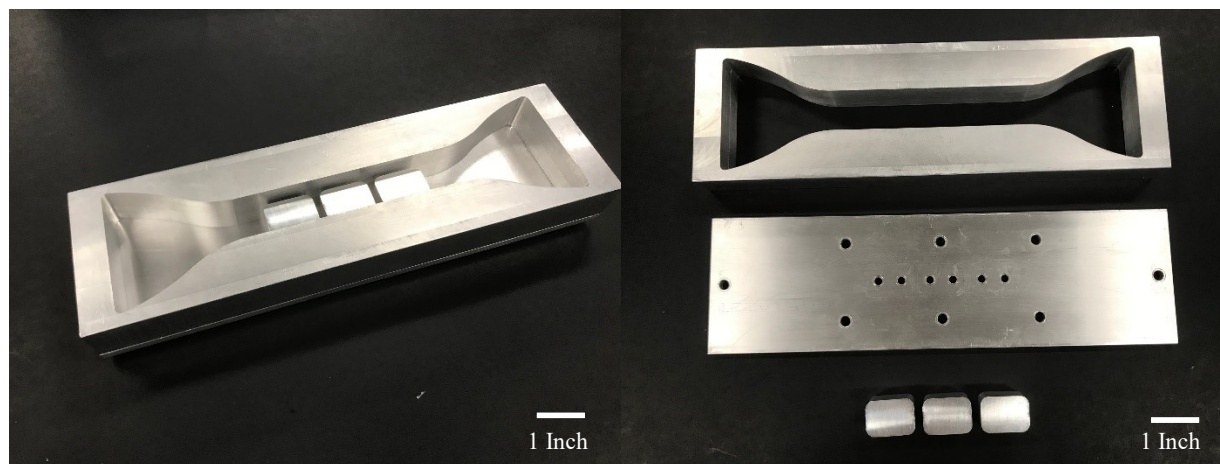


Figure 40. 5-piece aluminum mold of well plate (left image: assembled; right image: dis-assembled)

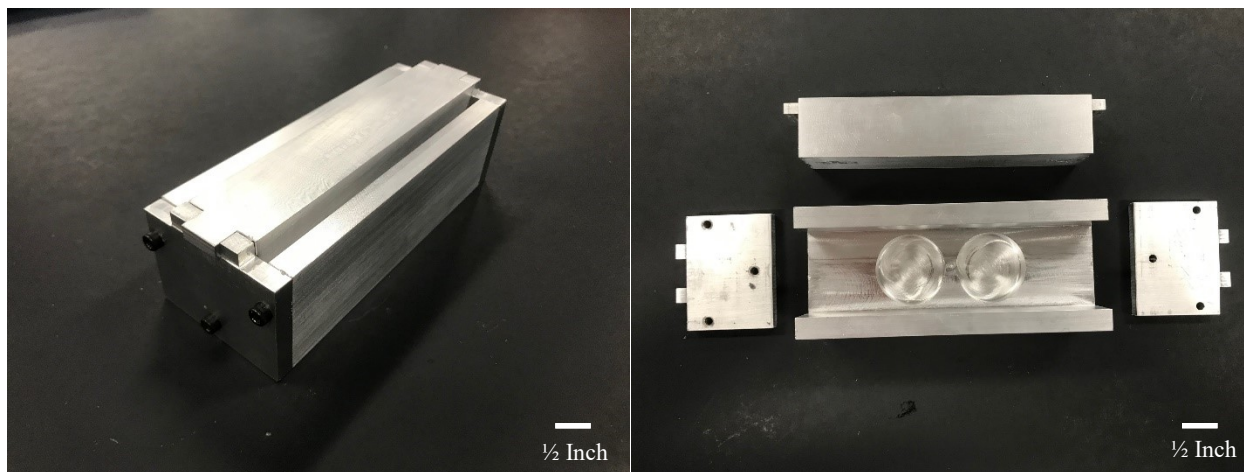


Figure 41. 4-piece aluminum mold of lid (left image: dis-assembled; right image: assembled)

The molds were held together by a series of screws which allowed for easy removal of the PDMS. The new molds proved very successful and so the team was able to carry on with experimentation. A procedure for using these molds can be found in Appendix C.

5.5 PDMS Well Plate Lid Testing Through pH Measurements

In order to validate the proper functionality of the PDMS well plate outlined in Section 4.11.2, a lid for a standard 6 well plate was designed and constructed out of PDMS with a ratio of 20:1 [68]. The preliminary design of this lid was used to validate its functionality by confirming consistent pH values of culture media within a standard polystyrene 6 well plate in an incubator. The point was to validate proper lid function before applying the lid design to the final well plate design. The PDMS lid is designed with three through-all extruded holes to fit T-75 flask filter caps around each hole. The purpose of the T-75 flask filter caps is to allow for proper gas and heat exchange between the outside environment and inner environment within the well plate. Each extruded hole is strategically placed between two wells of each row to allow for proper filtration while also minimizing thermal usage of T-75 flask filter caps.

To test whether proficient gas exchange was occurring within a 37°C and 5% CO₂ incubator, a two-day study was run to measure the pH of culture media within a polystyrene 6 well plate and lid as the control and a polystyrene 6 well plate and PDMS lid with filter caps as the experimental group. The culture media consisted of DMEM, 1X (Dulbecco's Modification of Eagle's Medium) with 4.5 g/L glucose, L-glutamine, and sodium pyruvate (Gibco, #11995-

065), 10% FBS (Gibco, #26140-087), GlutaMAX, 1X (Gibco, #3505-061), and Penicillin Streptomycin (Gibco, #15140-122) which was placed within each well of the control and experimental group. The pH of the system was tested using pH indicator strips 6.5-10 from EMD-Millipore. The pH of the culture media was tested following two days of incubation and the pH within both well plates decreased to the same value of 7.2. This experiment was run three times to prove efficacy of the pH measurements. Due to the same incremental decrease of pH in both incubated well plates, it is presumed that the PDMS lid has sufficient gas exchange through its T-75 flask filter caps (see Figure 42 below).

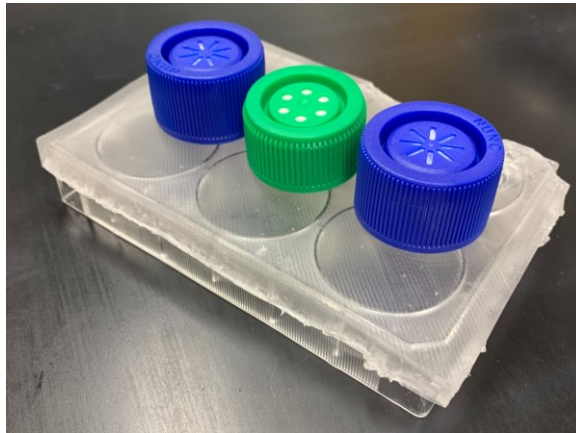


Figure 42. Picture of PDMS lid with 3 T75 flask filter caps on a standard 6 well plate

Once the final PDMS well plate and final PDMS lid are molded, the same experiment explained above will be run to test whether consistent pH values exist for all experimental groups.

5.6 Final Design

After going through preliminary testing, the final design was created as shown in Figure 43 and 44. It was placed in an incubator to sustain proper growth conditions. The well plate and lid was molded out of PDMS using the machined aluminum molds (Figure 40 and Figure 41). Together, the well plate and lid was fitted into the final mechanical system and secured with clamps on each end of the well plate. The mechanical system operated based off of a stepper motor and lead screw series which was further controlled by connecting wires extending out of

the incubator to an Arduino. A power cord was also connected to the Arduino as a constant source of power supply.

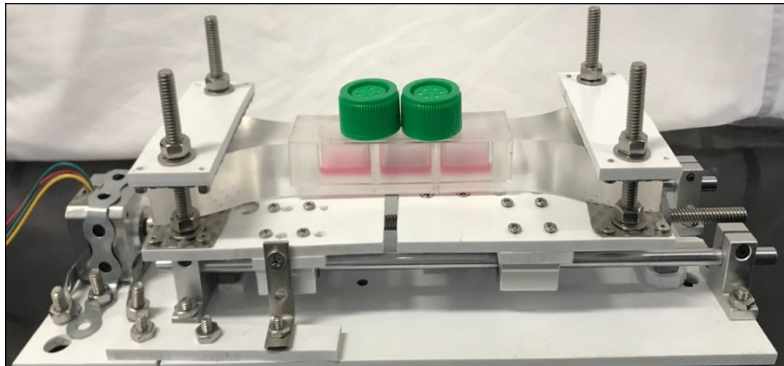


Figure 43. Fully assembled final design

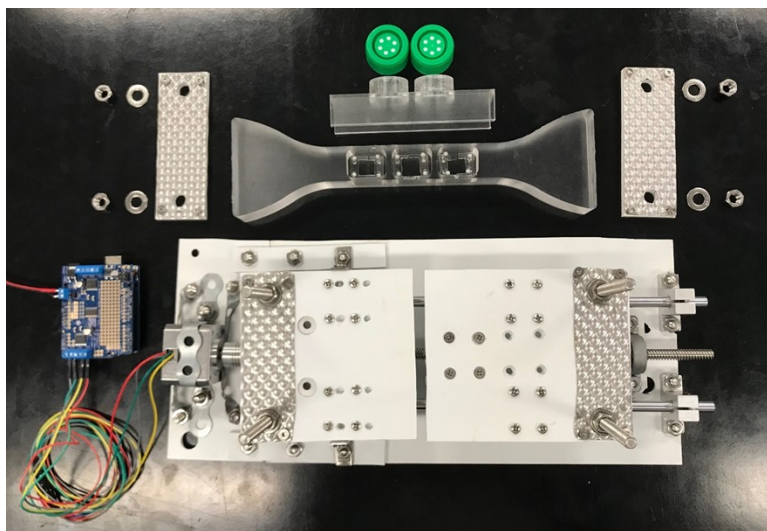


Figure 44. Final broken down into all components

6. Validation of the Final Design

6.1 Validation of the Mechanical System

6.1.1 Instron Testing of PDMS Well Plate

To determine whether the geometry and mechanical properties of the PDMS well plate could yield a uniform strain in the well region where the cardiac patches would be anchored, cyclic mechanical stretch was performed using an Instron 5544. The protocol that was used for the Instron testing as well as the image analysis can be found in Appendix C. Similar to the preliminary testing, a mounted camera was used to record each test, and a 50 mm piece of plastic was placed in-plane with the well plate to set a proper scale for image analysis. A PDMS frame was placed into each of the three wells, and the four corners of the PDMS frames were anchored into the bottom of the well using stainless steel pins. Three separate well plates were fabricated and tested three times each resulting in a total of nine tests. Each test consisted of five cycles to 10% elongation of the gauge length (12.8mm) and back. The team measured the width of the grips and drew lines on the PDMS plate in order to guide where the plate would be clamped. Ten images were extracted from the video using a custom MATLAB (R2018b, MathWorks, Natick, MA) program, and the images containing the minimum and maximum stretch were analyzed. ImageJ (NIH, Bethesda, MD) was used to measure the distances between a fixed reference point, in this case the edge of the lower Instron grip, and the heads of the stainless-steel pins used to anchor each PDMS frame in place. By comparing the distance of each pin head from the reference point in the unstretched and stretched image, the strain in each well could be calculated. Figure 45 below shows an example measurement.

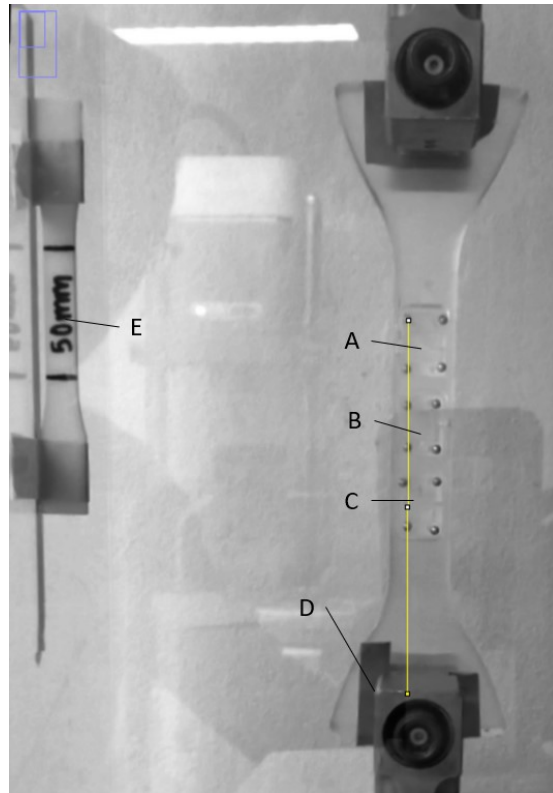


Figure 45. PDMS well plate Instron test, measured using ImageJ. Yellow line denotes measurement line from the reference point (D). Image also contains a 50mm known length for scale (E), the top well (A), middle well (B), and bottom well (C).

Five cycles were performed for every test; these cycles were averaged for each of the nine tests. Figure 46 below shows data collected for this test.

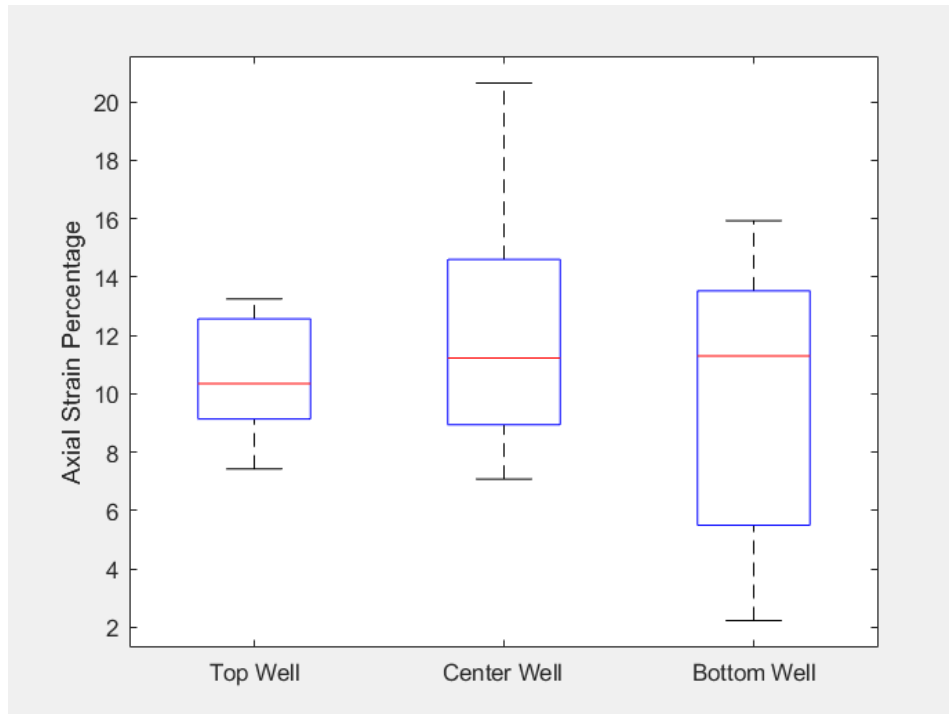


Figure 46. Boxplot of axial strain during Instron testing. Wells (x-axis) are labeled in Figure 43

Mean strain values and standard deviations are shown below in Table 12.

Table 12. Mean axial strain during Instron testing

Well	Mean (%)	Standard Deviation (%)
Top	10.68	2.01
Center	12.08	4.50
Bottom	9.98	4.59

The mean strains in all wells measured within the nominal range of 5-15% in accordance with our specifications. An Anderson-Darling normality test was performed to confirm the distribution of the data and found that the data was normal. Since the data was confirmed to be normal, a one-way analysis of variance (ANOVA) test was conducted (see Appendix J for ANOVA table). The null hypothesis stated that there is no significant difference in the mean strain in each of the three wells. The test returned a p-value of 0.5137, failing to reject the null

hypothesis and indicating that there was no statistically significant difference in the mean strain and variation in each well.

6.1.2 Mechanical Stimulation Benchtop Testing

The mechanical stimulation system was tested on the benchtop using a similar protocol to the Instron testing described in Section 5.3.1. The PDMS well plate was secured in the grips of the mechanical stimulator and the clamps were tightened. A PDMS frame was pinned into each well in the same way described in the previous section. A stand was used to hold the camera above the mechanical stimulator while it filmed each test. A 12 V AA battery pack was used to power the stepper motor, and the Arduino microcontroller was powered via computer USB. The Arduino was programmed to produce a strain rate of 170 mm/min with the goal of first applying predictable strains at low speed. Image analysis was performed using MATLAB and ImageJ according to supplemental protocols in Appendix C. A representative image showing the test setup and a sample ImageJ measurement is shown below in Figure 47.

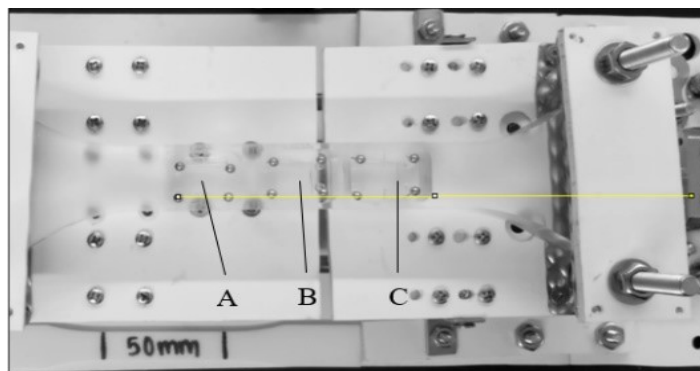


Figure 47. Image from mechanical stimulator testing. Yellow line denotes measurement from reference point on stepper motor. Image also contains labeled top well (A), center well (B), and bottom well (C).

Three well plates were each tested once and stretch measurements from each of the five cycles were averaged. Figure 48 below illustrates the test results.

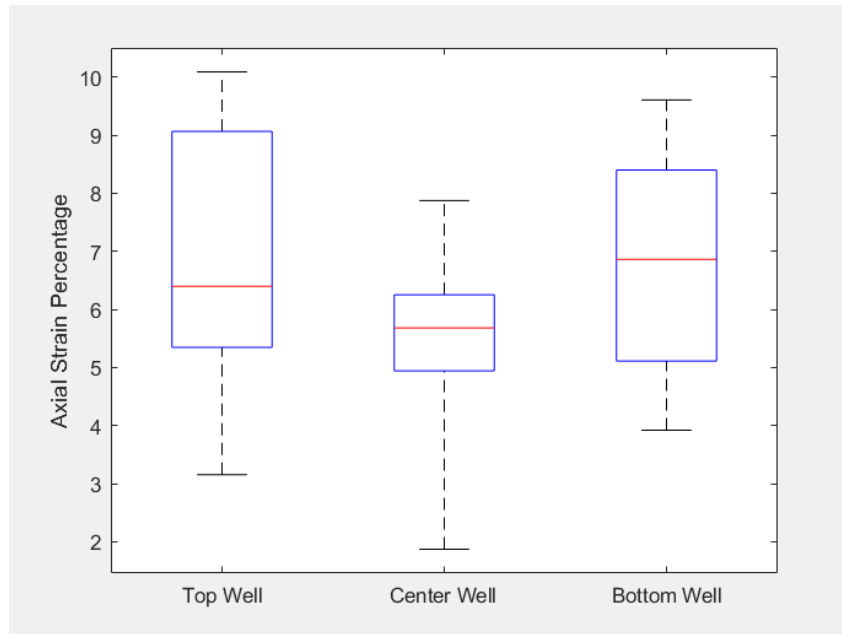


Figure 48. Box plot of axial strain in each well during mechanical stimulation. Wells (x-axis) are labeled in Fig. 45.

Table 13 below includes mean strains and standard deviations.

Table 13. Mean axial strain during mechanical stimulator testing

Well	Mean (%)	Standard Deviation (%)
Top	6.74	2.54
Center	5.38	1.99
Bottom	6.79	2.08

As with the Instron testing of the PDMS well plate detailed in Section 6.1.1, an Anderson-Darling normality test was performed, and confirmed that the data is normal. A one-way ANOVA was performed on this data (see Appendix J for ANOVA table) and returned a p-value of 0.4770 (n=6), indicating that the null hypothesis that there is no difference in the mean strain in each of the three wells cannot be rejected.

6.2 Well Plate and Lid Validation

To ensure the PDMS well plate and PDMS lid functioned properly and allowed for proper heat and gas exchange, measurements of pH were taken on initial day 0 and after 2 days from 10% FBS DMEM cell culture media inserted into the wells. pH is easily affected by change in heat or gas, thus by testing the pH of the media after 2 days, the team can validate whether or

not the PDMS well plate and PDMS lid can achieve this goal. In order to account for all possible variables, five different tests were set up; three without cells and two with cells. The first three experiments set up included a controlled well plate, a static PDMS well plate with a PDMS lid, and a dynamic PDMS well plate with a PDMS lid. The first test was the controlled experiment which utilized a standard polystyrene six well plate with a polystyrene lid.

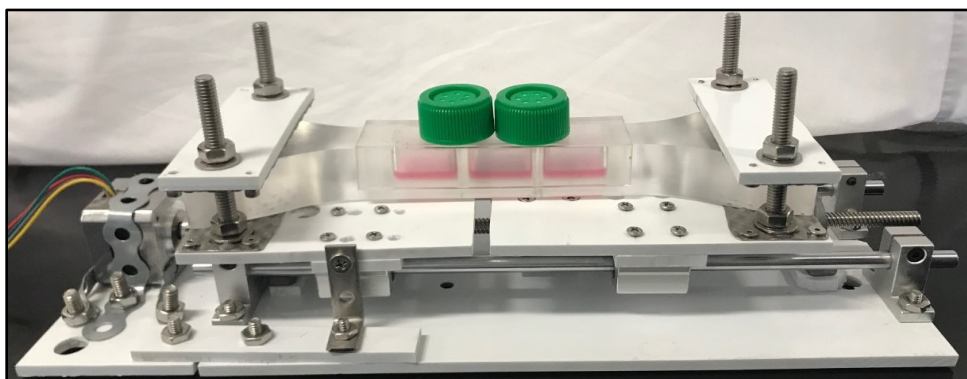


Figure 49. PDMS well plate with PDMS lid in mechanical system containing 10% FBS DMEM culture media

The second test used the team's finalized custom PDMS well plate and custom PMDS lid in static, while the third test used the team's final design in combination with the mechanical system to dynamically stimulate the well plate as shown in Figure 47. All experiments were allotted 3mL of standard 10% FBS supplemented DMEM, 1X (Dulbecco's Modification of Eagle's Medium) with 4.5 g/L glucose, L-glutamine, and sodium pyruvate (Gibco, California) cell culture media in each well and initial pH readings were taken from the cell culture media on day 0 then left for 2 days inside a standard lab incubator with set conditions. After 2 days, three different pH strips were used to validate each experiment. Table 14 below shows all the obtained pH values of the first three experiments mentioned previously. The data shows consistent pH values which proved proper gas and heat exchange was established. Likewise, two additionally tests were also run with the fabricated C2C12 tissue engineered muscle scaffolds. This was run in both a control well plate and dynamic PDMS well plate with PDMS lid. Table 15 shows the data for these experiments and also validates consistent pH values, thus proving proper gas and heat exchange once again.

Table 14. pH values of 10% FBS DMEM culture media without cells

pH Values of 10% FBS DMEM Culture Media Without Cells					
Without Cells	Initial Reading (t=0 day)	Strip 1 (t=2 days)	Strip 2 (t=2 days)	Strip 3 (t=2 days)	Average
Control	7.4	7.4	7.4	7.4	7.4
PDMS Well Plate Static	7.4	7.4	7.4	7.4	7.4
PDMS Well Plate Dynamic	7.4	7.3	7.3	7.3	7.3

Table 15. pH values of 10% FBS DMEM culture media with cells

pH Values of 10% FBS DMEM Culture Media With Cells					
With Cells	Initial Reading (t=0 day)	Strip 1 (t=2 days)	Strip 2 (t=2 days)	Strip 3 (t=2 days)	Average
Control	7.4	7.2	7.2	7.2	7.2
PDMS Well Plate Dynamic	7.4	7.2	7.2	7.2	7.2

6.3 Fibrin Microthread Diameter Comparison Study

In order to validate our fibrin-based scaffold, fibrin microthreads were synthesized, extruded, and analyzed for comparable thread diameter. In order to synthesize fibrin microthreads, the following procedures were executed. Fibrinogen and thrombin aliquots (Sigma, St. Louis, MO) were obtained from a -20 °C freezer and thawed at room temperature. An 850 uL volume of 40 mM solution of CaCl₂ was combined with the 150 uL volume of thawed thrombin. The same volume of fibrinogen and thrombin/CaCl₂ solutions were loaded into separate 1 mL syringes and inputted into a blending connector tip (SA-3670; Micromedics Inc., MN). Prior to the extrusion, a 10mM HEPES buffer solution was created and the pH was measured to be 7.4, to allow for formation of the fibrin microthreads. The solutions were extruded via a dual syringe pump through both the blending connector tip and attached polyethylene tubing (0.86 mm inner diameter) at an extrusion rate of 0.225 mL/min. The threads were drawn for about 15-20 seconds each on a Teflon-coated pan in order to create and obtain proper thread diameter. The fibrin microthreads were extruded within the Teflon coated pan filled with 300 mL of HEPES buffer solution. Once the solution has polymerized (about 10-15 minutes post extrusion), the fibrin microthreads were carefully removed and stretched to

approximately 125-175% of their original length. They were hung to dry in tension of their own weight.

To create fibrin microthreads with similar diameters, it became essential to extrude each thread at the same time interval. In order to validate that the team's threads were of appropriate diameter, the team extruded each thread for about 15-20 seconds and compared the diameters to those published by Grasman et al. in the Pins Lab [69]. The average diameter of the team's dry microthreads was 41.1 ± 7.8 μm and the average diameter of the team's wet microthreads was 127.0 ± 29.3 μm (see Appendix G). The Pins Lab dry microthread diameters of stretching percentage for 125-175% were: 53 ± 13 μm , 43 ± 10 μm , and 47 ± 11 μm . The team discovered that according to a stretch of about 150% of the original length, the team's diameters fell in the range of the Pins Lab dry diameter range (see Appendix G). The Pins Lab's wet microthread diameters of stretching percentage for 125-175 were: 97 ± 30 μm , 77 ± 25 μm , and 86 ± 22 μm . The team's threads fell well within the range of the Pins Lab wet and dry microthread diameters showing uniformity from batch to batch (see Figure 50 below).

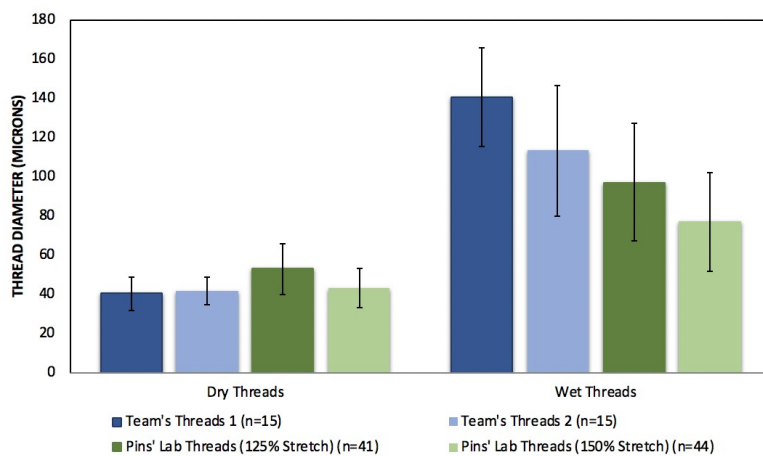


Figure 50. Bar graph showing team's & Pins' Lab dry and wet microthread diameters

6.4 Final Experiment

The entire device must be able to run inside a standard lab incubator with set conditions of 95% humidity, 5% CO_2 , and 37°C . The system operated on a duty cycle of 1 hour on 5 hours off and produce 5-15% strain for two weeks. Therefore, the device proved to be fully functional without supervision or concerns pertaining to sterility or overstretching.

As a final validation experiment, the entire device ran for a total of 6 days within the mechanical stimulator system with the duty cycle continuously running for the 6 days. The team also wanted to confirm the specification set that the system should be able to run overnight un-monitored for 12 hours (see Table 9). For proof of concept, C2C12-seeded fibrin patches were fabricated in accordance with Pins' Lab protocol found in Appendix C. The team made sure to build the entire mechanical system with stainless steel or corrosion-resistant parts and materials to allow the device to be properly sterilized. To validate this, the team monitored the final experiment and inspected the system for signs of corrosion or malfunction.

Following verification of the experiments described in the previous sections in Chapter 6, the team conducted a final experiment to assess the functionality of the mechanical stimulator system to promote myotube formation as well as cell elongation and alignment in the C2C12 cells within the fibrin-based engineered tissue. To ensure for proper sterilization of all device components, the PDMS well plate, PDMS lid, and PDMS frames were sterilized via autoclave, while the stainless-steel pins and the entire mechanical stimulator system were sterilized using isopropanol.

C2C12 cells, murine skeletal myoblasts, were cultured in culture media containing DMEM (1X) (Gibco, #11995-065), 10% FBS (Gibco, #26140-087), and GlutaMAX (100X) (Gibco, #35050-061) and maintained in a 100 mm petri dish in a standard incubator. Since the cardiac patches required about 400,000-600,000 cells per patch, C2C12 cells were sub-cultured when they reached a confluency of 80-90% to allow for the synthesis of multiple patches at one time. The day prior to seeding the C2C12s in the fibrin gel, media was supplemented with 0.4% aprotinin (ThermoFisher, #78432) to prevent the degradation of the fibrin due to cellular responses and vellum frames with threads were sterilized with isopropanol to allow for proper sterilization of the constructs (see Appendix C for fibrin microthreads sterilization protocol). An hour before seeding, the fibrin microthreads and vellum constructs are left to hydrate in autoclaved deionized water and the PDMS casting frames are left to soak top down in 1% Pluronic to allow for adherence of the gel to the PDMS for proper polymerization of the gel into the size of the vellum frame. Each of the patches is composed with 102 uL of cell suspension (containing 400,000 cells), 42 uL of 11 mg/mL fibrinogen, and 6 uL of 40 U/mL. Once all of these components are combined, it is imperative for the mixture to be placed on the PDMS

casting frames as soon as possible before polymerization occurs. The gel was then removed 10 minutes following the casting and placed on the cut PDMS frame and then inserted into each well in the PDMS well plate. Stainless steel pins were then inserted into each corner of the frames to hold the patch with the vellum frame from rising up once media was added to the wells. The lid with T75 Flask filter caps was placed on top of the well plate and the well plate was placed within the mechanical stimulation system. The mechanical stimulation system displaced the well plate 170 mm/min with a duty cycle of 1 hour on and 5 hours off. The team compared results of patches from three experimental groups- a standard 6 well plate (as the control group), a static well plate, and a dynamic well plate (within the mechanical system). The plates were incubated in an incubator for one day and six days to show the effects of time on morphological changes. For the 6-day experiment, culture media was exchanged two days following patch synthesis with differentiation media, which contained 48% DMEM, 48% F12, 2% Horse Serum, 1% Penicillin Streptomycin, 1% ITS, and 0.4% Aprotinin, to allow for differentiation and maturation of the C2C12 cells.

In order to visualize the morphological changes imparted to the C2C12 cells seeded in the fibrin patches, they were removed from the PDMS well plate and staining protocols for displaying the nucleus and cytoskeletal organization (see Appendix C) were followed. Patches were carefully removed from the PDMS well plates following 1 day and 6 days of mechanical stimulation and analyzed for morphological analysis. Briefly, the tissues were fixed with 4% paraformaldehyde and stained with 1:40 Alexa Fluor 488 Phalloidin and 1:6000 Hoechst (See Appendix C).

The stained, fluorescent images of the C2C12 cells within the fibrin-based scaffolds can be seen in Appendix J. Three experimental groups were run: the control group, a static group, and a dynamic group. The control group consisted of patches contained in a standard 6 well plate. The static group consisted of the team's PDMS well plate and PDMS lid without mechanical stimulation. The dynamic group consisted of the team's PDMS well plate and PDMS lid in the mechanical stimulation system.

The stained images from the 1 day and 6 day static and dynamic systems can be seen in Figure 51 below. The nuclei are illustrated in Figure 51 as the white arrows in the dynamic systems. The actin cytoskeleton (green) is shown with the white circles in Figure 51. The

elongation of the actin cytoskeleton can be seen when comparing the static system to the dynamic system. The direction of the loading is denoted by the red, dashed arrow in the dynamic images in Figure 51. It can be seen that the presence of the actin cytoskeleton (green) increases with time, from the 1-day dynamic system to the 6-day dynamic system. The 6-day dynamic system illustrates how the direction of the cytoskeletal elongation is in the same direction of the loading force.

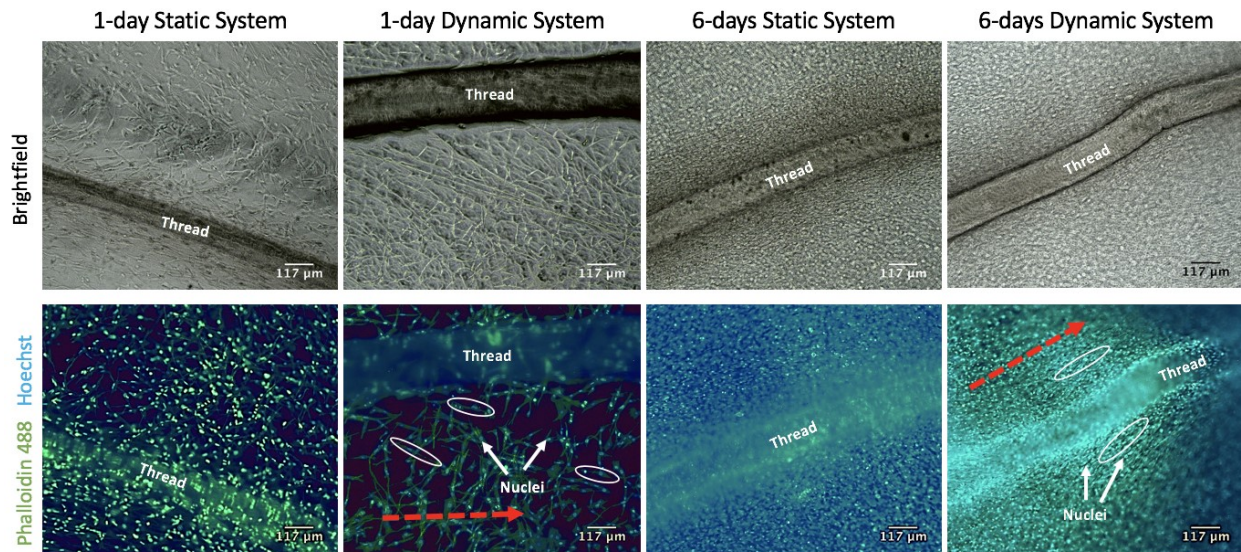


Figure 51. Fluorescence images of C2C12 cells within fibrin-based scaffolds that show the nuclei (blue) and the actin cytoskeleton (green), as well as the presence of the fibrin microthread. The white arrows indicate the nuclei, the white circles indicate the actin cytoskeleton, and the red, dashed arrows indicate the direction of the applied loading force.

7. Discussion

This chapter discusses the results obtained from the verification experiments performed in Chapter 6. These results will be used to provide evidence that the team has met previous design objectives, functions, and specifications previously stated in Chapter 3.

7.1 Mechanical System Analysis

The goal of the Instron validation test was to ensure that the inside of the wells could be stretched between 5-15% strain and to ensure that uniform strain could be accomplished through

all three wells. This was validated by performing a five-cycle tensile test on three of the plates. After analyzing the images, the strains in each well were seen to be 10.68, 12.08, and 9.98%. The standard deviations for these means were higher than expected, but the statistical analysis yielded that there was no statistically significant difference in the mean strain across each of the three wells. The variation of strain between each of the wells could have been due to small image analysis errors or the fact that the Instron grips do not reach across the entire width of the well plate. From this test, the team confirmed that the shape of the well plate was suitable for creating uniform strain in each of the three wells.

The goal of the mechanical system validation test was to ensure that the system could stretch the plate to achieve between 5-15% in each of the three wells. It was used to ensure that the strain in the wells would be consistent. Additionally, the test was performed to ensure that the mechanical system could cyclically stretch the plate. After the image analysis, the test showed that the mechanical stimulator was able to stretch the inside of the wells to 6.74, 5.38, and 6.79% strain. Again, the standard deviations were higher than expected, but after statistical analysis, the data showed that there was no statistically significant difference in the strain between the three wells. The mechanical stimulator was unable to stretch the plate to achieve 10% strain in each well, which was a benchmark goal, though it did fall within the 5-15% strain specification established by the team. Replacing the current stepper motor with a unit with higher moving torque would allow the mechanical stimulator to stretch the wells to 10% strain as well as increase the frequency of cyclic stimulation.

Comparing this data to the stimulation parameters found in the literature (shown in Table 2), it can be seen that the range of strains this device imparts on cardiac patches (5-7%) falls in line with other studies of mechanical stimulation, where strains between 5 and 15% were used. However, this device was unable to achieve a cyclic frequency of 1 Hz, which is also common in the studies shown in Table 2 and approximates the human heart rate. As mentioned, the team believes a stepper motor with a higher moving torque would improve the ability of the mechanical system to achieve a 1 Hz cyclic frequency and higher strain, if desired.

7.2 Well Plate and Lid Analysis

The objective of the well plate and lid validation test was to ensure proper heat and gas exchange was possible. This was validated by measuring the pH of the cell culture media after 2 days in the team's well plate with the lid as mentioned in Chapter 6. The data showed consistent pH values which confirmed the presence of proper heat and gas exchange. For the dynamic PDMS well plate with PDMS lid test, pH values averaged out to be about 7.3 instead of the accepted 7.4 value. This may be due to the PDMS's permeability in comparison to the polystyrene well plate. Since CO₂ decreases pH and PDMS is more permeable than polystyrene, this could explain why the pH decreased by .1 [70]. Though this may be the case, the team decided this was still an acceptable value considering its low standard deviation. For the validation tests containing cells, the data showed consistent pH values were carried out for both the control and dynamic test. The test containing cells however showed a decrease in pH which resulted in a consistent value of 7.2.

7.3 Fibrin Microthread Diameter Analysis

The microthread diameter data shown previously in Figure 50 shows that the diameters of the microthreads created by the team fall within the mean and standard deviation of the diameters previously reported by the Pins Lab. This validation is important because the diameter of the microthread can influence the orientation of cells near the microthread as well as the stiffness of the cardiac patch [9]. With the team's thread diameters in the same range as threads created using the same protocol, the team felt comfortable concluding that any observations made in later experiments were not a result of the thread diameters.

7.4 Final Design Analysis

The final experiment was conducted to verify that the device was able to impart mechanical stimulation to fibrin-based patches seeded with C2C12 cells and induce morphological changes. It was determined that no signs of contamination within the well plate occurred. After running the final experiment, it was determined that proper environmental conditions were maintained with no signs of corrosion or damage after 6 days of cyclically stimulating the patches for 1 hour on and five hours off.

The 1-day control group and 1-day static group showed similar results seen in Figure 51, showing disorganization of the actin cytoskeleton (green) (see Appendix J). The 1-day dynamic experimental group showed the elongation of the actin cytoskeleton (green) of the C2C12 cells, suggesting that the mechanical system causes cytoskeletal alignment in the direction of the force. Numerous studies involving mechanical stimulation have shown improvements to cell alignment; though cytoskeletal alignment does not necessarily mean improvements to cell alignment, the day 1 images showed promising results in that direction [33, 35, 39, 49]. The 6-day static and dynamic groups all showed an increase in cell proliferation which can be seen through increased amount of fluorescence of the nuclei and actin cytoskeleton. Much like the cardiomyocyte cell lines discussed in Chapter 2.4, the C2C12 murine skeletal myoblast cells morphologically respond depending on the mechanical stimulation applied. The 6-day dynamic group showed elongation and alignment of the C2C12 cells parallel to the fibrin microthreads (see Figure 51) as well as in the direction of the applied force. These improvements to cell alignment directly correspond with similar findings in the literature [33, 35, 39, 49]. This suggests that the 6-7% strain imparted on the patches by the mechanical stimulation device allowed for morphological changes that were more similar to native myocardial tissue. More testing could be done to the patches to measure myotube formation as well as elongation and alignment of the myotubes, however, long-term cell culture would be necessary for this visualization.

7.5 Impact Analysis

7.5.1 Economic Impact

Our device provides a low-cost platform for mechanical conditioning of tissue-engineered cardiomyocyte cardiac patches. Our system will save a research laboratory money compared to commercial cell stretchers on the market in terms of bill-of-materials cost (see Appendix K), as some custom-made stretching systems are reported to cost \$1000 USD or more, and the FlexCell FX-6000 tension system discussed in Section 2.7 costs roughly \$30,000 USD [71, 72]. It is reusable, and any components that fail after some amount of use are easily replaceable with common hardware and materials. This would reduce the overhead costs for conducting experiments related to how mechanical conditioning improves the functionality of

tissue-engineered cardiac patches. This presents an opportunity for smaller labs as well as undergraduate students to conduct these experiments, providing more data and knowledge towards the goal of creating tissue-engineered solutions that are a functional replacement for heart tissue damaged by myocardial infarction.

7.5.2 Environmental Impact

The production of all the components would create a minimal impact on the environment. Due to the re-sterilization capabilities of the mechanical stimulation system and the Arduino components controlling the stepper motor, the mechanical system is reusable. In terms of electrical waste, since the stepper motor in the mechanical stimulation system does not require an excess amount of voltage with a duty cycle of one hour of operation followed by five hours off, the environment will not be drastically impacted from the heat loss. Due to re-sterilization and reusability of the PDMS well plate, PDMS lid, PDMS casting frames, O-rings, and stainless-steel pins, the team's design will not have to be discarded on a regular basis thus creating less hazardous waste than the typical usage of a disposable 6 well plate. The negative environmental implications may be due to the amount of biohazardous waste created and the amount of water and heat needed to autoclave the PDMS components. The cell culturing prior to the synthesis of the fibrin-based patches requires the use of several petri dishes, serological pipettes, and pipette tips, which must be discarded in the receptacles containing biohazardous waste or biohazardous sharps. The C2C12-seeded fibrin-based patches must also be discarded in the biohazardous waste receptacle following staining and imaging. Many of these biohazardous materials are then taken to facilities where they are sterilized or incinerated thus using more energy or causing an increase in airborne pathogens.

7.5.3 Societal Impact

The use of our device will allow for improved functional properties of tissue engineered models. The use of a simple device to stimulate three-dimensional tissue constructs will be brought to the public attention as a next standard method of tissue engineering. The attention of this design will aid the direction of biomedical research towards further advancements in more efficient and complex models. Other lines of work will also focus attention on the effect

stimulation has to three-dimensional tissue constructs on a biological, chemical, and physical microscopic level. The use of our device can also be used on a broader scale to not only analyze and stimulate healthy tissue, but to see the effects of diseased tissue as well. For example, the Pins Lab cardiac patch could be used in conjunction with our mechanical stimulator system to create a benchtop model of mature, contractile heart tissue in order to test the effects of different drugs on human heart tissue without requiring *in vivo* implantation. The cost efficiency and accurate output of our design will also provide labs with a cheap and efficient way to stimulate cells, thus keeping it affordable for the client and user to use.

7.5.4 Political Ramifications

A significant barrier restraining tissue engineering and the medical research field in general is the cost of experiments and clinical trials. Academic institutions are often on the cutting edge of new ideas in medical research but derive funding through donations and grants rather than a shareholder and profit-funded budget. With this more limited funding source, finding solutions that can provide the desired experimental outcomes while lowering operating costs is important. Reducing the costs associated with development of regenerative tissue-engineered muscle can allow for more labs to contribute data and potentially accelerate the path to clinical trials and eventually to market for tissue-engineered muscle. Some decellularized extracellular matrix-based scaffolds have received approval from the U.S. Food and Drug Administration (FDA) as 510(k) medical devices for surgical applications (discussed in Section 2.3), but developers of tissue-engineered myocardial constructs would likely need to seek approval through the pre-market approval (PMA) pathway without a predicate solution and surgical method of implementation on the market already. This cardiac patch presents a high risk to the patient, as the heart is a critical organ and failure of the patch could cause further damage. As such, regulators may need to take additional steps to set appropriate quality and efficacy standards for this product. Companies eventually producing cardiac patches for clinical use would need to work with regulators to revise their internal quality policies to reflect more stringent requirements. If this product were successfully approved by the FDA for clinical use in humans, it is likely that a substantial decrease in the number of patients seeking heart transplants would occur. This would make it easier for patients who are in greatest need of a heart transplant

to find one. It may also reduce the number of patients who require invasive and expensive bypass surgeries, reducing the monetary and emotional load of heart disease on society.

7.5.5 Health and Safety Concerns

The device features electrical components that could be harmful to the user especially if exposed to the incubator environment improperly. Special concern should be taken for the stepper motor operating inside the incubator as it should not operate in an environment with a temperature above 80°C. Other associated electrical parts, such as the Arduino, power supply, and connecting wires can also pose a potential electrocuting hazard. The Arduino and stepper motor are powered by 120 V AC-DC power adapters that plug into a standard wall outlet, which is an electrocution risk if not handled with care. The amount of moving parts used in the stimulation should be monitored to ensure that there are no loose parts or potential risk each time the device is used. Sterilization of the device's components should be performed according to the guidelines set forth by OSHA. This device is also designed to work with fibrin cardiac patches, which contain a variety of biohazardous components. The scaffold gel and microthreads in the patch are derived from fibrinogen, which is a blood component, and could confer bloodborne pathogens to those working with them. Additionally, cells used to seed the fibrin scaffold are biohazardous. Preventative measures should be taken by individuals preparing these biohazardous components by wearing eye protection, gloves, and a lab coat, working inside a Class 2 biosafety cabinet, and disposing of biohazardous materials and sharps components according to the appropriate protocols.

7.5.6 Ethical Concerns

Many of the ethical concerns of this device feature what types of cells may be used to seed the construct. Cells that are derived from embryonic stem cells are most often up for ethical debate. However, any cell line previously discussed, such as iPSCs, human embryonic, and animal embryonic stem cells all offer their own line of ethical questions. Concerning this proof of concept using C2C12 cells, these cells are derived from mice and came from clonal culture. The ethical issues that surround this project are more forward-thinking concerning cell lines. Since this is an immortalized cell line, there are more ethical concerns regarding this project's

future work. In the future this device would ideally be tested using a cardiac cell line such as neonatal rat cardiac cells or induced pluripotent or embryonic stem cells. Significant ethical related caution should be exercised with the use of these cell lines. There could be concern around the killing of neonatal rats, and of using and altering human or animal stem cells. There are also many ethical issues concerning the use of unborn embryo cells in scientific research [73, 74].

7.5.7 Sustainable Usage

Our device is a sustainable system in a laboratory setting. The completely sterilizable design of the mechanical stimulation system with the reusable PDMS well plate produces minimal waste. Due to the growing application of 3D engineered biomaterials, the multi-purpose usage of the mechanical stimulation system broadens the cardiac application to a more universal application allowing for the usage of different cell lines, biomaterials, and applications.

7.5.8 Manufacturability

The initial cost of this device, \$254.57, is low compared to other devices currently on the market (see Appendix K for bill of materials). The reusability of the majority of the device components, including the mechanical stimulator, PDMS well plates, and PDMS lids reduces the per-use cost once the initial upfront cost has been paid. The mechanical stimulator system is constructed with common hardware and components available from the hardware store, online parts stores, or online manufacturers. Once assembled, most device components remain in place aside from nuts used to clamp the PDMS well plate. Manufacturing of the aluminum molds used to cast the PDMS well plate and lid is possible using standard 3-axis milling, and only needs to be done a single time. When building this device for laboratory use, there are no significant obstacles to manufacturability in terms of both cost and fabrication method. The bill of materials for this device can be found in Appendix K.

7.5.9 Applicable Standards

The final dog-bone shape of the PDMS well plate was inspired by shape specifications for elastomer tensile test specimens found in ASTM D412. When selecting components to power

the mechanical stimulator, care was taken to obtain power supplies and wires that are RoHS (Restriction of Hazardous Substances) – compliant.

8. Conclusions and Recommendations

The validation testing detailed in Sections 6 and 7 showed that the device developed by the team is capable of providing cyclic mechanical stimulation to engineered cardiac patches. This was achieved in a controllable and measurable way while maintaining environmental conditions necessary for the growth and survival of the cells seeded in the patch. This device is adaptable to test functional properties of cardiac patches at varying mechanical stimulation conditions such as frequency, cyclic strain, and duty cycle. Optimal settings for mechanical stimulation could be found that would yield the greatest improvements to cardiac patch cell alignment, cell size, and contractile force. The end goal with use of a device such as this would be to mechanically condition cardiac patches until their mechanical and electrical properties match those of native myocardium. This would make them a clinically viable replacement for heart tissue damaged by myocardial infarction.

Though this device met the project goals as laid out in the revised client statement, the team has several recommendations for ways the device can be improved. First, implementation of a stronger stepper motor that produces higher torque would make the system capable of a wider range of strains and cyclic frequencies. Particularly, a stronger stepper motor would allow the system to achieve stimulation at 1 Hz, which approximates the heart rate of a human increasing the device's biomimetic capabilities.

The mechanical stimulator system runs completely without user input once the test is started. However, incorporating an app that connects to the Arduino microcontroller via Bluetooth or Wi-Fi would allow the device user to monitor the status of the experiment in real time, or make changes to the protocol on the fly. Additionally, if the PDMS well plate, lid, and stages of the mechanical stimulator were optically clear, a microscope imaging system could be incorporated in order to visualize changes to the cardiac patch throughout the experiment.

The system should also be tested with a cardiomyocyte cell line that the Pins Lab plans to use in the cardiac patches moving forward, such as iPS-CMs. While the murine skeletal

myoblasts (C2C12s) were an excellent low- cost analog for cardiomyocytes, the system needs to be validated with the cell type ultimately being used in the cardiac patch.

Collection of more data for the validation studies would provide greater sample sizes for analysis and improve the power of the conclusions the team drew from them. Since the team was not able to test the device continuously for a two-week experiment, conducting a two week or longer experiment would be useful to understanding morphological changes with respect to time and the mechanical stimulation.

Finally, the design of this device leaves room to implement an electrical stimulation system utilizing in-well electrodes or an electrical field generated by parallel plates. Section 2.5 of this paper details the positive effects on myocyte maturity that come from exposure to electric fields, so incorporation of electrical stimulation into our system could add a second pathway for improving the functional properties of cardiac patches.

References

1. *Cardiovascular Diseases*. Available from: [https://www.who.int/news-room/fact-sheets/detail/cardiovascular-diseases-\(cvds\)](https://www.who.int/news-room/fact-sheets/detail/cardiovascular-diseases-(cvds)).
2. *Treatment of a Heart Attack*. Available from: <https://www.heart.org/en/health-topics/heart-attack/treatment-of-a-heart-attack>.
3. Christman, K.L., *Biomaterials for tissue repair*. Science, 2019. **363**(6425): p. 340-341.
4. Jawad, H., et al., *Myocardial tissue engineering: a review*. J Tissue Eng Regen Med, 2007. **1**(5): p. 327-42.
5. Ye, L., et al., *Patching the Heart: Cardiac Repair from Within and Outside*. Circulation research, 2013. **113**(7): p. 10.1161/CIRCRESAHA.113.300216.
6. Zimmermann, W.-H., I. Melnychenko, and T. Eschenhagen, *Engineered heart tissue for regeneration of diseased hearts*. Biomaterials, 2004. **25**(9): p. 1639-1647.
7. Ozcelik, B., *7 - Degradable hydrogel systems for biomedical applications*, in *Biosynthetic Polymers for Medical Applications*, L. Poole-Warren, P. Martens, and R. Green, Editors. 2016, Woodhead Publishing. p. 173-188.
8. Hinds, S., et al., *The role of extracellular matrix composition in structure and function of bioengineered skeletal muscle*. Biomaterials, 2011. **32**(14): p. 3575-83.
9. Chrobak, M.O., et al., *Design of a Fibrin Microthread-Based Composite Layer for Use in a Cardiac Patch*. ACS Biomaterials Science & Engineering, 2017. **3**(7): p. 1394-1403.
10. Montgomery, M., et al., *Flexible shape-memory scaffold for minimally invasive delivery of functional tissues*. Nat Mater, 2017. **16**(10): p. 1038-1046.
11. *Heart disease*. [Web]; Available from: <https://www.mayoclinic.org/diseases-conditions/heart-disease/symptoms-causes/syc-20353118>.

12. Reed, G.W., J.E. Rossi, and C.P. Cannon, *Acute myocardial infarction*. The Lancet, 2017. **389**(10065): p. 197-210.
13. National Heart, L., and Blood Institute. *Heart Failure*. [Web] [cited 2019; Available from: <https://www.nhlbi.nih.gov/health-topics/heart-failure>].
14. Mehta, L.S., et al., *Acute Myocardial Infarction in Women: A Scientific Statement From the American Heart Association*. Circulation, 2016. **133**(9): p. 916-47.
15. *Left Ventricular Assist Device (LVAD): Overview*. Available from: <https://stanfordhealthcare.org/medical-treatments/l/lvad.html>.
16. Golob, M., R.L. Moss, and N.C. Chesler, *Cardiac tissue structure, properties, and performance: a materials science perspective*. J Annals of Biomedical Engineering, 2014. **42**(10): p. 2003-2013.
17. Abbasi, M., et al., *Characterization of three-dimensional anisotropic heart valve tissue mechanical properties using inverse finite element analysis*. Journal of the Mechanical Behavior of Biomedical Materials, 2016. **62**: p. 33-44.
18. Radisic, M. and K.L. Christman, *Materials Science and Tissue Engineering: Repairing the Heart*. Mayo Clinic Proceedings, 2013. **88**(8): p. 884-898.
19. Woodcock, E.A. and S.J. Matkovich, *Cardiomyocytes structure, function and associated pathologies*. The international journal of biochemistry & cell biology, 2005. **37**(9): p. 1746-1751.
20. Peter, A.K., M.A. Bjerke, and L.A. Leinwand, *Biology of the cardiac myocyte in heart disease*. Mol Biol Cell, 2016. **27**(14): p. 2149-60.
21. Park, M. and Y.S. Yoon, *Cardiac Regeneration with Human Pluripotent Stem Cell-Derived Cardiomyocytes*. Korean Circ J, 2018. **48**(11): p. 974-988.
22. Simpson, D. and S. Dudley Jr, *Lost in Translation: What is Limiting Cardiomyoplasty and Can Tissue Engineering Help?* Current Stem Cell Research & Therapy, 2009. **4**(3): p. 210-223.
23. Juhas, M., et al., *Biomimetic engineered muscle with capacity for vascular integration and functional maturation in vivo*. Proc Natl Acad Sci U S A, 2014. **111**(15): p. 5508-13.
24. Yildirim, Y., et al., *Development of a biological ventricular assist device: preliminary data from a small animal model*. Circulation, 2007. **116**(11 Suppl): p. I16-23.
25. Berry, M.F., et al., *Mesenchymal stem cell injection after myocardial infarction improves myocardial compliance*. American Journal of Physiology-Heart and Circulatory Physiology, 2006. **290**(6): p. H2196-H2203.
26. Fomovsky, G.M. and J.W. Holmes, *Evolution of scar structure, mechanics, and ventricular function after myocardial infarction in the rat*. American Journal of Physiology-Heart and Circulatory Physiology, 2009. **298**(1): p. H221-H228.
27. Fernandes, I.R., et al., *Fibroblast sources: Where can we get them?* Cytotechnology, 2016. **68**(2): p. 223-8.
28. Zhang, D., et al., *Tissue-engineered cardiac patch for advanced functional maturation of human ESC-derived cardiomyocytes*. Biomaterials, 2013. **34**(23): p. 5813-20.
29. Vunjak-Novakovic, G., et al., *Challenges in Cardiac Tissue Engineering*. Tissue Engineering. Part B, Reviews, 2010. **16**(2): p. 169-187.
30. Malki, M., et al., *Gold Nanorod-Based Engineered Cardiac Patch for Suture-Free Engraftment by Near IR*. Nano Letters, 2018. **18**(7): p. 4069-4073.
31. Roberts, E.G., et al., *Engineering Myocardial Tissue Patches with Hierarchical Structure-Function*. Annals of biomedical engineering, 2015. **43**(3): p. 762-773.

32. Stoppel, W.L., D.L. Kaplan, and L.D. Black, 3rd, *Electrical and mechanical stimulation of cardiac cells and tissue constructs*. *Adv Drug Deliv Rev*, 2016. **96**: p. 135-55.
33. Nguyen, M.-D., et al., *Effects of physiologic mechanical stimulation on embryonic chick cardiomyocytes using a microfluidic cardiac cell culture model*. *Analytical chemistry*, 2015. **87**(4): p. 2107-2113.
34. Taber, L.A., *Mechanical aspects of cardiac development*. *Progress in biophysics and molecular biology*, 1998. **69**(2-3): p. 237-255.
35. Vandenburg, H.H., et al., *Response of neonatal rat cardiomyocytes to repetitive mechanical stimulation in vitro*. *Annals of the New York Academy of Sciences*, 1995. **752**(1): p. 19-29.
36. Jacot, J.G., J.C. Martin, and D.L. Hunt, *Mechanobiology of cardiomyocyte development*. *Journal of biomechanics*, 2010. **43**(1): p. 93-98.
37. Zimmermann, W.-H., et al., *Tissue engineering of a differentiated cardiac muscle construct*. *Circulation research*, 2002. **90**(2): p. 223-230.
38. Ruan, J.-L., et al., *Mechanical stress conditioning and electrical stimulation promote contractility and force maturation of induced pluripotent stem cell-derived human cardiac tissue*. *Circulation*, 2016: p. CIRCULATIONAHA. 114.014998.
39. Shimko, V.F. and W.C. Claycomb, *Effect of mechanical loading on three-dimensional cultures of embryonic stem cell-derived cardiomyocytes*. *Tissue Engineering Part A*, 2008. **14**(1): p. 49-58.
40. Lux, M., et al., *In vitro maturation of large-scale cardiac patches based on a perfusable starter matrix by cyclic mechanical stimulation*. *Acta Biomaterialia*, 2016. **30**: p. 177-187.
41. Rangarajan, S., L. Madden, and N. Bursac, *Use of Flow, Electrical, and Mechanical Stimulation to Promote Engineering of Striated Muscles*. *Annals of Biomedical Engineering*, 2014. **42**(7): p. 1391-1405.
42. Marieb, E. and K. Hoehn, *Human Anatomy and Physiology*. 10 ed. 2015, United States: Pearson.
43. Stevens, K., et al., *Physiological function and transplantation of scaffold-free and vascularized human cardiac muscle tissue*. *Proceedings of the National Academy of Sciences*, 2009. **106**(39): p. 16568-16573.
44. Massai, D., et al., *Bioreactors as engineering support to treat cardiac muscle and vascular disease*. *Journal of healthcare engineering*, 2013. **4**(3): p. 329-370.
45. *Matrigel Matrix*. 2018; Available from: <https://www.corning.com/worldwide/en/products/life-sciences/products/surfaces/matrigel-matrix.html>.
46. *C-Pace EM 100 User Manual*. 2017 Sep 2017; Available from: <http://www.ionoptix.com/wp-content/uploads/2018/07/CPaceEM-UserManual.pdf>.
47. Gerbin, K.A., et al., *Enhanced electrical integration of engineered human myocardium via intramyocardial versus epicardial delivery in infarcted rat hearts*. *PLoS One*, 2015. **10**(7): p. e0131446.
48. Rupert, C.E. and K.L. Coulombe, *IGF1 and NRG1 enhance proliferation, metabolic maturity, and the force-frequency response in hESC-derived engineered cardiac tissues*. *Stem cells international*, 2017. **2017**.

49. Ruan, J.L., et al., *Mechanical Stress Conditioning and Electrical Stimulation Promote Contractility and Force Maturation of Induced Pluripotent Stem Cell-Derived Human Cardiac Tissue*. *Circulation*, 2016. **134**(20): p. 1557-1567.
50. Hirt, M.N., et al., *Functional improvement and maturation of rat and human engineered heart tissue by chronic electrical stimulation*. *Journal of molecular and cellular cardiology*, 2014. **74**: p. 151-161.
51. Barash, Y., et al., *Electric field stimulation integrated into perfusion bioreactor for cardiac tissue engineering*. *Tissue Eng Part C Methods*, 2010. **16**(6): p. 1417-26.
52. Hansen, K.J., M.A. Laflamme, and G.R. Gaudette, *Development of a contractile cardiac Fiber From Pluripotent stem cell Derived cardiomyocytes*. *Frontiers in Cardiovascular Medicine*, 2018. **5**.
53. Shiba, Y., et al., *Human ES-cell-derived cardiomyocytes electrically couple and suppress arrhythmias in injured hearts*. *Nature*, 2012. **489**(7415): p. 322.
54. Corporation, F. *FX-6000 Tension System*. 2019 [cited 2019 April]; Available from: <http://www.flexcellint.com/FX6000T.htm>.
55. IonOptix. *C-Stretch*. 2019 [cited 2019 18 April 2019]; Available from: <http://www.ionoptix.com/product/c-stretch/>.
56. CellScale. *Products*. 2019 [cited 2019 18 April 2019]; Available from: <https://cellscale.com/products/>.
57. Liao, I.C., et al., *Effect of Electromechanical Stimulation on the Maturation of Myotubes on Aligned Electrospun Fibers*. *Cell Mol Bioeng*, 2008. **1**(2-3): p. 133-145.
58. Skaalure, S.C., S.C. Oppegard, and D.T. Eddington, *Characterization of sterilization techniques on a microfluidic oxygen delivery device*. *The Journal of Undergraduate Research at the University of Illinois at Chicago*, 2008. **2**(1).
59. Subramanian, G., et al., *Creating homogenous strain distribution within 3D cell-encapsulated constructs using a simple and cost-effective uniaxial tensile bioreactor: Design and validation study*. *Biotechnol Bioeng*, 2017. **114**(8): p. 1878-1887.
60. Yost, M.J., et al., *Design and construction of a uniaxial cell stretcher*. *Am J Physiol Heart Circ Physiol*, 2000. **279**(6): p. H3124-30.
61. Shachar, M., N. Benishti, and S. Cohen, *Effects of mechanical stimulation induced by compression and medium perfusion on cardiac tissue engineering*. *Biotechnol Prog*, 2012. **28**(6): p. 1551-9.
62. Yeh, R., R.A. Conant, and K.S. Pister. *Mechanical digital-to-analog converters*. in *Tenth International Solid-State Sensors and Actuators Conference (Sendai, Japan, 1999)*. 1999.
63. *The Stepper Motor Basics: Types, Working Operation and Applications*. ElProCus - Electronic Projects for Engineering Students; Available from: <https://www.elprocus.com/stepper-motor-types-advantages-applications/>.
64. Schneider, F., et al., *Process and material properties of polydimethylsiloxane (PDMS) for Optical MEMS*. *Sensors and Actuators A: Physical*, 2009. **151**(2): p. 95-99.
65. Johnston, I., et al., *Mechanical characterization of bulk Sylgard 184 for microfluidics and microengineering*. *Journal of Micromechanics*, 2014. **24**(3): p. 035017.
66. International, A., *ASTM D412-16 Standard Test Methods for Vulcanized Rubber and Thermoplastic Elastomers—Tension*. 2016: West Conshohocken, PA.
67. *Ball & Acme Lead Screw Technical Information*. [cited 2019].
68. *Dow SYLGARD™ 184 Silicone Encapsulant Clear 0.5 kg Kit*.

69. Grasman, J.M., et al., *Static axial stretching enhances the mechanical properties and cellular responses of fibrin microthreads*. *Acta biomaterialia*, 2014. **10**(10): p. 4367-4376.
70. Barillas, M.K., et al., *The CO₂ permeability and mixed gas CO₂/H₂ selectivity of membranes composed of CO₂-philic polymers*. *Journal of Membrane Science*, 2011. **372**(1): p. 29-39.
71. Toume, S., A. Gefen, and D. Weihs, *Printable low-cost, sustained and dynamic cell stretching apparatus*. *Journal of Biomechanics*, 2016. **49**(8): p. 1336-1339.
72. Billiar, K., *FlexCell Device Cost*, A. Rosenthal, Editor. 2019.
73. Soriano-Arroquia, A., et al., *Preparation and Culture of Myogenic Precursor Cells/Primary Myoblasts from Skeletal Muscle of Adult and Aged Humans*. *J Vis Exp*, 2017(120): p. e55047.
74. Cornelison, D.D.W., *Context matters: In vivo and in vitro influences on muscle satellite cell activity*. 2008. **105**(3): p. 663-669.

Appendix A: Pairwise Comparison Chart

User PCC								
Top-Level Objective	Reliability	Ease of Use	Growth Environment	Visualization	Sustainability/Environmental Impact	Cost-Efficient	Reproducible	Total Score
Reliability		0.5	0	1	1	0.5	0	3
Ease of Use	0.5		0	1	1	0.5	0.5	3.5
Growth Environment	1	1		1	1	0.5	0.5	5
Visualization	0	0	0		1	0	0	1
Sustainability/Environmental Impact	0	0	0	0		0	0	0
Cost-efficient	0.5	0.5	0.5	1	1		0.5	4
Reproducible	1	0.5	0.5	1	1	0.5		4.5
Reliability	Organized	Corrosion Resistant	Damage Resistant	Limited Monitoring Required	Reusable	Total Score		
Organized		0.5	0.5	0	1	2		
Corrosion Resistant	0.5		0.5	0	1	2		
Damage Resistant	0.5	0.5		0	1	2		
Limited Monitoring Required	1	1	1		1	4		
Reusable	0	0	0	0		0		
Ease Of Use	Easy to Program	Easy to Clean	Easy to Assemble	Easy To Monitor/Read Outputs	Minimal Training Required	Limited monitoring required	Total Score	
Easy to Program		0.5	0	0.5	1	0		2
Easy to Clean	0.5		1	0.5	1	0		3
Easy to Assemble	1	0		0.5	1	0		2.5
Easy to Monitor/Read Outputs	0.5	0.5	0.5		1	0		2.5
Minimal Training Required	0	0	0	0		0		0
Limited Monitoring Required	1	1	1	1	1			5
Growth Environment	Mechanical Stimulation	CO2	Humidity	Temperature	Nutrients	Electrical Stimulation	Sterility	Total Score
Mechanical Stimulation		0.5	0.5	0.5	0.5	0.5	0.5	3
CO2	0.5		0.5	0.5	0.5	0.5	0.5	3
Humidity	0.5	0.5		0.5	0.5	0.5	0.5	3
Temperature	0.5	0.5	0.5		0.5	0.5	0.5	3
Nutrients	0.5	0.5	0.5	0.5		0.5	0.5	3
Electrical Stimulation	0.5	0.5	0.5	0.5	0.5		0.5	3
Sterility	0.5	0.5	0.5	0.5	0.5	0.5		3
Visualization	Cell Alignment	Cell Hypertrophy	Gene Expression	Construct Structure	Total Score			
Cell Alignment		1	0	0	1			
Cell Hypertrophy	0		0	0	0			
Gene Expression	1	1		0.5	2.5			
Construct Structure	1	1	0.5		2.5			
Sustainability/Environmental Impact	Minimal Waste Production	Minimize Environmental Toxicity	Total Score:					
Minimal Waste Production		0.5	0.5					
Minimize Environmental Toxicity	0.5		0.5					
Reproducible	Accurate	Precise	Total Score					
Accurate		0.5	0.5					
Precise	0.5		0.5					

Client PCC								
Top-Level Objective	Reliability	Ease of Use	Growth Environment	Visualization	Sustainability/Environmental Impact	Cost-Efficient	Reproducible	Total Score
Reliability			1	0	0.5	1	1	0.5
Ease of Use	0		0	0	0	1	1	0
Growth Environment	1	1		0.5	0.5	1	1	0.5
Visualization	0.5	1	0.5		0	1	1	0.5
Sustainability/Environmental Impact	0	0	0	0		0	0	0
Cost-efficient	0	0	0	0	0	1	0	0
Reproducible	0.5	1	0.5	0.5	1	1	1	0.5
Reliability	Organized	Corrosion Resistant	Damage Resistant	Limited Monitoring Required	Reusable	Total Score		
Organized			0	0	0	0	0	0
Corrosion Resistant	1		0.5	1	0.5	3		
Damage Resistant	1	0.5		1	0.5	3		
Limited Monitoring Required	1	0	0		0	1		
Reusable	1	0.5	0.5	1		3		
Ease Of Use	Easy to Program	Easy to Clean	Easy to Assemble	Easy To Monitor/Read Outputs	Minimal Training Required	Limited monitoring required	Total Score	
Easy to Program		0	0	0	1	1	2	
Easy to Clean	1		0.5	0	1	1	3.5	
Easy to Assemble	1	0.5		0	1	1	3.5	
Easy to Monitor/Read Outputs	1	1	1		1	1	5	
Minimal Training Required	0	0	0	0		1	1	
Limited Monitoring Required	0	0	0	0	0	0	0	
Growth Environment	Mechanical Stimulation	CO2	Humidity	Temperature	Nutrients	Electrical Stimulation	Sterility	Total Score
Mechanical Stimulation		0	1	0	0	0.5	0	1.5
CO2	1		1	0	0	1	0	3
Humidity	0	0		0	0	0	0	0
Temperature	1	1	1		0.5	1	0.5	5
Nutrients	1	1	1	0.5		1	0.5	5
Electrical Stimulation	0.5	0	1	0	0		0	1.5
Sterility	1	1	1	0.5	0.5	1		5
Visualization	Cell Alignment	Cell Hypertrophy	Gene Expression	Construct Structure	Total Score			
Cell Alignment		1	1	0.5	2.5			
Cell Hypertrophy	0		1	0.5	1.5			
Gene Expression	0	0		0	0			
Construct Structure	0.5	0.5	1		2			
Sustainability/Environmental Impact	Minimal Waste Production	Minimize Environmental Toxicity	Total Score:					
Minimal Waste Production		1	1					
Minimize Environmental Toxicity	0		0					
Reproducible	Accurate	Precise	Total Score					
Accurate		0	0					
Precise	1		1					

Designer PCC								
Top-Level Objective	Reliability	Ease of Use	Growth Environment	Visualization	Sustainability/Environmental Impact	Cost-Efficient	Reproducible	Total Score
Reliability	1	0.5	0.5	1	1	0.5	0.5	4.5
Ease of Use	0	1	0	0	1	0.5	0	1.5
Growth Environment	0.5	1	1	1	1	1	0.5	5
Visualization	0.5	1	0	1	1	1	0.5	4
Sustainability/Environmental Impact	0	0	0	0	1	0.5	0	0.5
Cost-efficient	0	0.5	0	0	0.5	1	0	1
Reproducible	0.5	1	0.5	0.5	1	1	0.5	4.5
Reliability	Organized	Corrosion Resistant	Damage Resistant	Limited Monitoring Required	Reusable	Total Score		
Organized	1	0	1	0.5	0.5	2		
Corrosion Resistant	1	1	1	1	1	4		
Damage Resistant	0	0	0	0	0.5	0.5		
Limited Monitoring Required	0.5	0	1	0.5	0.5	2		
Reusable	0.5	0	0.5	0.5	0.5	1.5		
Ease Of Use	Easy to Program	Easy to Clean	Easy to Assemble	Easy To Monitor/Read Outputs	Minimal Training Required	Limited Monitoring Required	Total Score	
Easy to Program	1	1	1	0.5	1	1	4.5	
Easy to Clean	0	0	0	0	0.5	0	0.5	
Easy to Assemble	0	1	0	0	0.5	0	1.5	
Easy to Monitor/Read Outputs	0.5	1	1	1	1	0.5	4	
Minimal Training Required	0	0.5	0.5	0	0	0	1	
Limited Monitoring Required	0	1	1	0.5	1	0.5	3.5	
Growth Environment	Mechanical Stimulation	CO2	Humidity	Temperature	Nutrients	Electrical Stimulation	Sterility	Total Score
Mechanical Stimulation	0.5	0.5	0.5	0.5	0.5	0.5	0	2.5
CO2	0.5	0.5	0.5	0.5	0.5	0.5	0	2.5
Humidity	0.5	0.5	0.5	0.5	0.5	0.5	0	2.5
Temperature	0.5	0.5	0.5	0.5	0.5	0.5	0	2.5
Nutrients	0.5	0.5	0.5	0.5	0.5	0.5	0	2.5
Electrical Stimulation	0.5	0.5	0.5	0.5	0.5	0.5	0	2.5
Sterility	1	1	1	1	1	1	0	6
Visualization	Cell Alignment	Cell Hypertrophy	Gene Expression	Construct Structure	Total Score			
Cell Alignment	1	0.5	1	0.5	2			
Cell Hypertrophy	0.5	1	1	0.5	2			
Gene Expression	0	0	0	0	0			
Construct Structure	0.5	0.5	1	0.5	2			
Sustainability/Environmental Impact	Minimal Waste Production	Minimize Environmental Toxicity	Total Score					
Minimal Waste Production	1	0	0					
Minimize Environmental Toxicity	1	1	1					
Reproducible	Accurate	Precise	Total Score					
Accurate	1	0	0					
Precise	1	1	1					

Appendix B: Pugh Matrices

Well Plate Material		PDMS	Glass Bottom	Polystyrene (standard)
Constraints				
C1	Sterile	Y	Y	Y
C2	Functions within Lab Incubator	Y	Y	Y
C3	Completed before April	Y	Y	Y
C4	Cost Below \$1000 Budget	Y	Y	Y
C5	Cell Viability	Y	Y	Y
Objectives:		Scores		
O1	Weight % Reliability			
17.60%	Durable	4	2	4
	Limited monitoring required			
	Reusable	2	1	1
Total Score:		6	3	5
Weighted Sum:		1.056	0.528	0.88
O2	Weight % Ease of Use			
11.90%	Easy to Program			
	Easy to Clean	5	5	5
	Easy to Assemble	4	5	5
	Minimal Training Required	4	5	5
Total Score:		13	15	15
Weighted Sum:		1.547	1.785	1.785
O3	Weight % Reproducible			
21.40%	Accurate			
	Precise			
Total Score:				
Weighted Sum:				
O4	Weight % Visualization			
14.30%	Imagable	4	5	5
	Total Score:	4	5	5
Weighted Sum:		0.572	0.715	0.715
O5	Weight % Cost Efficient			
10.50%		4	4	5
	Total Score:	4	4	5
Weighted Sum:		0.42	0.42	0.525
Total Score:		3.595	3.448	3.905

Construct Anchoring		Built Into Well	Vellum Frame	Inverted Vellum Frame
Constraints				
C1	Sterile	Y	Y	Y
C2	Functions within Lab Incubator	Y	Y	Y
C3	Completed before April	Y	Y	Y
C4	Cost Below \$1000 Budget	Y	Y	Y
C5	Cell Viability	Y	Y	Y
Objectives:		Scores		
O1	Weight % Reliability			
17.60%	Durable	4	2	3
	Limited monitoring required			
	Reusable			
Total Score:		4	2	3
Weighted Sum:		0.704	0.352	0.528
O2	Weight % Ease of Use			
11.90%	Easy to Program			
	Easy to Clean	5	5	5
	Easy to Assemble	4	4	4
	Minimal Training Required	4	4	4
Total Score:		13	13	13
Weighted Sum:		1.547	1.547	1.547
O3	Weight % Reproducible			
21.40%	Accurate			
	Precise			
Total Score:				
Weighted Sum:				
O4	Weight % Visualization			
14.30%	Imagable	2	5	5
	Total Score:	2	5	5
Weighted Sum:		0.286	0.715	0.715
O5	Weight % Cost Efficient			
10.50%		4	5	4
	Total Score:	4	5	4
Weighted Sum:		0.42	0.525	0.42
Total Score:		2.957	3.139	3.21

Mechanical Stim. Technique		Uniaxial	Multiaxial	Shear Flow	Mechanical Stim. Technique		Uniaxial	Shear Flow
Constraints					Constraints			
C1	Sterile	Y	Y	Y	C1	Sterile	Y	Y
C2	Functions within Lab Incubator	Y	Y	Y	C2	Functions within Lab Incubator	Y	Y
C3	Completed before April	Y	Y	Y	C3	Completed before April	Y	Y
C4	Cost Below \$1000 Budget	Y	Y	Y	C4	Cost Below \$1000 Budget	Y	Y
C5	Cell Viability	Y	Y	Y	C5	Cell Viability	Y	Y
Objectives:		Scores			Objectives:		Scores	
O1 Weight % Reliability					O1 Weight % Reliability			
17.60%	Durable				17.60%	Durable		
	Limited monitoring required	4	4	4		Limited monitoring required	4	4
	Reusable	4	4	2		Reusable	4	2
Total Score:		8	8	6	Total Score:		8	6
Weighted Sum:		1.408	1.408	1.056	Weighted Sum:		1.408	1.056
O2 Weight % Ease of Use					O2 Weight % Ease of Use			
11.90%	Easy to Program	4	3	3	11.90%	Easy to Program	4	3
	Easy to Clean					Easy to Clean		
	Easy to Assemble	4	3	2		Easy to Assemble	4	2
	Minimal Training Required					Minimal Training Required		
Total Score:		8	6	5	Total Score:		8	5
Weighted Sum:		0.952	0.714	0.595	Weighted Sum:		0.952	0.595
O3 Weight % Reproducible					O3 Weight % Reproducible			
21.40%	Accurate	3	5	2	21.40%	Accurate	3	2
	Precise	3	4	3		Precise	3	3
Total Score:		6	9	5	Total Score:		6	5
Weighted Sum:		1.284	1.926	1.07	Weighted Sum:		1.284	1.07
O4 Weight % Visualization					O4 Weight % Visualization			
14.30%	Imagable				14.30%	Imagable		
Total Score:					Total Score:			
Weighted Sum:					Weighted Sum:			
O5 Weight % Cost Efficient					O5 Weight % Cost Efficient			
10.50%		4	3	2	10.50%		4	2
Total Score:		4	3	2	Total Score:		4	2
Weighted Sum:		0.402	0.3015	0.201	Weighted Sum:		0.402	0.201
Total Score:		4.046	4.350	2.922	Total Score:		4.046	2.922

Force Analysis		Load Cell	Displacement
Constraints			
C1	Sterile	Y	Y
C2	Functions within Lab Incubator	Y	Y
C3	Completed before April	Y	Y
C4	Cost Below \$1000 Budget	Y	Y
C5	Cell Viability	Y	Y
Objectives:		Scores	
O1	Weight %	Reliability	
	17.60%	Durable	4 5
		Limited monitoring	5 3
		Reusable	5 5
		Total Score:	14 13
		Weighted Sum:	2.464 2.288
O2	Weight %	Ease of Use	
	11.90%	Easy to Program	5 2
		Easy to Clean	
		Easy to Assemble	
		Minimal Training	4 3
		Total Score:	9 5
		Weighted Sum:	1.071 0.595
O3	Weight %	Reproducible	
	21.40%	Accurate	5 3
		Precise	5 3
		Total Score:	10 6
		Weighted Sum:	2.14 1.284
O4	Weight %	Visualization	
	14.30%	Imagable	
		Total Score:	
		Weighted Sum:	
O5	Weight %	Cost Efficient	
	10.50%		3 3
		Total Score:	3 3
		Weighted Sum:	0.3015 0.3015
		Total Score:	5.977 4.469

Force Production		Stepper Motor	Vacuum Pressure	Magnetic Beads
Constraints				
C1	Sterile	Y	Y	M
C2	Functions within Lab Incubator	Y	Y	M
C3	Completed before April	Y	Y	Y
C4	Cost Below \$1000 Budget	Y	Y	Y
C5	Cell Viability	Y	Y	Y
Objectives:		Scores		
O1	Weight %	Reliability		
	17.60%	Durable	4 4	
		Limited monitoring	4 4	
		Reusable	4 4	
		Total Score:	12 12	
		Weighted Sum:	2.112 2.112	
O2	Weight %	Ease of Use		
	11.90%	Easy to Program	4 4	
		Easy to Clean	4 4	
		Easy to Assemble	4 3	
		Minimal Training	4 3	
		Total Score:	16 14	
		Weighted Sum:	1.904 1.666	
O3	Weight %	Reproducible		
	21.40%	Accurate	2 3	
		Precise	4 3	
		Total Score:	6 6	
		Weighted Sum:	1.284 1.284	
O4	Weight %	Visualization		
	14.30%	Imagable		
		Total Score:		
		Weighted Sum:		
O5	Weight %	Cost Efficient		
	10.50%		3 3	
		Total Score:	3 3	
		Weighted Sum:	0.3015 0.3015	
		Total Score:	5.602 5.364	

Appendix C: Experimental Protocols

Instron Well Plate Deformation Test Method

Purpose:

The purpose of this test method is to measure the deformation of a dog-bone shaped polydimethylsiloxane (PDMS) well plate and cardiac patch substitutes placed in its wells when stretched in uniaxial tension.

Scope: This is to inform the validation testing of components from a device fabricated from an MQP at Worcester Polytechnic Institute

Materials:

- Instron 5544 Universal Testing Machine
- Diamond-tip grippers
- PDMS well plate
- 3 PDMS frames
- 12 stainless steel pins
- Rice paper
- 6 Velum frames
- “Special Lab Glue”
- Calipers
- Video recording device
- Grip position overlay
- Permanent marker

Personal Protective Equipment:

- Safety glasses
- Instron safety shield

Procedure:

1. Turn on the computer next to the Instron 5544 and log in. Then open Bluehill 3 and log in with your username and password.
 - a. Sign the Instron log book with your name(s) and the date and time.
2. Turn on the Instron 5544 using the switch at the back. Put on safety goggles at this time.
3. Load the PDMS_Tensile_Test Bluehill 3 method.
4. Ensure all parameters are in line with those listed in the Table 1 below.

Table 1. Test Parameters

General	Units	SI		
	Assign specimen parameters from	Method default		
Sample	Notes	NA		
	Number Inputs	NA		
	Text Inputs	NA		
Specimen	Properties	Specimen label	User discretion	
		Geometry	Rectangular	
		Width	26mm	
		Thickness	15.8 mm	
		Length	269.302 mm	
		Final width	26 mm	
		Final thickness	17.38 mm	
	Final length	309.8 mm		
	Notes	NA		
	Number inputs	NA		
	Text inputs	NA		
	Choice inputs	NA		
Measurement types	Load			
	Torque			
	Strain			
	User-defined			
	Expression			
	Corrected extension			
Calculations	NA			
Test control	Start test	By the start button		
	Strain	Primary source	Extension	
Pretest	Temperature soak	NA		
	Preload	NA		
	Autobalance	NA		
	Precycling	Cycles		4
		Control mode		Extension
		Rate		500 mm/min
		Maximum measurement		Extension
		Maximum value		12.8 mm
Minimum measurement		Extension		
Minimum value		0		

Test	Ramp 1	Control Mode	Extension
			Rate 1
End of Test	Criteria 1	Measurement Event	
		Measurement 1	Extension
		Value 1	12.8 mm
	End of Test Action	Stop	
Console	Selected Live Displays	Extension	
		Load	
Workspace	N/A		
Exports	Export Raw Data	Modulus (automatic Young's)	
		Geometry	
		Length	
		Thickness	
		Width	
Prompted Test	N/A		

5. With the grips empty, calibrate the 2 kN load cell.
6. Ensure the mechanical stops on the side of the Instron 5544 are set appropriately to prevent the load cell from crashing.
7. Balance the load cell with the grips empty.
8. To ensure the grips are centered on the well plate, draw squares in permanent marker on the PDMS well plate according to the overlay provided.
9. Cut 3 X by Y rectangles from the rice paper. Place the Velum frames over the PDMS frames, then glue the ends of the rice paper onto the Velum frames. Wait for the glue to dry.
10. Using a pair of scissors, cut the long edges of the PDMS frame and Velum frame in the centers, being careful not to cut the rice paper.
11. Center the PDMS frames in each well, then using the stainless steel pins, drive a pin through each corner of the frame into the well plate.
12. Put the bottom end of the PDMS well plate into the lower grip with the edges of the grip face lined up with the drawn square and tighten the grips.
13. Put the top end of the PDMS well plate into the upper grip with the edges of the grip face lined up with the drawn square and tighten the grips.
14. Apply a 1 N \pm 0.05 tare load.
15. Zero the extension.
16. Attach an object of a known length to the Instron so that it is in the **same** field of view as the well plate.
17. Set up the safety shield.
18. Set up the video equipment so that the wells are seen in the foreground of the video.
19. Ensure that the video capture equipment is secure and steady, and start recording.
20. On the Bluehill 3 software, begin the test.
21. Ensure the test is running smoothly and ensure that the grips do not come too close to the mechanical stops.
22. After the test is done running, click stop and stop the recording.
23. Hit the “return” button to jog the load cell back to the initial position.

24. Save the results of the test to a flash drive.
25. Remove the safety shield and the well plate from the Instron 5544.
26. Turn off the Instron and click the exit button on the BlueHill 3 software.
27. Replace the safety shield.

Mechanical Stimulator Well Plate Deformation Test Method

Purpose:

The purpose of this test method is to validate the ability of a mechanical stimulation system to stretch a dog bone shaped PDMS well plate to achieve 10% in each of the three wells.

Scope: This is to inform the validation testing of components from a device fabricated from an MQP at Worcester Polytechnic Institute.

Materials:

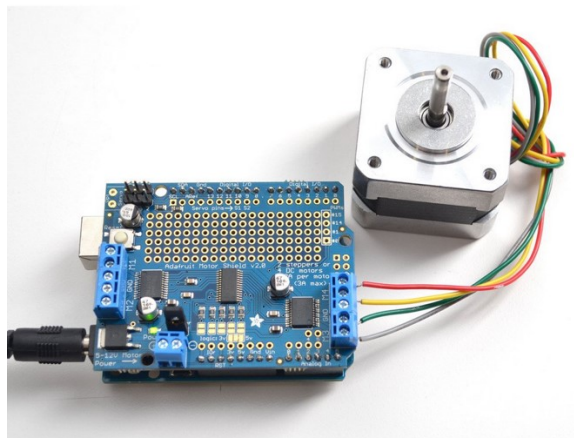
- Mechanical stimulation system and associated small parts
- PDMS well plate
- 3 PDMS frames
- 12 stainless steel pins
- Rice paper
- 3 Velum frames
- Glue
- Calipers
- Video recording device
- Grip position overlay
- Permanent marker
- Arduino operation code

Personal Protective Equipment:

- Safety glasses

Procedure:

1. On the benchtop, attach wires from the stepper motor in the mechanical stimulator to the Arduino.



*** The stepper motor wires connect to the M3 and M4 port on the side of the Arduino **exactly as shown in the above picture**. Plug the positive and negative leads of the AC/DC converter for the stepper motor into the positive and negative terminals of the motor power housing (bottom edge of Arduino).

2. Separately, place the vellum frame on top of the PDMS frame ensuring proper alignment.
3. Place the PDMS frame into the well and secure with stainless steel pins in all four corners.
4. Soak and cut a piece of rice paper the size of a cardiac patch and place it on the frame.
5. Glue the rice paper to the vellum and allow a two minutes for glue to dry.
6. Place the well plate on the mechanical stimulator and secure the grips so that the well plate is edge to edge with the grips.
7. Ensure that there is the same distance on each side of the well plate at both the left and the right ends of the mechanical stimulator.
8. Secure the well plate in the grips by tightening the nuts on the screws protruding from the top of the stimulator grips.
9. Mount the video recording device so the experiment can be seen from a top view.
10. Ensure the Arduino code (shown in Appendix of this protocol) is uploaded to the Arduino by plugging the Arduino into the computer, confirming that the code has the desired parameters (running for 5 cycles, speed = 5 RPM translating to 170 mm/min actuation), and flashing the code to the Arduino. Then, unplug the Arduino from the computer.
11. Ensure that the mechanical system, well plate, and camera are in place, then plug the Arduino into an AC/DC power supply to start the test.
12. Run the test for five cycles and stop the video.
13. Save the video for future ImageJ analysis.
14. Repeat this protocol with two additional well plates.

Image Analysis of Well Plate Deformation Protocol

Purpose:

The purpose of this protocol is to quantify and analyze the deformation of a cardiac patch substitute within a dog-bone shaped polydimethylsiloxane (PDMS) well plate when stretched in uniaxial tension. This will be done through analyzing images obtained after performing the Instron Testing Protocol. This protocol is used to validate that an even 10% strain distribution would be acquired during mechanical stimulation.

Scope: This is to inform the validation testing of components from a device fabricated from an MQP at Worcester Polytechnic Institute.

Materials:

- ImageJ software
- Video recording of Instron test

Personal Protective Equipment:

- N/A

Procedure:

1. Transfer the video file from the video capture device to a computer.
2. Each test video should supply ten images, five of the well plate in the unstretched position, and five of the well plate in the stretched position.
3. The video file will be run through the appropriate MATLAB code according to the MATLAB code protocol. Ten images for each video will be outputted from this.
4. Once all images have been taken from the video, open ImageJ software.
5. On the taskbar, under file, click open.
6. Locate the photo from the test that you would like to analyze.
7. After the image opens, click this icon  in order to draw a straight line on the image.
8. Locate the item of a known distance that was used in the Instron Test Method, and zoom in on the item using this icon .
9. Click the mouse on the starting point of the measurement line and drag to the end point.
10. Once a yellow line is visible on the scale, under analyze on the taskbar, click set scale.
11. A pop-up window will appear and next to "Known Distance" enter the length of the item in the photograph of a known length.
12. Underneath, next to unit of length, input the units for the known length inputted in step 11 and click OK.
13. Following this zoom in on the top well in the photo but ensure that the bottom crosshead of the instron is visible in the photo.
14. Click and drag a straight line from the marker on the cardiac patch at the top left corner of the well to the cross head of the instron. An example can be seen below.

15. A results pane will appear and the measurement that was just taken can be seen under the length column.
16. The same should be done on the right side of the well from the top marker. Which can also be seen in the image below.
17. Steps 13-15 should be repeated for the markers at the bottom end of the cardiac patch and for all following wells in the image.
18. Once all measurements have been taken of an image, click File and Save As in the results pane.
19. The results will save to an excel file for further analysis. Be sure to keep track of order of measurement in the results file.
20. Next exit out of the image but not the ImageJ software.
21. Open the next image and repeat steps 5-20.
22. Once all the measurements have been taken, click File and Save As on the window that shows the data. The data will save as a comma delimited excel file for future analysis.

Assembly of Fibrin Microthreads on the Vellum Frames Using a Pressurized Vacuum Chamber Protocol

Purpose:

The purpose of this protocol is to have a uniform mechanism of spacing out the fibrin microthreads on the vellum frames without user variability. The team used a past MQP's pressurized vacuum chamber to uniformly space these fibrin microthreads.

Scope: This is to inform the uniformity of the fibrin microthreads on the vellum frames as part of a design component from an MQP at Worcester Polytechnic Institute.

Materials:

- Pins Lab pressurized vacuum chamber
- Tape
- Forceps
- Scissors
- Vellum frames
- Epoxy glue

Personal Protective Equipment:

- Safety glasses
- Gloves

Procedure:

1. Equally space out and place 5 fibrin microthreads within the pressurized vacuum chamber
2. Tape both sides of the pressurized vacuum chamber to allow for removal of threads
3. Place thread on top of two vellum frames
4. Glue the threads down on both sides of the vellum frames and let dry overnight

Ethanol Sterilization of the Fibrin Microthreads on the Vellum Frames Protocol

Purpose:

The purpose of this protocol is to sterilize the fibrin microthreads on the vellum frames to allow for proper sterilization of the patch components. This will eliminate the possibility of exposing the cells to any pathogens that will cause bacterial contamination.

Scope: This is to inform the sterilization of the fibrin microthreads as a design requirement from an MQP at Worcester Polytechnic Institute.

Materials:

- Autoclaved DI water
- Ethanol
- Forceps
- 1 Well Plate

Personal Protective Equipment:

- Gloves
- Biosafety Cabinet

Procedure:

1. Hydrate the fibrin microthreads on the vellum frame with autoclaved water for 1 hour
2. Hydrate in ethanol for 2-3 hours
3. Rinse 2-3 time with autoclaved water
4. Leave to dry overnight propped up on the side of the well plate

Note: Make sure all threads are still intact.

Assembling the Patch with C2C12 Cells Protocol

Purpose:

The purpose of this protocol is to provide a guide for synthesizing the fibrin-based patches with C2C12 cells in full assembly within the team's PDMS well plate.

Scope: This is to inform the synthesis of the fibrin-based patches as fabricated a design component from an MQP at Worcester Polytechnic Institute.

Materials:

Material	Number needed	Supplier	Sterilizing method
Forceps	2		Autoclave
Scissors	1		Autoclave
Sterile 6 well plate	1		NA
PDMS well plate	1	Dow Sylgard 184 (10:1)	Autoclave
PDMS lid	1	Dow Sylgard 184 (20:1)	Autoclave
PDMS casting devices	8	Dow Sylgard 184 (10:1)	Autoclave
PDMS culturing devices	8	Dow Sylgard 184 (10:1)	Autoclave
Stainless steel pins	12		Autoclave, Ethanol
Sterile Vacuum grease	1 syringe	Dow Corning, Z273554	Autoclave
PBS (1X, pH = 7.4)	500 mL	Sigma Aldrich, P3813	Autoclave
1% Pluronic F-127	500 mL	Sigma Aldrich, P2443	Autoclave
C2C12 Prolif Media (DMEM 1X, 10% FBS, GlutaMAX, PenStrep, 0.4% Aprotinin)	500 mL	Gibco: 1195-065, 26140-087, 3505-061, 15140-122 ThermoFisher: 78432	Prepare in sterile conditions
11 mg/mL Fibrinogen	1000 uL	Sigma Aldrich, F8630	Sterile filter
40 U/mL Thrombin	500 uL	Sigma Aldrich, T4648	Sterile filter
Ice	Enough to fill the styrofoam		NA
Styrofoam	1 -Small		NA

C2C12 Cells	400,000 cells/patch		NA
Sterile T75 Flask Filter Caps	2 per plate		NA
Vellum Frame with Fibrin Microthreads	3		Ethanol

Personal Protective Equipment:

- Gloves
- Biosafety Cabinet

Procedure:

1. Rehydrate samples in PBS 1 hour
2. 1% Pluronics coating of PDMS slabs and devices 1 hour
3. Thaw fibrinogen and thrombin to room T.
4. Sterile filter all gel components.
5. Place gel components on ice in hood.
6. Trypsinize/ Take cell count
 - a. Factor in the entire volume of liquid for an accurate count.
 - b. Mix cell suspension thoroughly.
 - c. Use trypan blue to ensure you can distinguish cells from debris.
 - i. 50 uL trypan blue, 40 ul PBS, 10 uL cell suspension (1:10 dilution)
 - d. Obtain cell count.
7. Spin cells down at 1000 rpm for 5 minutes.
8. Re-suspend cells:

$$\frac{400,000 \text{ cells}}{68\% \times 150 \text{ uL}} = \frac{\text{Cell count obtained}}{X}$$

9. Cast samples
 - a. Take a 1 well plate with casting devices and fill with hydrated samples.
 - b. Mix gel components on ice.
 - c. Only cast 2 samples at a time (or 1 if more comfortable!)

COMPONENT	VOLUME/ BATCH OF 2 (X3)	VOLUME/ BATCH OF 1 (X1)	TOTAL VOLUME PER GROUP
FIBRINOGEN	84	42	252
CELL SUSPENSION	204	102	612
THROMBIN (ADD LAST)	12	6	36

TOTAL **300 uL** **150 uL**

10. Allow 10 minutes for polymerization, then move vellum frame with the patch to the cut PDMS frames

11. Cut vellum frame in half where PDMS frame is cut in half to allow for tension of the device
12. Place the PDMS frame with the patch inside each of the 3 wells in the PDMS well plate
13. Put 1 mL of media within each well
14. Place 1 pin in each of the 4 corners of the PDMS frame to secure the vellum frame to the PDMS plate
15. Aspirate the media and add 3 mL of media to each well
16. Following 2-3 days, change the culture media to differentiation media to allow cells to differentiate and begin their maturation process.

Removing the patch:

1. Aspirate media from each well
2. Remove pins from all 4 corners of the PDMS frame
3. Gently remove the patch and place within a 6 well plate

C2C12 Actin Cytoskeleton and Nucleus Staining Protocol

Actin Staining Protocol from Thermo Fisher for Alexa Fluor 488 Phalloidin (Life Technologies #A12379, lot #1670151) & Hoechst 33342 (Invitrogen #H3570, lot #822698)

Purpose:

The purpose of this protocol is to visualize the nucleus and actin cytoskeleton of fixed C2C12 murine skeletal myoblast cells. The fluorescence staining allows the team to see the differing results between the experimental groups- the control group, the static group, and the dynamic group. This will be done through analyzing microscopic images obtained from the stained patches from the 1-day and 6-day experiments.

Scope: This is to inform the validation of the fibrin-based patches from a device fabricated from an MQP at Worcester Polytechnic Institute.

Materials:

- Phosphate Buffered Saline, 1X (PBS)
- 4% Paraformaldehyde
- 0.1% Triton X-100
- 1:40 μ L Alexa Fluor 488 Phalloidin
- 1:6000 Hoechst

Personal Protective Equipment:

- Gloves

Procedure:

1. Wash patch twice with prewarmed phosphate-buffered saline, pH 7.4 (PBS).
2. Fix the sample in 4% paraformaldehyde solution in PBS for 30 minutes at room temperature.
Note: Methanol can disrupt actin during the fixation process. Therefore, it is best to avoid any methanol containing fixatives. The preferred fixative is methanol-free formaldehyde.
3. Wash 3x with PBS.
4. Add 0.1% Triton X-100 in PBS for 20 minutes.
5. Wash 3x with PBS.
6. Dilute 5 μ L of Alexa Fluor 488 Phalloidin into 200 μ L PBS for each patch to be stained with. Stain for 20 minutes at room temperature.
Note: A total of 300 μ L of 1:40 Alexa Fluor 488 Phalloidin was used for each patch.
7. Wash 3x with PBS.
8. Counterstain with 1:6000 Hoechst for 10 minutes. Keep in the dark.
9. Wash 3x with PBS.
10. Leave PBS with patches if not immediately imaged and store in the dark at 2-6°C.

Molding the PDMS Frames and Casting Frames Protocol

Purpose:

The purpose of this test method is to make polydimethylsiloxane (PDMS) frames and casting frame for fabrication of fibrin microthread based tissue scaffolds.

Scope:

This is to inform the validation testing of the PMDS frames and casting frames fabricated from an MQP at Worcester Polytechnic Institute.

Materials:

- SYLGARD 184 Silicone Elastomer Base Agent
- SYLGARD 184 Silicone Elastomer Curing Agent
- Oven
- Large weigh boats
- Scale
- Spoon
- Ethanol
- Autoclave bag
- Autoclave machine
- Disposable plastic pipet
- Degasser chamber
- Aluminum
- Razor blade

Personal Protective Equipment:

- Safety glasses
- Gloves
- Lab Coat

Procedure:

1. Place one large weigh boat on the scale and zero it.
2. Using a spoon, weigh out approximately 10.8 grams of the Silicone Elastomer Base Agent onto the weigh boat.
3. Using the disposable plastic pipet, weigh out approximately 1.2 grams of the Silicone Elastomer Curing Agent onto the weigh boat with the base agent.
4. Thoroughly mix the two agents for 2 minutes to achieve a proper PDMS ratio of 10:1.
5. Carefully pour the uncured PDMS onto the aluminum mold and evenly spread it using a plastic pipet.
6. Place the aluminum mold with PMDS into the degasser and let it stand until no bubbles remain.
7. Take out the mold out of the degasser and pop any remaining bubbles carefully using a gauge needle.

8. Place mold in oven at 85 degrees celsius for 100 minutes.
9. Remove mold from oven, let cool for a while, and carefully peel the PDMS off of the mold.
10. Using a razor blade, carefully cut the excess PDMS from each PDMS frame and casting frame
11. For the PDMS frames, carefully cut a small rectangle in the center of the frame.
12. Place the PDMS frames and PDMS casting frames in an autoclave bag and seal.
13. Place autoclave bag inside the autoclave machine and run the wrapped cycle for 30 minutes.

Molding the PDMS Lid Protocol

Purpose:

The purpose of this test method is to make a polydimethylsiloxane (PDMS) lid for the custom PDMS dog-bone shaped well plate.

Scope:

This is to inform the validation testing of the PMDS lid a device fabricated from an MQP at Worcester Polytechnic Institute.

Materials:

- SYLGARD 184 Silicone Elastomer Base Agent
- SYLGARD 184 Silicone Elastomer Curing Agent
- Oven
- Large weigh boats
- Scale
- Spoon
- Ethanol
- Autoclave bag
- Autoclave machine
- Disposable plastic pipet
- Degasser chamber
- Four piece aluminum mold
- 6 T25 hex screws
- T25 star screw driver

Personal Protective Equipment:

- Safety glasses
- Gloves
- Lab Coat

Procedure:

1. Place one large weigh boat on the scale and zero it.
2. Using a spoon, weigh out approximately 52.25 grams of the Silicone Elastomer Base Agent onto the weigh boat.
3. Using the disposable plastic pipet, weigh out approximately 2.75 grams of the Silicone Elastomer Curing Agent onto the weigh boat with the base agent.
4. Thoroughly mix the two agents for 2 minutes to achieve a proper PDMS ratio of 20:1.
5. Ensure the bottom and two sides of the aluminum mold are properly secured using the allen wrench to tighten all the screws into place (do NOT include the top mold)
6. Place the three piece mold on the scale and zero it.
7. Carefully pour and weigh out about 45 grams of the uncured PDMS into the three piece mold.
8. Next, place mold with PDMS into the degasser and leave in until no bubbles remain.

9. Take out of degasser and place top mold onto the rest of the three piece mold (make sure it is properly set).
10. Place mold back in degasser and leave in until no more bubbles rise after 10 minutes.
11. Place mold in oven at 85 degrees celsius for 130 minutes.
12. Remove mold from oven, let cool for a while (you may put in fridge/freezer) and unscrew all hex screws.
13. Remove side pieces first, followed by the top piece.
14. Very carefully, remove cured PDMS from mold.
15. Using the 15mm circle cutter, puncture one hole at the center of each prong on the PDMS lid.
16. Wipe down any excess PDMS from the aluminum mold and resemble mold.
17. Wipe down any excess PDMS from the PDMS lid, place in autoclave bag, and seal.
18. Place PDMS well plate in autoclave bag inside the autoclave machine and run the wrapped cycle for 30 minutes.

*When working under the hood, place one T75 Filter Flask cap on each prong of the lid

Molding the PDMS Well Plate Protocol

Purpose:

The purpose of this test method is to make a dog-bone shaped well plate out of polydimethylsiloxane (PDMS) with three wells.

Scope:

This is to inform the validation testing of the PMDS well plate a device fabricated from an MQP at Worcester Polytechnic Institute.

Materials:

- SYLGARD 184 Silicone Elastomer Base Agent
- SYLGARD 184 Silicone Elastomer Curing Agent
- Oven
- Large weigh boats
- Scale
- Spoon
- Vacuum Grease
- Cotton Swab
- Kimwipes
- Ethanol
- Autoclave bag
- Autoclave machine
- Disposable plastic pipet
- Degasser chamber
- Five Piece Aluminum Mold
- 6 5/32 hex screws
- 8 3/16 hex screws
- 5/32 allen wrench
- 3/16 allen wrench

Personal Protective Equipment:

- Safety glasses
- Gloves
- Lab Coat

Procedure:

1. Place one large weigh boat on the scale and zero it.
2. Using a spoon, weigh out approximately 119.3 grams of the Silicone Elastomer Base Agent onto the weigh boat.
3. Using the disposable plastic pipet, weigh out approximately 13.26 grams of the Silicone Elastomer Curing Agent onto the weigh boat with the base agent.
4. Thoroughly mix the two agents for 2 minutes to achieve a proper PDMS ratio of 10:1.
5. Place the weigh boat with the uncured PDMS into the degasser and leave in until all bubbles have been removed.

6. Repeat steps 1 through 5 so a second weigh boat of uncured PDMS is obtained.
7. Using the two-part aluminum mold, make sure all pieces are properly secured using the allen wrench to tighten all the screws into place.
8. On the bottom circumference of each well, apply a small amount of vacuum grease and use the cotton swab to carefully spread it along the circumference so a thin, but proper seal is made.
9. Carefully wipe any excess vacuum grease by using a kimwipe or cotton swab.
10. Pour the two weigh boats of uncured PDMS carefully into the mold so it fills to the brim.
11. Using a syringe XX gauge tip needle, pop the leftover bubbles.
12. Once all bubbles are removed, place the mold in a curing oven at 85 degrees Celsius for 100 minutes.
13. Remove mold from oven, let cool for a while (you may put in fridge/freezer) and unscrew all hex screws.
14. Separate the bottom mold plate from the rest of the mold and carefully remove the now cured PDMS dog-shape well plate.
15. Next, remove the three aluminum blocks from each well in the PDMS plate.
16. Clean any excess PDMS off the aluminum with ethanol and reassemble the mold.
17. Clean any excess PDMS off the PDMS well plate with ethanol, place inside an autoclave bag, and seal.
18. Place PDMS well plate in autoclave bag inside the autoclave machine and run the wrapped cycle for 30 minutes.

Fibrin Microthread Extrusion Protocol

Aliquot Preparation

Materials:

Fibrinogen (F8630, Sigma)
Thrombin (T4648, Sigma) – 1 KU
Calcium Chloride (CaCl₂; MW: 110.99)
Sodium Chloride (NaCl; MW: 58.44)
HEPES (MW: 238.3)

Procedure:

HEPES buffered saline (HBS) preparation

1. Definition: HBS contains 20 mM HEPES and 0.9% (w/v) NaCl
2. Add the following reagents to 200 mL:
 - a. 2.25g of NaCl
 - b. 1.1915g of HEPES
3. pH solution to 7.4 using NaOH/HCl.
4. Bring final volume to 250 mL.
5. Store at room temperature.

Fibrinogen aliquots (70 mg/mL)

1. Measure 14.3 mL of HBS into a 50 mL conical tube.
2. Weigh 1.00 gram of fibrinogen and pour into conical tube.
3. Put conical tube on rocker plate, adjusting the position every 30-40 minutes until fibrinogen goes into solution.
NEVER SHAKE/VORTEX FIBRINOGEN SOLUTION!!!! THIS WILL CAUSE FIBRINOGEN TO FALL OUT OF SOLUTION AND BIND TO ITSELF!!!!
4. Incubate conical tube at 37 C overnight to ensure fibrinogen is completely dissolved.
5. The next morning, measure 1 mL aliquots in eppendorfs and store at -20 °C.

Thrombin aliquots (40 U/mL)

1. Add 25 mL HBS to bottle of 1KU thrombin, mix well.
2. Aliquot 200 µL into eppendorfs and store at -20 °C (Final concentration: 8U / 200 µL).

Calcium chloride preparation (40 mM)

1. Add 0.1776 g of CaCl₂ to 40 mL of diH₂O.
2. Store at 4 °C.

HEPES buffer bath stock solution

1. Definition: Stock solution will be prepared at 10X of 10 mM HEPES buffer (100mM).
2. Add 23.83g of HEPES to 900 mL of diH₂O.
3. pH to 7.4 using NaOH/HCl
WILL REQUIRE LARGE AMOUNTS OF ACID/BASE- USE HIGHER CONCENTRATIONS CAREFULLY.
4. Bring final volume to 1000 mL.
5. Store at room temperature.

Extrusion Procedure

Materials:

Fibrinogen aliquot (warmed to room temperature)
Thrombin aliquot (warmed to room temperature)
Calcium chloride solution (40mM, warmed to room temperature)
HEPES buffer bath stock solution (10X)
Metal non-stick pan
25 Gauge blunt end needle
0.86 mm I.D. polyethylene tubing (Intramedic PE90 427421)
2 1 mL syringes
Blending connector (SA-3670; Micromedics, MN)

Setup:

1. Place blunt end needle (25 gauge, BD) into 0.86 mm I.D. polyethylene tubing.
CAN REUSE THESE MATERIALS IF PREVIOUS USER WASHED PROPERLY
2. Leur lock blunt end needle/tubing onto the front end of blending connector.
3. Turn syringe pump on.
 - a. Press SELECT.
 - b. Toggle to Table, press SELECT.
 - c. Toggle to Bec. Dic. Plastic, press SELECT.
 - d. Toggle to 1 cc 4.70 mm, press SELECT.
 - e. Enter volume: 1.0 mL, press ENTER.
 - f. Enter extrusion rate: 0.225 mL/min, press ENTER.
4. Place a metal non-stick pan next to the syringe pump.
5. Prepare 300 mL of 1X HEPES buffer solution (30 mL of stock solution and 270 mL diH₂O), pH to 7.4
6. Fill pan with 300 mL HEPES buffer solution
7. Add 150 μ L of thrombin aliquot to 850 μ L of calcium chloride solution, mix well.

Extrusion:

1. "Prime" 2 1 mL syringes by moving the plunger several times.
2. Collect all of the thrombin and fibrinogen solutions into 1 mL syringes.
COLLECT THE FIBRINOGEN SOLUTION SLOWLY AND CAREFULLY, FAILURE TO DO SO MAY RESULT IN INSOLUBLE FIBRINOGEN FORMATION!!
3. Invert syringe, remove all bubbles, and ensure that both syringes have equal volumes.
4. Place each 1 mL syringe of fibrinogen and thrombin solutions into the back end of the blending applicator.
ALWAYS PUT FIBRINOGEN SOLUTION IN THE BLENDING APPLICATOR OPENING WITH THE CIRCLE ON IT.
5. Secure syringe/blending applicator construct into syringe pump.
6. Press RUN on the syringe pump and wait for fibrin solution to flow out of the tip of the tubing.
7. Using a metal bar if necessary, draw threads into the buffer solution, taking 6-10 seconds to draw each thread.
8. If the pump does not automatically stop when the syringes empty, press STOP.

9. Wash tubing/blending applicator with cold water and a 5 mL syringe, plugging the other opening with your thumb (at least 5 water rinses per blending applicator opening).
10. Flush water out of blending applicator/tubing repeating step 9 using an empty 5 mL syringe.
11. Fibers can be removed from the bath after 10-15 minutes and stretch threads to make 3 threads along the cardboard box (~7.5 inch threads).

Appendix D: Instron Testing of Polyurethane Well Plate

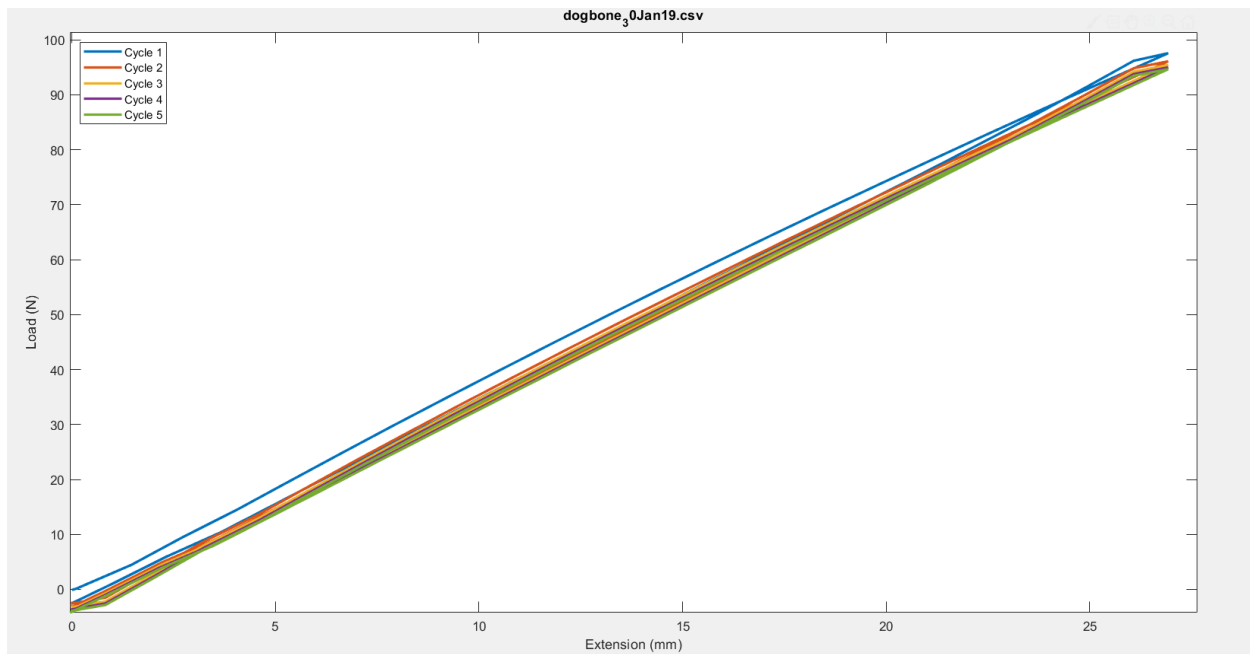


Figure 1: Force-Displacement Curve of Dog-Bone Well Plate outputted by the Bluehill Software

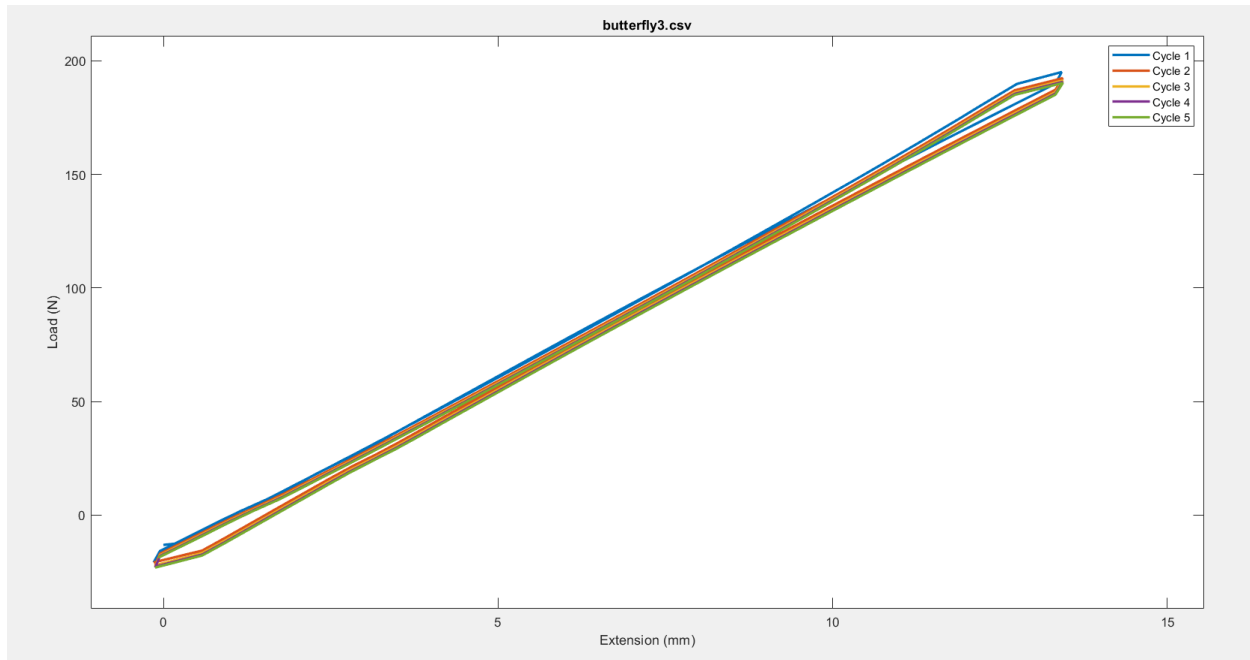


Figure 2: Force-Displacement Curve for “Butterfly Squares” Well Plate outputted by the Bluehill Software

Table 1. ImageJ Summary Data

10% Elongation of Well Plate (n=5)		
Well Measured	Mean Strain	Standard Deviation
Top Well-Left	14.69%	5.39%
Top Well-Right	20.74%	3.11%
Center Well-Left	14.71%	4.31%
Center Well-Right	15.93%	0.26%
Bottom Well-Left	15.66%	1.93%
Bottom Well-Right	18.41%	3.10%

8.6% Elongation of Well Plate (n=5)		
Well Measured	Mean	Standard Deviation
Top Well-Left	12.59%	3.31%
Top Well-Right	17.04%	3.73%
Center Well-Left	13.21%	2.55%
Center Well-Right	13.13%	4.10%
Bottom Well-Left	16.05%	1.44%
Bottom Well-Right	14.33%	3.44%

6.2% Elongation of Well Plate (n=5)		
Well Measured	Mean Strain	Standard Deviation
Top Well-Left	10.70%	1.76%
Top Well-Right	11.24%	2.81%
Center Well-Left	11.88%	2.66%
Center Well-Right	11.60%	1.13%
Bottom Well-Left	12.17%	2.38%
Bottom Well-Right	13.04%	3.87%

Appendix E: CAD Files of PDMS Lid on 6-Well Standard Well Plate

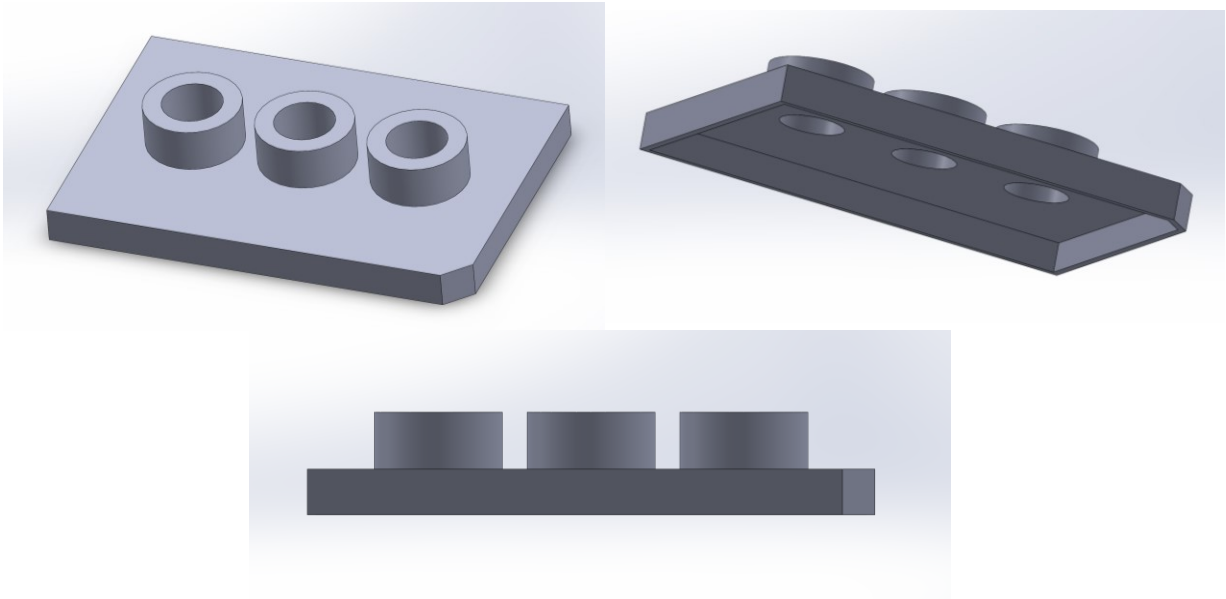


Figure 1. (Top left image): Isometric top view of the PDMS lid for a 6 well plate.
Figure 2. (Top right image): Isometric bottom view of the PDMS lid for a 6 well plate.
Figure 3. (Bottom image): Side view of the PDMS lid for a 6 well plate.

Appendix F: Stepper Motor Control Arduino Code

```
#include <Wire.h>
#include <Adafruit_MotorShield.h>

// Create the motor shield object with the default I2C address
Adafruit_MotorShield AFMS = Adafruit_MotorShield();
// Or, create it with a different I2C address (say for stacking)
// Adafruit_MotorShield AFMS = Adafruit_MotorShield(0x61);

// Connect a stepper motor with 200 steps per revolution (1.8 degree)
// to motor port #2 (M3 and M4)
Adafruit_StepperMotor *myMotor = AFMS.getStepper(200, 2);

unsigned long previousMillis = 0;
long onTime = 3600000; // 1 hour on, in ms
long offTime = 18000000; // 5 hours off, in ms
int completeCycle = 0; // 1 indicates that a cycle has been completed
int cycleCount = 0; // counts the cycles completed
void setup() {
  Serial.begin(9600); // set up Serial library at 9600 bps
  Serial.println("Stepper test!");
  Wire.setClock(400000);

  AFMS.begin(); // create with the default frequency 1.6KHz
  //AFMS.begin(1000); // OR with a different frequency, say 1KHz

  myMotor->setSpeed(5); // THIS IS HOW YOU CHANGE THE SPEED. IT'S IN RPM
}

void loop() {
  // Check to see if it's time to switch motor on or off
  unsigned long currentMillis = millis();
  Serial.println(currentMillis);
  Serial.println(currentMillis - previousMillis);
  if ((currentMillis - previousMillis) > onTime) // If the motor has been running for greater than the "on time"
  {

    Serial.println("Waiting for off time");
    // Stop the motor only once it has completed the current cycle

    myMotor->release(); // actually turn off the motor
    delay(offTime);
    cycleCount = 0;
    previousMillis = millis(); // Reset the clock to reflect when the delay ends
  }

  else
  {
    // actually turn on the motor
    myMotor->step(240, FORWARD, DOUBLE); // THE FIRST ARGUMENT IS THE NUMBER OF STEPS. 10% ELONGATION IS APPROX. 320 STEPS!
    myMotor->step(240, BACKWARD, DOUBLE);
    Serial.println("Cycle Completed");

    cycleCount = cycleCount + 1; // add 1 to the cycle count
  }
}
```

Set number of steps forward and backward to complete one cycle. Steps are in 1.8 deg increments, 12.8 mm stretch (10% elongation) is roughly 320 steps with the current lead screw.

Appendix G: Fibrin Microthread Diameter Tables

Table 1. Team's Dry/Wet Microthread Diameters

Batch No.	Sample Size	Dry Diameter (um)	Wet Diameter (um)
1	n=15	40.5 ± 8.5	140.8 ± 25.3
2	n=15	41.7 ± 7.1	113.2 ± 33.3
Total	n=30	41.1 ± 7.8	127.0 ± 29.3

Table 2. Pins' Dry/Wet Microthread Diameters [69]

Percent Stretch	Sample Size	Dry Diameter (um)	Wet Diameter (um)
125 %	n=41	53 ± 13	97 ± 30
150 %	n=44	43 ± 10	77 ± 25
175 %	n=58	47 ± 11	86 ± 22

Appendix H: MATLAB Code

```
%% Well Plate Strain Measurements following ImageJ Method (Apdx. C)
% Aaron Rosenthal

clc; clear; close all;
% Input filenames
% fileNamesAll = {'Data_1_1.xlsx', 'Data_1_2.xlsx', 'Data_1_3.xlsx',
'Data_2_1.xlsx'...,
% 'Data_2_2.xlsx', 'Data_2_3.xlsx', 'Data_3_1.xlsx', 'Data_3_2.xlsx',
'Data_3_3.xlsx'};
% Initialize export structure
export = struct;
% Initialize mean strain variable to plot later
meanStrainforPlots = [];
% Turn on/off plotting data from each well plate measurement
plotMeasurements = 0; % starts at 0 (off)
% Loop through all data
for files = 1:length(fileNamesAll)
    % Import well plate dot displacement data
    data = xlsread(fileNamesAll{files}, 'B2:K13');

    % Separate the data for the stretched and unstretched wells
    unstretched = data(:,1:2:end);
    stretched = data(:,2:2:end);

    % Take the mean values for each of the 5
    runs together

    ustrDifferences = unstretched(1:2:end,:) - unstretched(2:2:end,:);
    strDifferences = stretched(1:2:end,:) - stretched(2:2:end,:);
    meanUnstretched = mean(ustrDifferences,2);
    meanStretched = mean(strDifferences, 2);
    % Calculate the strains in each well order goes (L, R) for each of 3
    wells
    strain = (meanStretched - meanUnstretched)./meanUnstretched;
    leftStrains = strain(1:2:end);
    rightStrains = strain(2:2:end);
    export(files).fileName = fileNamesAll{files};
    export(files).wellStrain = [leftStrains rightStrains];
    meanStrainforPlots = [meanStrainforPlots mean([leftStrains
rightStrains],2)];
end
%% Plot Data from Each Well Plate
topWell = meanStrainforPlots(1,:);
centerWell = meanStrainforPlots(2,:);
bottomWell = meanStrainforPlots(3,:);
figure
xVals1 = zeros(length(topWell),1);
xVals3 = ones(length(topWell),1);
xVals2 = xVals3./2;
scatter(xVals1, topWell, 'filled')
xlim([-0.5 1.5])
ylim([0 max(meanStrainforPlots(:))+.05])
```

```

set(gca, 'xtick', [0 0.5 1], 'xticklabel', {'Top Well' 'Center Well' 'Bottom
Well'});
hold on;
scatter(xVals2, centerWell, 'filled')
scatter(xVals3, bottomWell, 'filled')
figure

% legend('Top Well', 'Center Well', 'Bottom Well', 'Location', 'northwest')
% title('Individual Value Plot of Well Strain at 10% Elongation')
% % ylabel('Strain (mm/mm)')

% Plot means on IVP
scatter(xVals1(1), mean(topWell), 50, '*')
scatter(xVals2(1), mean(centerWell), 50, '*')
scatter(xVals3(1), mean(bottomWell), 50, '*')

boxplot([topWell(:).*100 centerWell(:).*100 bottomWell(:).*100], 'Labels',
{'Top Well' 'Center Well' 'Bottom Well'}, 'Whisker', 3)
ylabel('Axial Strain Percentage')
if adtest(topWell) == 0 && adtest(centerWell) == 0 && adtest(bottomWell) == 0
    fprintf('The data are normal by the Anderson-Darling normality test \n')
    pValANOVA = anova1([topWell(:) centerWell(:) bottomWell(:)]);
    fprintf('p=%4.4f', pValANOVA)
else
    fprintf('The data are not normally distributed by the Anderson-Darling
normality test')
    pValueKW = kruskalwallis(topWell(:), centerWell(:), bottomWell(:));
    fprintf('p=%4.4f', pValKW)
end

%% Well Plate Video Analysis for ImageJ Processing
% Aaron Rosenthal
clear; clc; close all;
%% Break up Video into Individual Frames
% Extract frames from video
[file, path] = uigetfile('.mp4', 'Select a video file', ...
    'C:\Users\rosen\OneDrive\Documents\WPI\MQP\Data');
addpath(path)
video = VideoReader(file);
% video.CurrentTime = 3; % Begin reading frames 3 sec from the beginning of
the video

% currentAxes = axes; % Create an axes object
% mkdir('images')
% addpath('images')
numFrames = video.NumberOfFrames;
video = VideoReader(file); % Re-extract frames b/c of stupid NumberOfFrames
property call
mkdir('Instron', file)
imgDirectory = convertCharsToStrings(fullfile('Instron', file)); % Folder to
save all the images in corresponding with the name of the video

```

```

for iFrames = 1:numFrames
    vidFrame = readFrame(video);
    grayScaleImg = rgb2gray(vidFrame);
    imwrite(grayScaleImg, strcat(imgDirectory, '\', 'image',
int2str(iFrames), '.png'), 'png');
    fprintf('Writing frame %i to image \n', iFrames)
end

%% Select the image that is the beginning of the Instron test.
[file2, path2] = uigetfile('.png', 'Select the first image of the test', ...
    imgDirectory);
imageID = [];
framesPerSec = 30;
testSpeed = 500; % in mm/min\
targetStretch = 12.8; % mm
framesPerCycle = 88; %(framesPerSec*60/testSpeed*targetStretch);
for i = 2:length(file2)
    [ithNumber, flag] = str2num(file2(i));
    if flag == 1
        numStr = num2str(ithNumber);
        imageID = strcat(imageID, numStr);
    end
end
selectedImages = []; % Initialize a variable containing the image #s
corresponding with the max and min stretch
for halfCycle = 1:10
    selectedImages = [selectedImages str2num(imageID) + (halfCycle-
1)*framesPerCycle];
end

%% Move selected images into a new folder

% Create a new folder where the images at no stretch and max stretch will be
stored
mkdir(imgDirectory, 'Min_Max_images')
imgDirectory2 = convertCharsToStrings(fullfile(imgDirectory,
'Min_Max_images'));
% Copy the files into the new folder
for j = 1:numel(selectedImages)
    copyfile(strcat(imgDirectory, '\', 'image',
num2str(int64(selectedImages(j))), ...
        '.png'), imgDirectory2)
end

```

Appendix I: CAD Drawing of Final Components

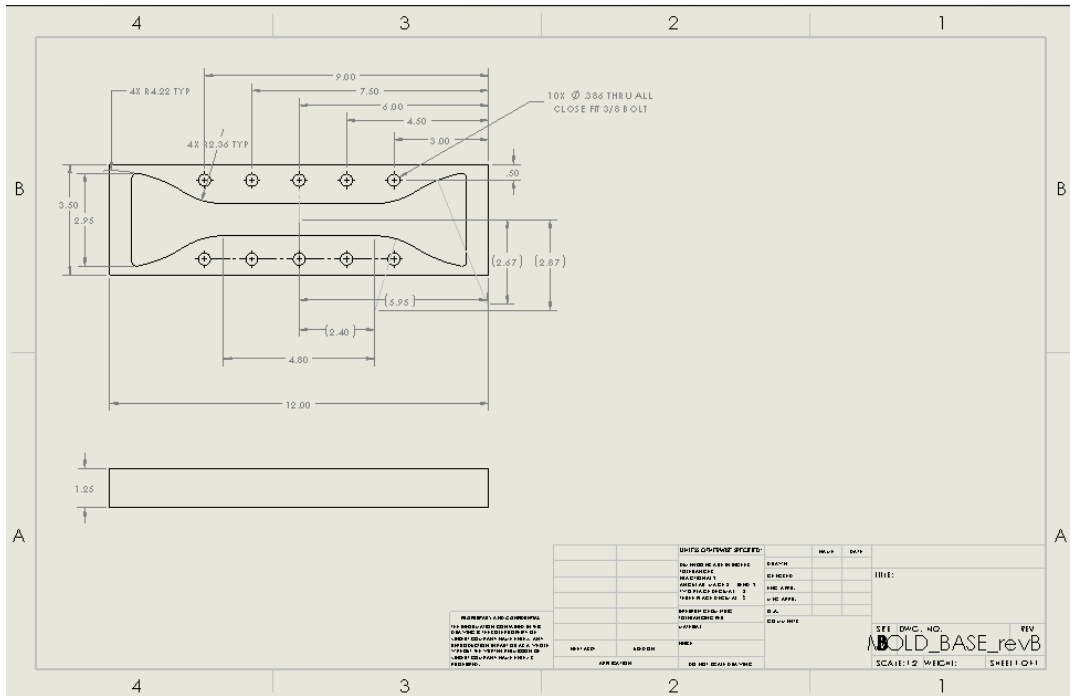


Figure 1. PDMS Aluminum Mold – Base Frame

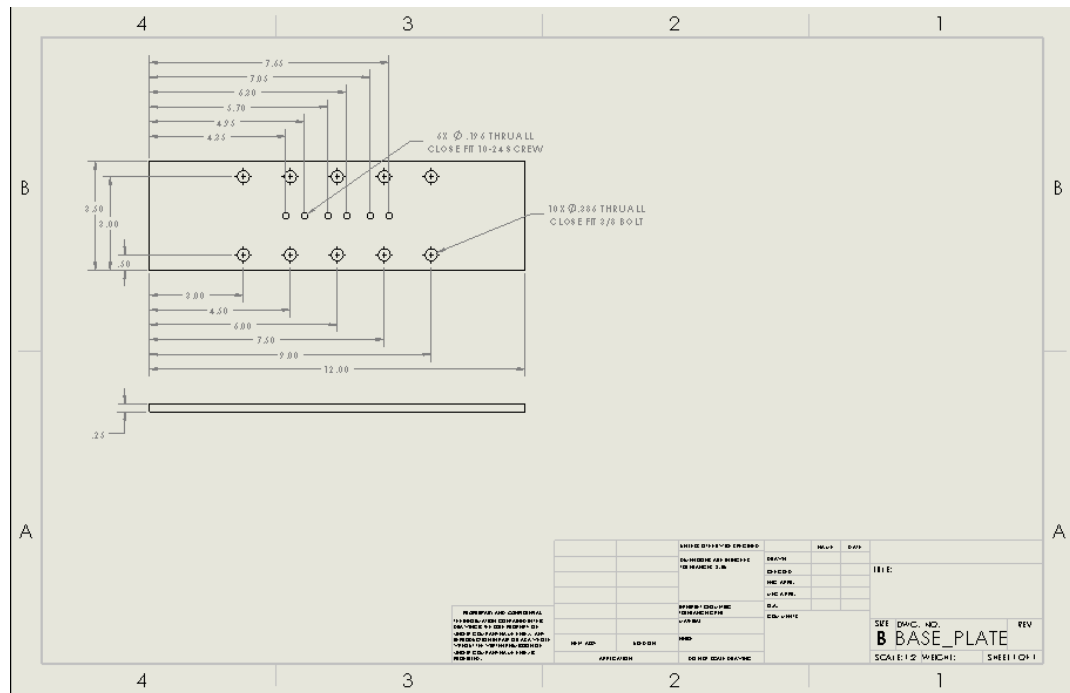


Figure 2. PDMS Aluminum Mold – Base Plate

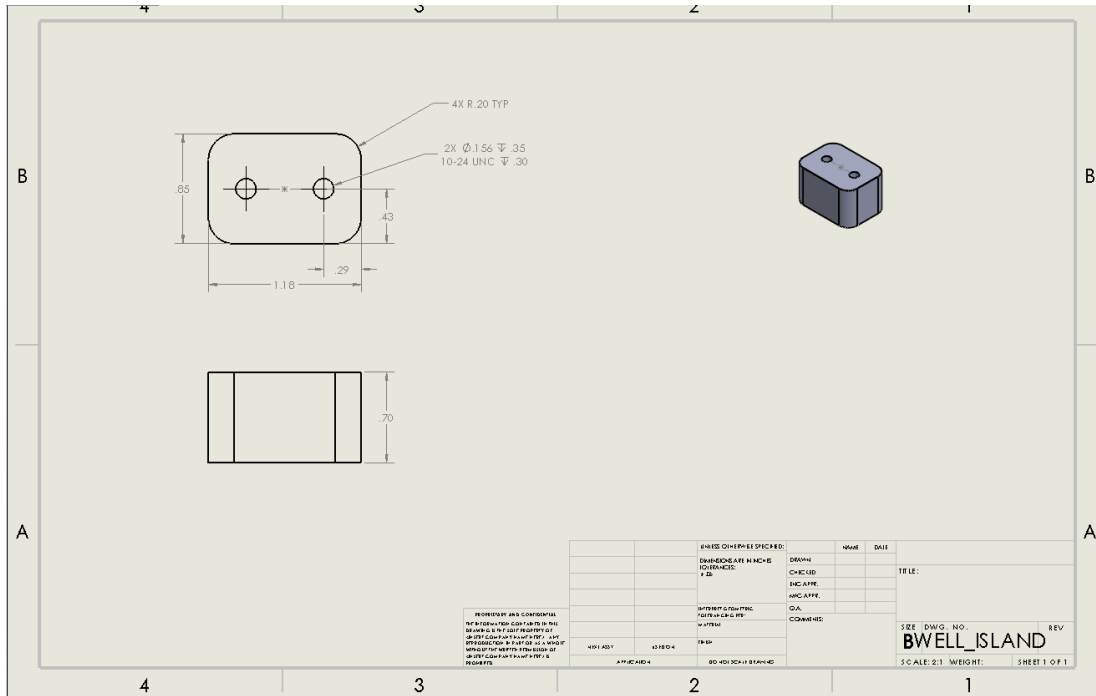


Figure 3. PDMS Aluminum Mold – “Islands”

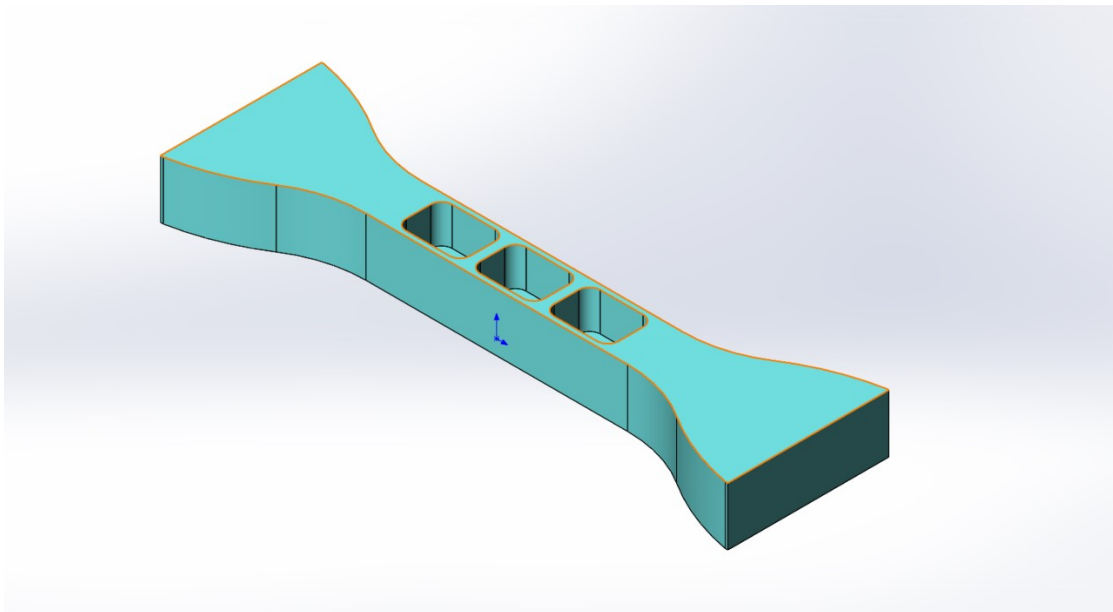


Figure 4. PDMS Well Plate Solid Model

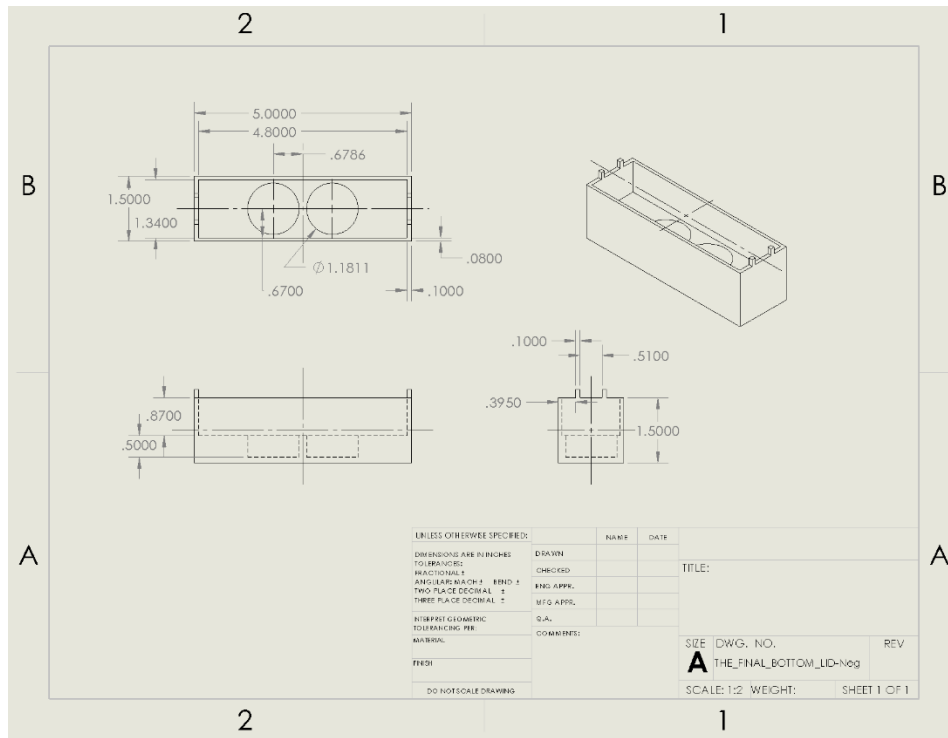


Figure 5. PDMS Aluminum Lid Mold – Bottom Piece

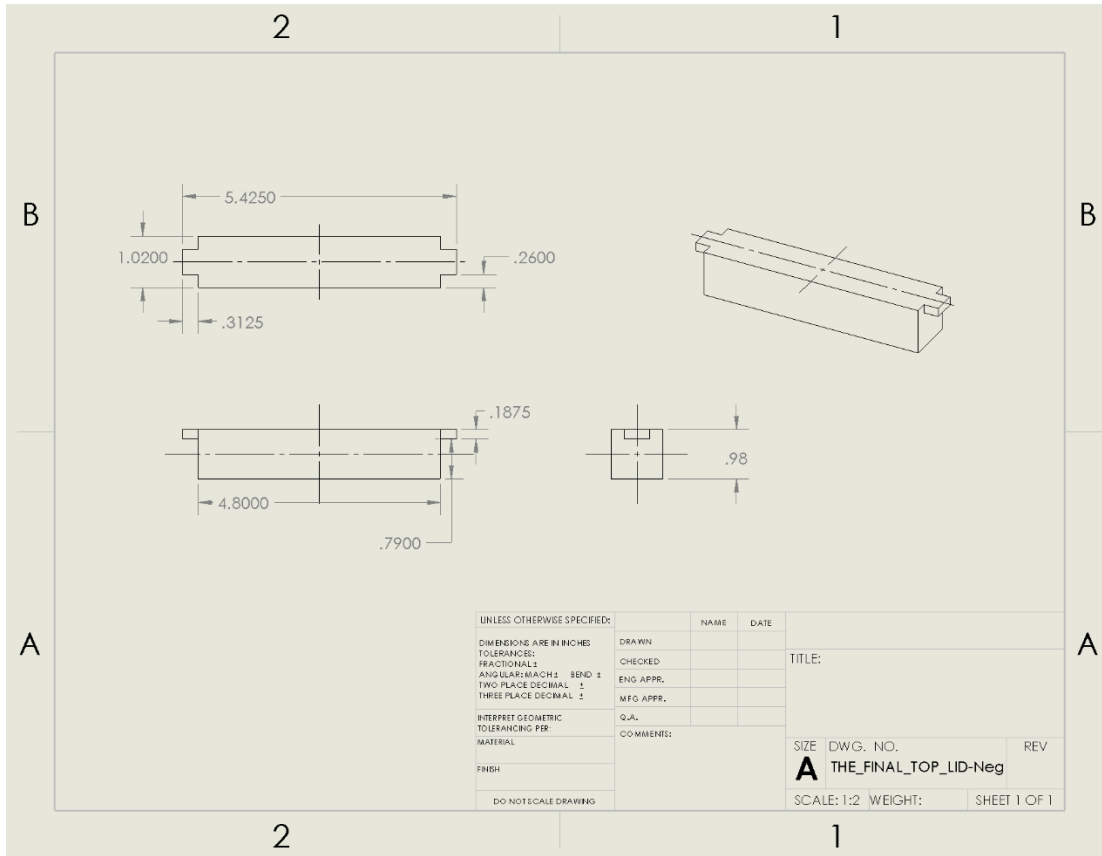


Figure 6. PDMS Aluminum Lid Mold – Top Piece

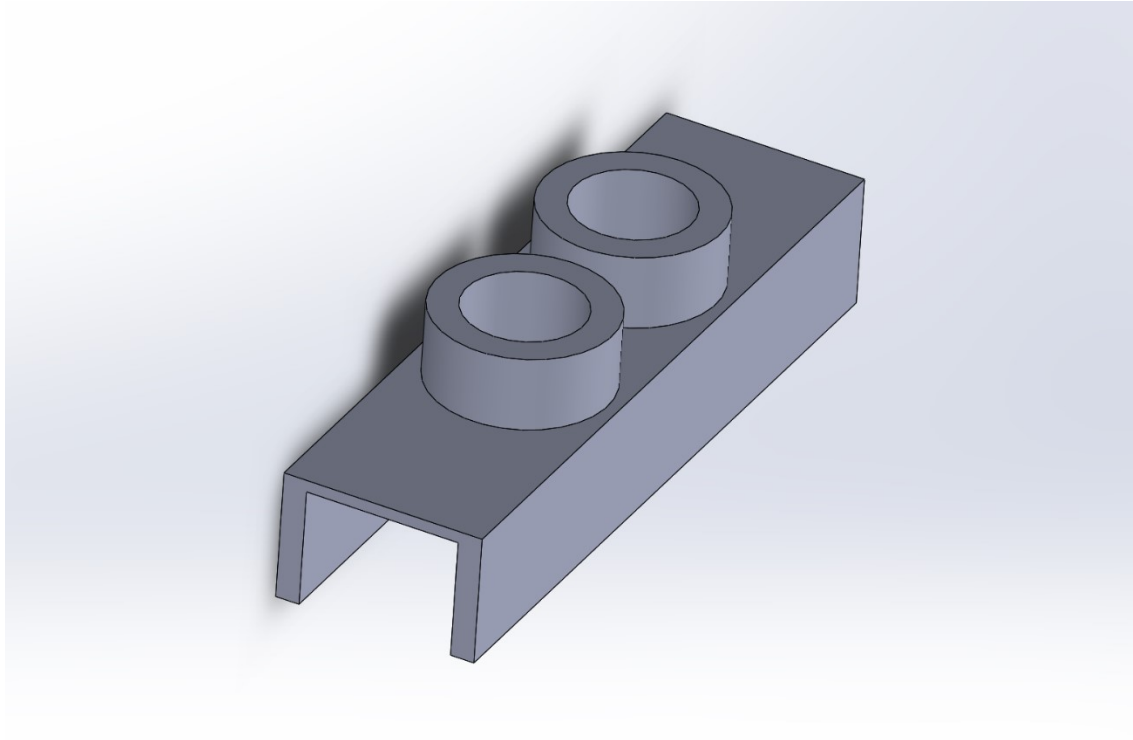


Figure 7. PDMS Lid Solid Model

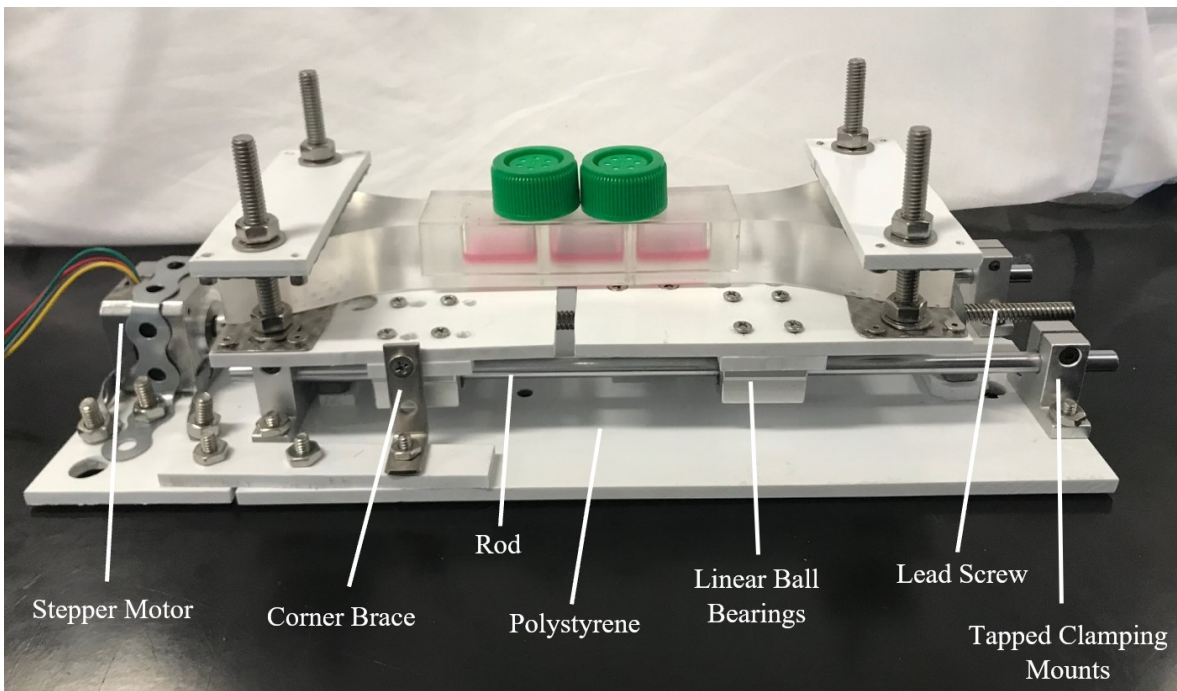


Figure 8. Front View of Mechanical System Labeled

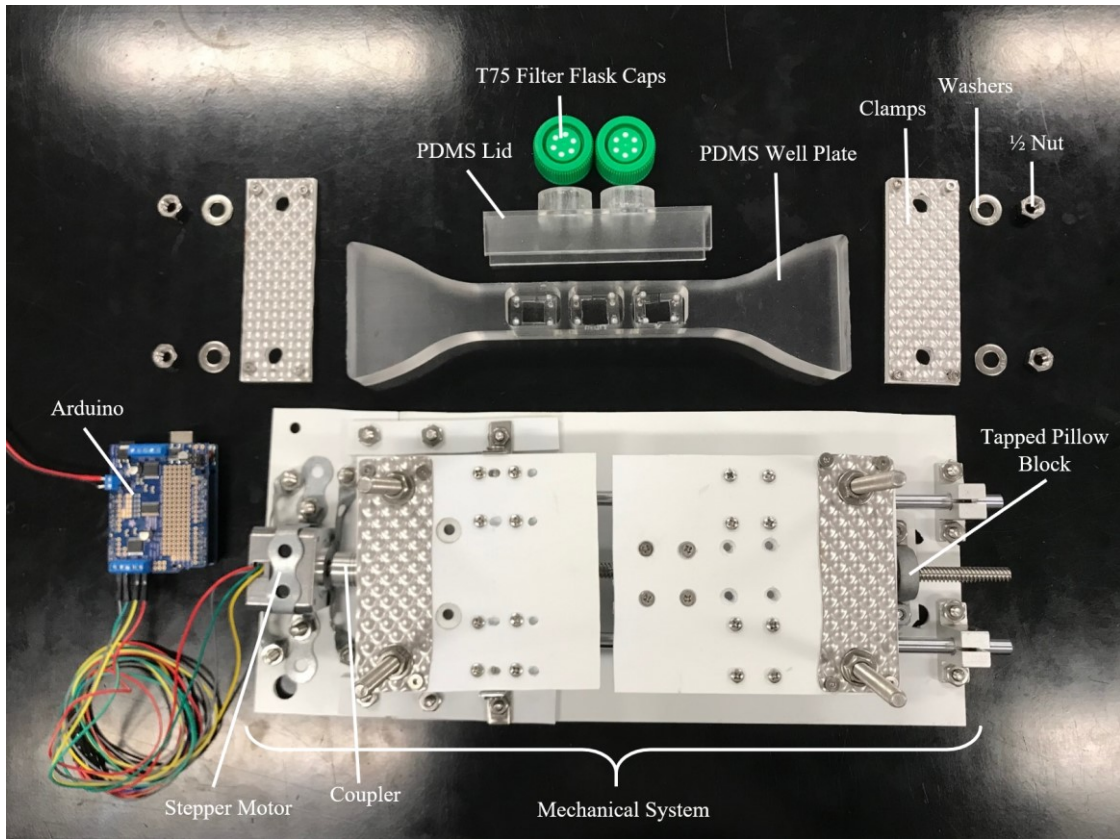
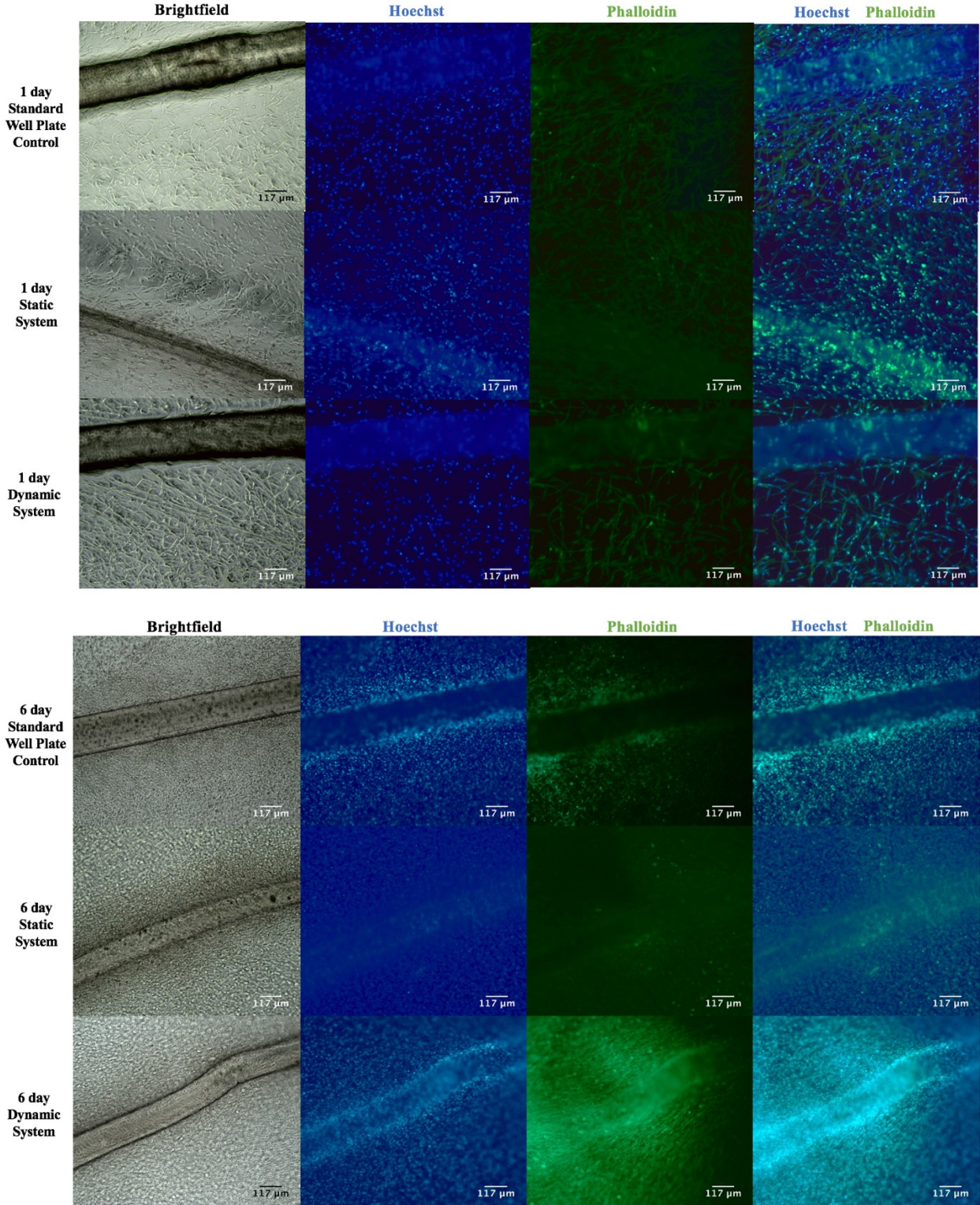


Figure 9. Top View of Final Components Labeled

Appendix J: Final Design Validation Data



ANOVA Table					
Source	SS	df	MS	F	Prob>F
Columns	0.00207	2	0.00104	0.69	0.5137
Error	0.03629	24	0.00151		
Total	0.03836	26			

Figure above: One-Way ANOVA Table for Section 6.1.1 Instron Testing of PDMS Well Plate

ANOVA Table					
Source	SS	df	MS	F	Prob>F
Columns	0.00077	2	0.00038	0.78	0.477
Error	0.00739	15	0.00049		
Total	0.00815	17			

Figure above: One-Way ANOVA Table for Section 6.1.2 Mechanical System Validation

Appendix K: Bill of Materials with Corresponding Prices

Materials and Price	
Sylgard 184 PDMS Well Plate	\$33.33
Sylgard 184 PDMS Lid	\$6.30
Adafruit Stepper Motor	\$14.00
Adafruit Motor Shield	\$19.95
Adafruit 5mm to 8mm Rod Connector	\$4.95
Stainless Steel Fixture Pins	\$5.00
Arduino Wire Extensions	\$11.19
Lead Screw	\$4.00
2 pcs x 8x400mm Steel Optical Axis 2 pcs x KP08 55x13x29mm Zinc Alloy Pillow Block Bearing	\$22.26

4 pcs x SK8 42x32x14mm Aluminum Rail Shaft Support 1 pcs x 400x8mm Stainless Steel Lead Screw Rod with Nut 4 pcs x SC8UU 8x34mm Slide Bushing 2 pcs x 5x8mm D19L25 Flexible Shaft Coupling	
1pc x T8 Screw Nut Bracket	\$15.30
Polystyrene Sheet	\$15.07
Diamond Textured Stainless Sheet	\$9.88
16 #6-32 Oval Head Screws	\$4.32
4 #10-24 Flat Head Screws	\$1.08
8 Half Diameter Washers	\$2.16
20 #12-24 Oval Head Screws	\$5.25
20 #12-24 Hex Nuts	\$2.25
4 1/2" Screws	\$4.32
4 Larger Washers	\$2.16
4 1/2" Hex Nuts	\$4.23
Corner Brace	\$2.44
Galvanized Steel	\$5.00
Aluminum Well Plate and Lid Molds	\$60.28
Total:	\$254.57